Binding Site Structure and Stoichiometry in Serotonin Type 3 Receptors

Thesis by

Timothy Francis Miles

In Partial Fulfillment of the Requirements

for the Degree of

Doctor of Philosophy

CALIFORNIA INSTITUTE OF TECHNOLOGY

Pasadena, California

2015

(Defended July 11, 2014)

Acknowledgements

I have had the good fortune to be surrounded by sterling people who have encouraged, motivated, and supported me. For this, I wish to express my deepest thanks to:

Dennis Dougherty, for being an ideal advisor, giving wide latitude to follow my research interests and counsel when I encountered stumbling blocks. His ability to find balance, his intellectual tenacity, and his talent for clarity in communication are all things to which I aspire;

Henry Lester, for providing insight and a unique perspective throughout my graduate training. Collaborating closely with Henry during my fluorescence microscopy studies was a great privilege and my research conduct is more rigorous and professional for it;

Ellen Rothenberg, for her invaluable support and advice concerning my teaching interests. TAing for her was both a pleasure and an education in effective pedagogy;

Sarah Lummis of the University of Cambridge, for sharing materials and expertise;

My thesis committee members, Doug Rees and Ray Deshaies, for their advice and support;

Rob Fairman of Haverford College, for introducing me to research and supporting me throughout my academic development. No single person has informed my scientific outlook more;

Bashkim Kokona of Haverford College, for helping me to adjust to the day-to-day practice of research and for challenging me to be a rigorous thinker;

My labmates, for providing a welcoming, stimulating, productive, and enjoyable environment in which to spend the past four years. You have made grad school a truly fun experience and I will miss you all. Noah Duffy showed me the ropes in lab during my rotation and was an invaluable source of advice and insight over the years. His quiet manner and kind words reassured me of my place in grad school in the early days and our technical conversations shaped my thinking countless times since. Angela Blum is a prolific worker and sharp thinker whose ethic was both slightly intimidating and highly motivating. I miss cycling and going to concerts with Ethan Van Arnam almost as much as I miss his zeal for science. Kristina Daeffler had a knack for making the inevitable pitfalls of research seem both amusing and tractable. Clint Regan is a supremely diligent researcher, leading a new branch of the lab. I'm left in awe when he gets on a roll at a research update meeting, excitedly detailing reactions and calculations. Chris Marotta holds the prize for somehow being the most warm and upbeat person in lab and the most likely to shout in exasperation at inanimate objects; his fellowship has been a great aid over the years. Oliver Shafaat is a rigorous thinker and is unafraid of big problems; these traits will carry him well. Matt Rienzo is often found preparing for 50+ mile day hikes in his free time; this gives some insight into his aptitude and affinity for enduring and accomplishing difficult tasks. I look forward to hearing what he sets his sights on next. I thank Mike Post for his dub-step Mondays that crept through the whole week and for being the bedrock of "North Bay Nation". Paul Walton is the most intelligent tornado I've met. His whirlwind of jokes belies his intellectual seriousness. Working with Matt

Davis has been a great experience. I admire his eagerness to follow a question wherever it takes him. I respect Kayla Busby's bravery and wish her luck in her future endeavors. Betty Wong, Catie Blunt, Annet Blom, and Bryce Jarman have been great additions to the Dougherty lab, both as supremely capable researchers and also as genuinely nice people. I look forward to seeing where their research takes them.

I thank Don Letts, Paul Bisceglio, Mike Hildner, Danny Guilfoyle, Greg Potestio, Ben Walker, Mac Sellars, Jossi Fritz-Maur, Emma O'Neill, and Jane Weber for their support and friendship, and the Goats for providing community and inspiration to avoid becoming a total sloth in graduate school.

Marco Allodi, Katie Kirby, Josh Kretchmer, and Danielle Ownby for being great housemates, friends, and sounding boards. I'm going to miss our grilling and game nights, our nerdy discussions of just about every topic, and our adventures around LA. I look forward to seeing where the future takes each of them.

Morgan Soloway for being my climbing partner, my sharer of adventures, my friend, and my love.

My sisters in-law Nadine and Chrissi, and all of my aunts, uncles, and cousins for their encouragement and support. I have been so fortunate to have been surrounded by such wonderful people.

Mommom Mary and Pop Frank for their interest in and support of my academics and my adventures. In all things I try to make them proud.

Mommom Marylou and Pop Jim, who are constantly in my thoughts. Some of my fondest memories are of doing anagrams with Mommom Marylou and falling asleep on Pop Jim's lap watching cartoons. I love and miss them.

My brothers Mike, John, and Andrew and my sister Jenn. They are my oldest and closest friends. Mike has always modeled for me seriousness of purpose, dedication to excellence, and doggedness in its pursuit. John is amazingly brave, following his own path. I admire his intellectual curiosity, his creativity, and his talent for finding meaning. Andrew's cheer is infectious. He teaches me patience and compassion, continually shows me new ways of viewing the world, and inspires me to make the most of my abilities. Though slightly younger, Jenn always felt like my big sister. She is caring and compassionate, intelligent and funny. I look forward to spending more time with her in the bay state next year.

And finally, I thank my parents for instilling high expectations, academic and otherwise, for modeling a strong work ethic and a compassionate disposition, and for creating an environment where I always felt loved, valued, and supported.

Abstract

This dissertation primarily describes studies of serotonin type 3 (5-HT_3) receptors of the Cys-loop super-family of ligand gated ion channels. The first chapter provides a general introduction to these important proteins and the methods used to interrogate their structure and function. The second chapter details the delineation of a structural unit of the ligand binding site of homomeric 5-HT_3A receptors on which the ligands serotonin (5-HT) and *m*-chlorophenyl biguanide (*m*CPBG) are reliant for effective receptor activation. Unnatural amino acid mutagenesis results show that the details of each ligand's interaction with this organizing feature of the binding site differ, providing insights into general principles of receptor activation.

The third chapter describes a study in which florescent protein fusions of the A and B subunits of the heteromeric 5-HT_3AB receptor are employed to determine the subunit stoichiometry and order within functional receptors. Strong evidence is found for an A_3B_2 stoichiometry with A-A-B-A-B order. The fourth chapter investigates the potential for ligand binding across heteromeric binding sites in the 5-HT_3AB receptor. Unlike serotonin, mCPBG is found to bind the receptor at heteromeric binding sites. Further mCPBG is capable of allosterically modulating the response of serotonin on the 5-HT_3AB receptor from these heteromeric sites.

Finally, the fifth chapter describes progress towards the application of unnatural amino acid mutagenesis to an important new class of proteins, transcription factors. Experiments optimizing novel methods for the detection of function are described, using RARα of the nuclear receptor family of transcription factors.

Table of Contents

List of Figures

List of Tables

Chapter 1

Introduction

1.1 Synaptic Transmission

The brain is the most complex structure on earth (*1*). It is principally a highly inter-connected web of specialized cells called neurons. These cells feature extended processes that reach out to form connections with other neurons termed synapses. Sensation, consciousness, and all the other marvelous functions that brains perform arise from the patterns of activation that travel along this neural web. Within a neuron, activation is coded as an electrical current that travels the length of the cell. This current is propagated by voltage-gated ion channels. Upon sensing a sufficient change in membrane potential, these proteins change shape to allow ion passage across the plasma membrane. The ion flux depolarizes adjacent regions of the membrane, thereby activating further voltage-gated ion channels nearby and forming the leading edge of a wave of current called an action potential.

This current is incapable of crossing the synapse and bridging cells. To solve this impasse, the activating electrical signal is converted to a chemical signal (Figure 1). When the action potential reaches the end of neural processes called axons, membrane vesicles are stimulated to fuse with the plasma membrane. Upon fusion, the vesicles dump their contents into the cleft between the two neurons of the synapse. The vesicle cargo is a class of small molecules called neurotransmitters. These neurotransmitters diffuse across the synaptic cleft and bind to protein receptors on the process of the

receiving neuron, referred to as a dendrite. This binding leads to ion flux that, depending on the identity and concentration of the neurotransmitters and receptors present, depolarizes the dendrite such that voltage-gated ion channels there are activated. This activation restarts the action potential in the receiving neuron where it rushes toward the cell body and its own axons, where the process will repeat.

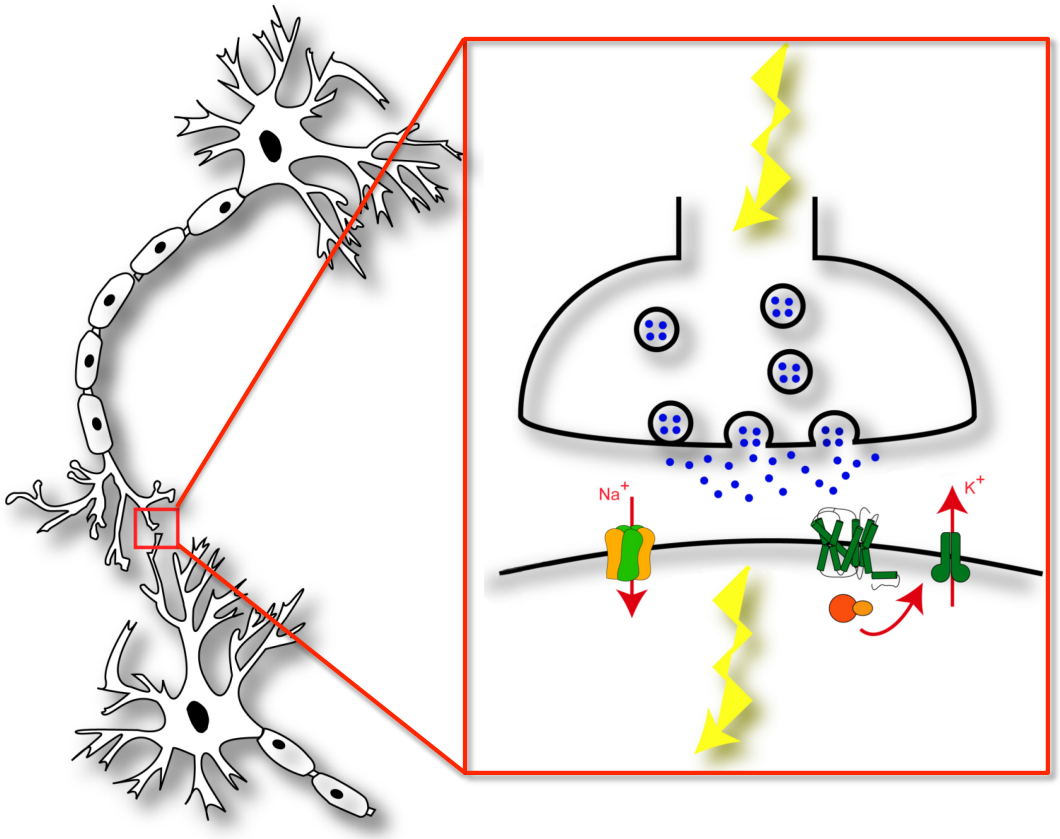

Figure 1.1 Synaptic transmission. (left) Two neurons forming a synapse. (right) Expansion of the synapse; axon at top and dendrite below; blue dots are neurotransmitters.

1.2 Cys-loop Receptors

There are two classes of protein receptors in the brain. The first class is G protein coupled receptors, or GPCRs. Neurotransmitter binding by these transmembrane proteins releases the G protein from the receptor, which then activates downstream intracellular

signaling cascades that indirectly modulate the membrane potential. The second class of protein receptors in the brain is ligand-gated ion channels. Ligand-gated ion channels may be classified by their oligomeric state: trimeric ATP-gated P2X receptors, tetrameric ionotropic glutamate receptors, and pentameric Cys-loop receptors. Like the voltage-gated ion channels, these proteins open a pore in the membrane, allowing ion flux that directly alters the membrane potential.

Cys-loop receptors are a broad family of ligand-gated ion channels that encompasses nicotinic acetylcholine, glycine, $GABA_A$, and serotonin type 3 receptors. Cys-loop receptor function has been implicated in numerous essential cognitive processes and their disfuction has been found to underlie many neurological disorders (*2-4*). Given this, they are active pharmaceutical targets.

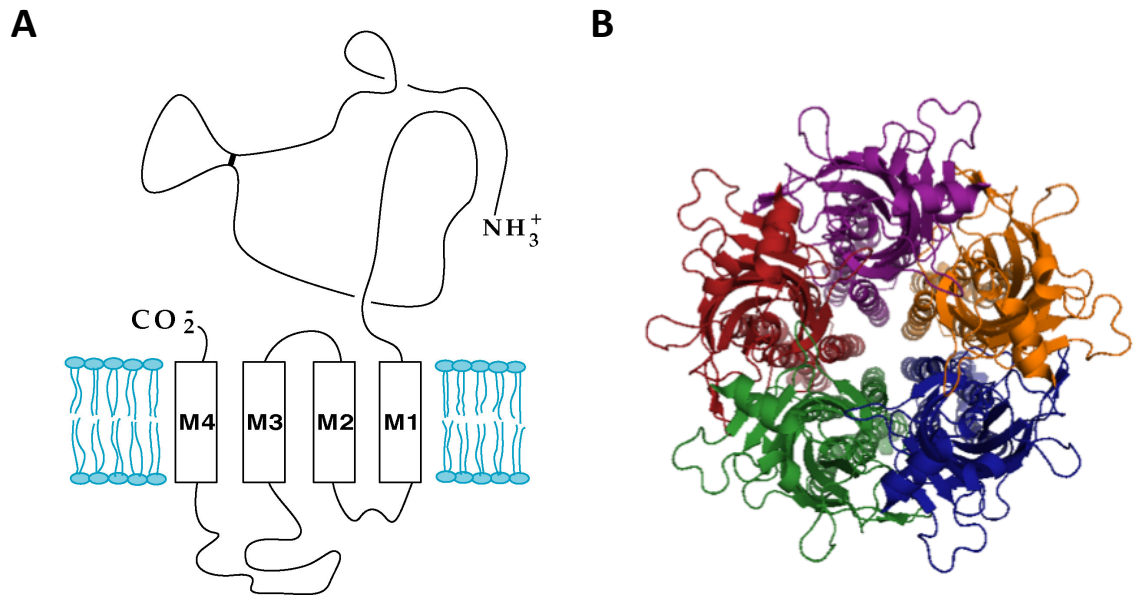

Figure 1.2 Cys-loop receptor structure. (A) Schematic of cys-loop receptor domain architecture. (B) Top-down view of Cys-loop receptor showing M2 α-helix lining the central pore.

Each of the five Cys-loop receptor subunits that form a functional receptor contains a large extracellular domain, four transmembrane helices, and an intracellular loop of variable length that bridges the third and fourth transmembrane helices (Figure 2A) (*5*). These subunits arrange semi-symmetrically around a central pore. Lining that pore is the second transmembrane helix (Figure 2B). The side chains of the residues on this helix occlude the channel pore in the resting state of the receptor.

Ligand binding occurs at the interface of the extracellular domains of adjacent subunits. The binding site is composed of six loops, three on the principal subunit (A-C), and three on the complementary subunit (D-F) (Figure 3A). On these six loops, five highly conserved aromatic residues have been identified: a tyrosine on loop A (TyrA), a tryptophan on loop B (TrpB), two tyrosines on loop C (TyrC1 and TyrC2), and a tryptophan on loop D (TrpD); these are collectively referred to as the "aromatic box" (Figure 3B). The location of the binding site is nearly 60Å from the occlusion of the channel pore. Thus, a broad conformational change must occur to link neurotransmitter binding with channel opening.

Each category of Cys-loop receptor listed above is itself a diverse family of receptors. In nicotinic acetylcholine receptors (nAChRs) for instance, there are 17 subunit types that are expressed in the brain (*6*). These different subunit types are able to co-assemble, creating even more potential unique heteromeric receptors. As ligand binding spans adjacent subunits, this diversity of receptor subunit composition affords the potential for markedly different responses to the same neurotransmitter. In fact, subtle sequence differences between the muscle and neuronal nAChRs have been shown to explain why cigarette smoking does not result in body-wide muscle contraction (*7*).

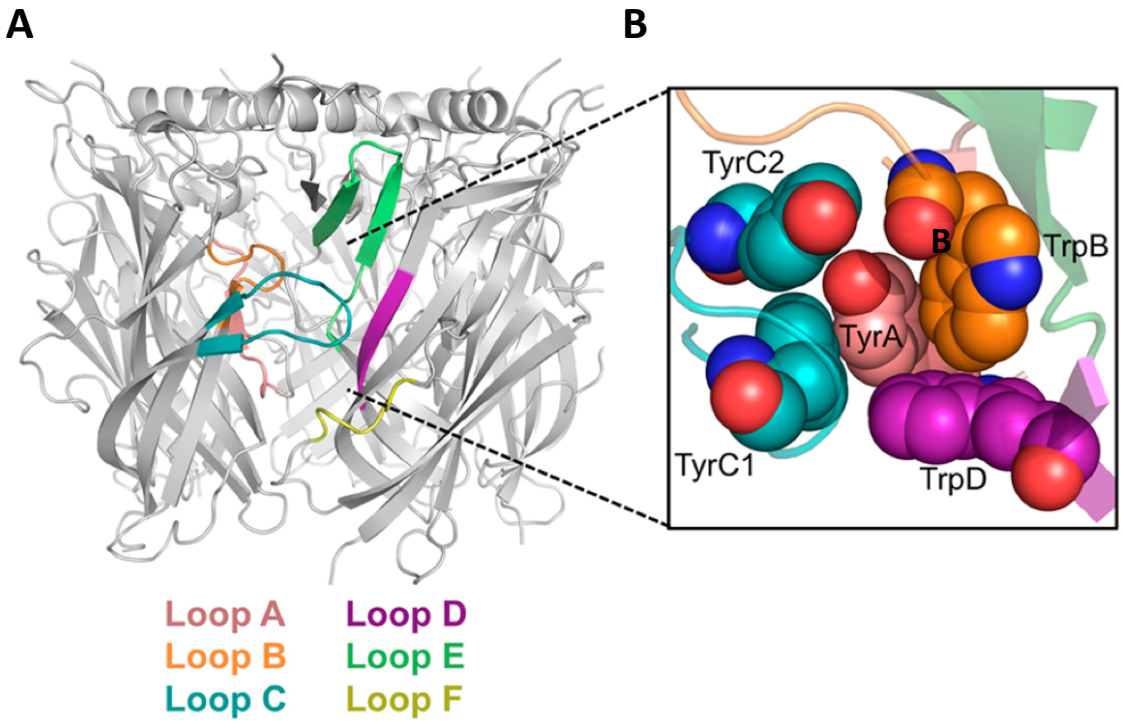

Figure 1.3 The Cys-loop receptor ligand-binding site. (A) Conserved loops of the binding site. (B) Conserved aromatic residues of the binding site. Adapted from (12).

In addition to the complexity generated by diversity in receptor composition, there is also the potential for variation in receptor subunit stoichiometry. Again, using nAChRs as our guide, the α4β2 subtype exists in both A(3)B(2) and A(2)B(3) stoichiometries. This subtle difference affords the receptors different sensitivities to neurotransmitter and different roles in the molecular pathology of addiction (*8, 9*).

Knowledge of Cys-loop receptors has been greatly advanced by the efforts of structural biologists (*10*). The first relevant structural information came from x-ray crystal structures of acetylcholine binding proteins (AChBP) (Figure 4A). These soluble proteins found in snails share homology with the extracellular domains of Cys-loop receptors, and structures bound with numerous ligands have been crystallized (*11*). These

structures have provided much insight into possible ligand binding interactions, but subsequent functional data have, unsurprisingly given their evolutionary distance and functional divergence, shown them to be imperfect models of the full-length human membrane receptors (*12*).

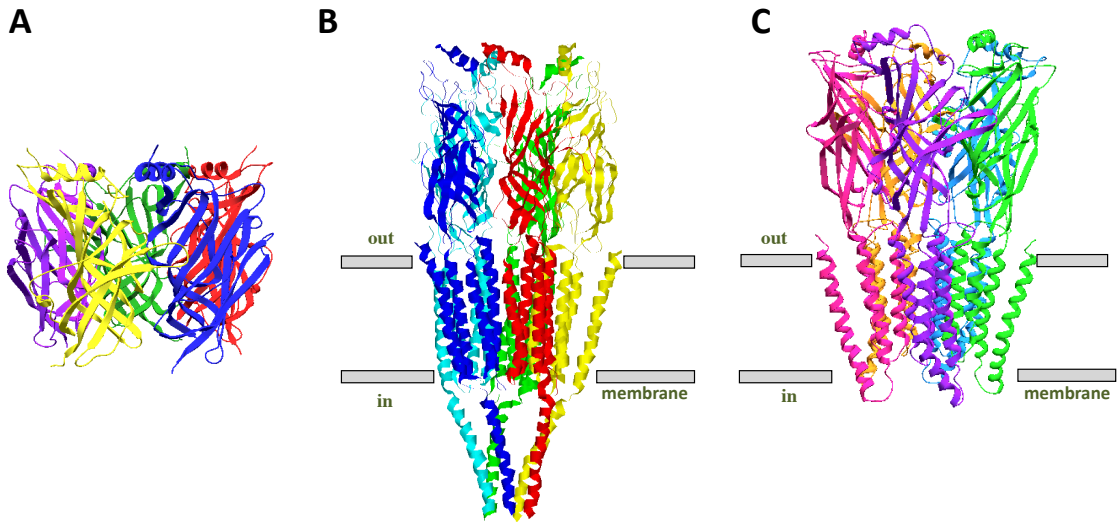

Figure 1.4 High resolution structures of relevance to Cys-loop receptors. (A) Acetylcholine binding protein crystal structure. PDB: IUW6. (B) *Torpedo* nAChR cryo-EM structure. PDB: 2BG9. (C) GluCl receptor crystal structure. PDB: 3RHW.

A cryo-electron microscopy structure of the nAChR from the *Torpedo* ray provided the first structural information on a full-length Cys-loop receptor (Figure 4B) (*13*). Unfortunately, the poor resolution of the structure limits its use to the demonstration of global receptor topology. More recently, the high resolution crystal structure of a full-length Cys-loop receptor found in *C. Elegans* was solved (Figure 4C). Glu-Cl is a glutamate binding receptor with a chloride selective pore (*14*). It shows similar global topology to the cryo-EM nAChR structure and for the first time reveals ligand-binding interactions in a Cys-loop receptor. It is difficult however to extrapolate from this one

snapshot to the many human Cys-loop receptors and the motions on which their functions depend.

1.3 Methods for Perturbing Receptor Function

1.3.1 Conventional Mutagenesis

The time-honored method for gaining insight into the relation of a protein's structure to that protein's function is to analyze the many ways in which one can break that relation. This can involve something as simple as heating the sample until the protein falls apart or as complicated as screening hundreds of thousands of potentially interfering small molecules.

A method that strikes a balance of technical ease and atomic level feedback is mutagenesis. Advances in the last twenty years have made it trivial to site-specifically change the coding sequence in the gene of a protein for *in vitro* or heterologous expression. By exchanging one codon for another, any amino acid can be swapped for one of its 19 conventional cousins. This has been extremely useful in determining sites crucial for protein function and for gaining some insight into what properties might be required at that site. The natural array of amino acids contains both hydrophobic and hydrophilic, bulky and diminutive, as well as positively, negatively, and non-charged side chains that allow for the importance of many features of a site of interest to be probed.

1.3.2 Unnatural Amino Acid Mutagenesis

Obviously, a repertoire of twenty amino acids cannot adequately cover chemical space, so many mutations actually change multiple features of the natural residue. This is highlighted by the case of the amino acid tryptophan. It has a large side chain capable of

forming extensive van der Waals contacts and filling a steric niche, an indole nitrogen capable of forming hydrogen bonds, and a conjugated aromatic system capable of forming interactions with other aromatic side chains or positive charges. The most subtle conventional alternative is to mutate to phenylalanine, which retains aromaticity, but this mutation both eliminates hydrogen bonding, changes steric bulk, and slightly weakens aromatic interactions. This ambiguity makes it difficult to confidently assign specific interactions of functional importance.

Synthetic methods allow for the chemical preparation of a vastly larger array of amino acids than those provided by nature. Referring again to the case of tryptophan, one can imagine substituting naphthyl-alanine to eliminate hydrogen bonding while retaining strong aromaticity and steric bulk. Or one could substitute tryptophan analogues featuring sequential fluorination of the indole that additively deplete the aromatic system of π-electron density, thereby selectively weakening aromatic interactions while leaving hydrogen bonding and steric contacts intact (*15*).

The challenge has long been not the synthesis of these molecules but their successful incorporation into proteins within a biological system. The critical consideration for a successful method is orthogonality (*16*). This is the concept that the unnatural amino acid incorporation should function alongside but completely independently of the existing machinery for conventional amino acids. In practice this requires that the unnatural amino acid should be charged only to a tRNA unique to it and that the unique tRNA should recognize an mRNA codon that is incompatible with all endogenous tRNAs. Additionally, the unnatural aminoacyl tRNA should then be an acceptable substrate for the ribosome.

To accomplish this, tRNAs from various bacteria and archea have been identified and further engineered to be unrecognizable to eukaryotic amino acyl synthetases that append conventional amino acids to their tRNAs (*17, 18*). To charge the engineered tRNA several groups have evolved new aminoacyl synthetases that selectively recognize the unnatural amino acid (*19*). Unfortunately this tactic requires the creation of nearly as many synthetases as unnatural amino acids, and also requires that the unnatural amino acids be sufficiently different from any natural analogue in order to generate acceptable specificity. These requirements create an experimental bottleneck and preclude the use of many subtly different unnatural amino acids of potential utility.

An alternative pursued here is to chemically append the desired unnatural amino acid directly to its tRNA (*20*). This occurs in two key steps (Figure 5). The unnatural amino acid is reacted with a DNA-RNA hybrid dinucleotide, dCA, to ensure its installation at a translationally competent hydroxyl on the terminal nucleotide. The amino acyl dCA is then enzymatically ligated to a 74mer RNA that has been *in vitro* transcribed, generating the full-length tRNA. This approach results in the creation of a stoichiometric reagent however, as the tRNA cannot be recharged with the unnatural amino acid in the cell, unlike its endogenous counterparts. This results in significantly lower expression of the unnatural amino acid containing protein.

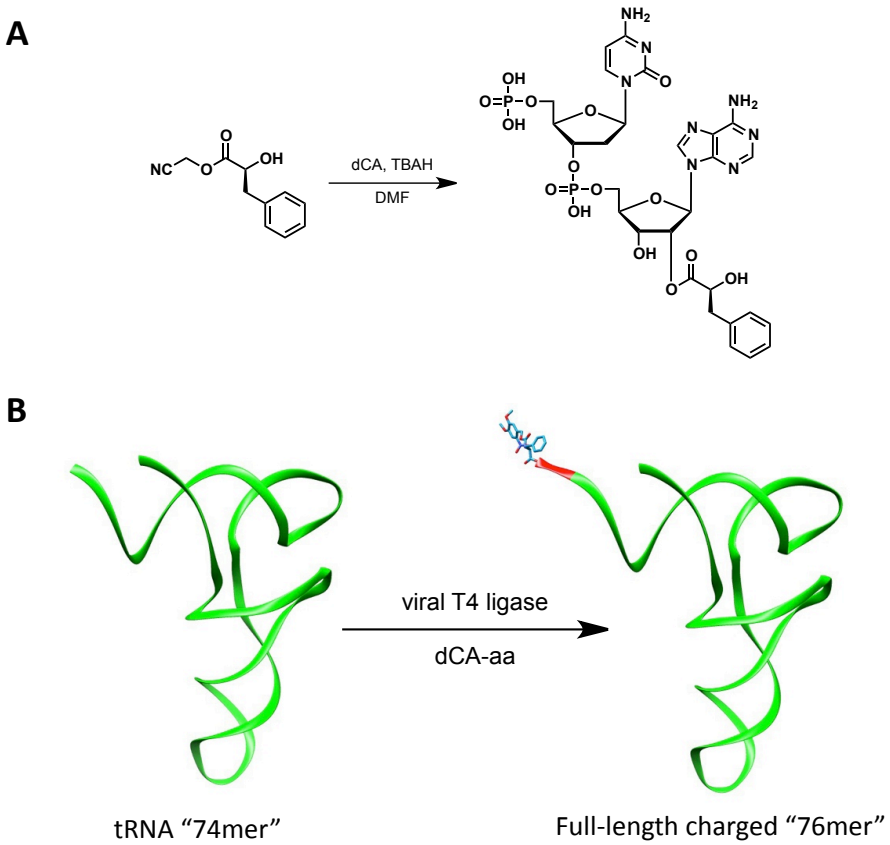

Figure 1.5 Direct chemical amino acylation of tRNA. (A) Reaction of protected amino acid with DNA/RNA hybrid dinucleotide dCA. (B) Enzymatic ligation of amino acyl dCA to *in vitro* transcribed 74mer to form full length amino acyl tRNA.

The next challenge is to install the amino acid site selectively. To accomplish this, nonsense suppression methodology is utilized (Figure 6) (*20*). This involves the repurposing of one of the three stop or nonsense codons, typically TAG. Normally upon reaching a stop codon, the ribosome stalls until a release factor protein liberates the amino acyl chain from the tRNA on the penultimate codon. If the unnatural amino acid-bearing, engineered tRNA is given an anticodon that pairs with the stop codon however, it will suppress the nonsense codon and the unnatural amino acid will be added to the growing amino acyl chain. This process will occur in competition with the endogenous

release factor though, further lowering expected yields of the unnatural amino acid containing protein.

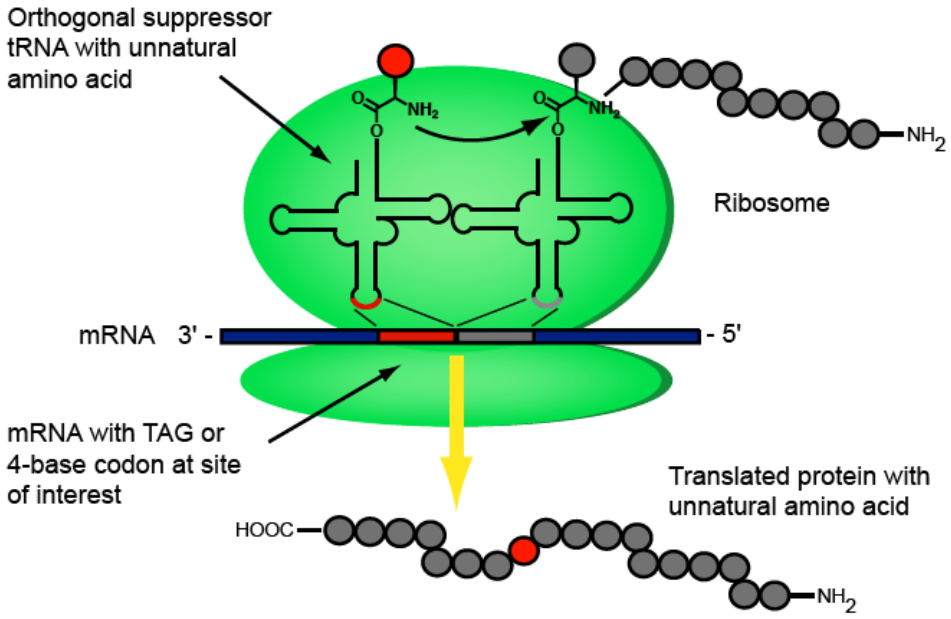

Figure 1.6 Nonsense suppression methodology.

The final challenge is ensuring the amino acid itself is capable of successfully passing through the ribosome and being added to the growing amino acyl chain. Thankfully, the ribosome is relatively blind to the properties of the amino acid and places limits only on especially bulky side chains. Using this methodology, a vast collection of unnatural amino acids have been successfully incorporated (Figure 7).

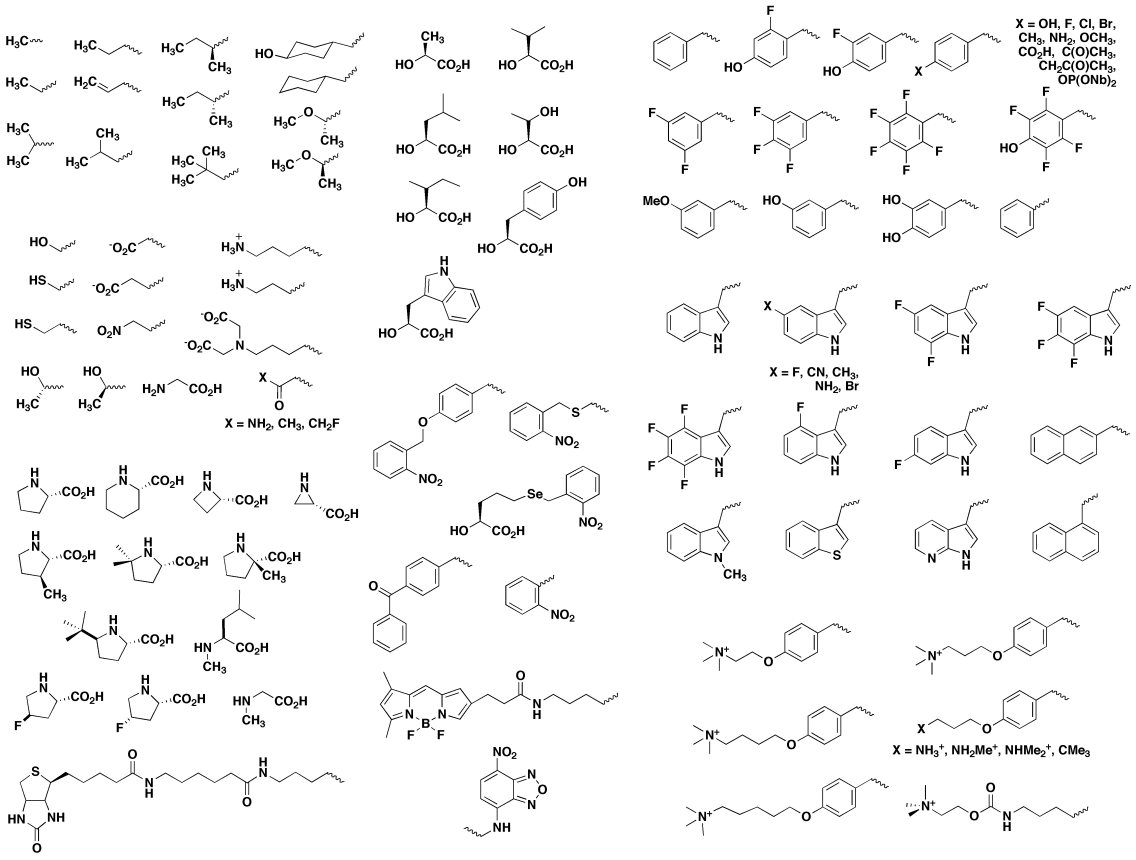

Figure 1.7 Unnatural amino acids successfully incorporated into proteins by direct chemical acylation of tRNA via nonsense suppression metholodology in *X. laevis* oocytes.

1.4 Methods for Detecting Functional Perturbations

1.4.1 Electrophysiology

As unnatural amino acid mutagenesis is an inefficient process, highly sensitive assays for assessing function are necessary. Thankfully, ligand-gated ion channels, by nature of their ability to generate electrical current in their activated state, afford just such an assay. Electrophysiology is an extremely sensitive and well-developed method that detects changes in electrical current. The version of electrophysiology employed here is two-electrode, voltage-clamped, whole cell electrophysiology.

In this method, reagents (mRNA only for conventional mutations, and both mRNA and aminoacyl tRNA for unnatural amino acid mutations) are micro-injected into *Xenopus laevis* oocytes (Figure 8A). Oocytes are a well precedented heterologous expression system for ion channels, in part because they are quite large (~1mm in diameter), allowing for easy delivery of reagents and easy access to the cytoplasm by penetrating electrodes (*21*).

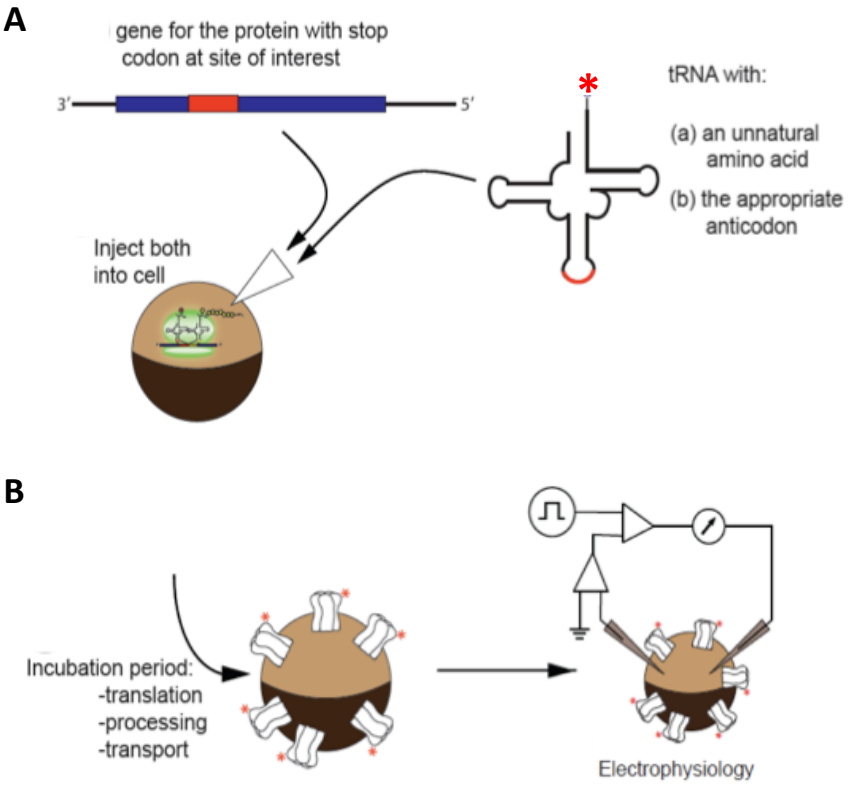

Figure 1.8 Heterologous expression in *X. laevis* oocytes for unnatural amino acid mutagenesis. (A) Microinjection of engineered amino acyl tRNA and stop codon containing mRNA into the oocyte. (B) Expression of protein containing mutation of interest and assaying of function by electrophysiology.

After sufficient time for the oocyte to translate, process, and assemble the receptor on the plasma membrane (usually 24–72 hours), the oocytes are impaled with two electrodes (Figure 8B). These are used to hold or clamp the cell at a specific voltage

compared to an external reference electrode. When activating ligands, called agonists, are applied to the cell, ions flow through the open pores of the activated receptors and a change in current necessary to maintain constant voltage is detected.

As higher concentrations of agonist are applied, a greater percentage of the total receptors on the oocyte is activated (Figure 9A). This results in increasing amounts of current until the receptors reach a saturating concentration at which maximal channel opening is achieved. From these data, a dose-response relationship can be plotted (Figure 9B). By fitting this relationship to the Hill equation, several important properties of the receptor can be obtained.

The EC_{50} is the concentration of agonist at which half maximal receptor activation occurs. Mutations that disrupt the ability of the receptor to activate result in a reduced sensitivity to the agonist. Thus, a loss of function mutation results in an increase in EC_{50} (Figure 9B). Conversely, mutations that improve channel function result in a decrease in EC_{50}. The Hill equation also provides a Hill coefficient that is a measure of receptor cooperativity. This measure provides some insight into the number of ligand binding sites required for efficient receptor activation.

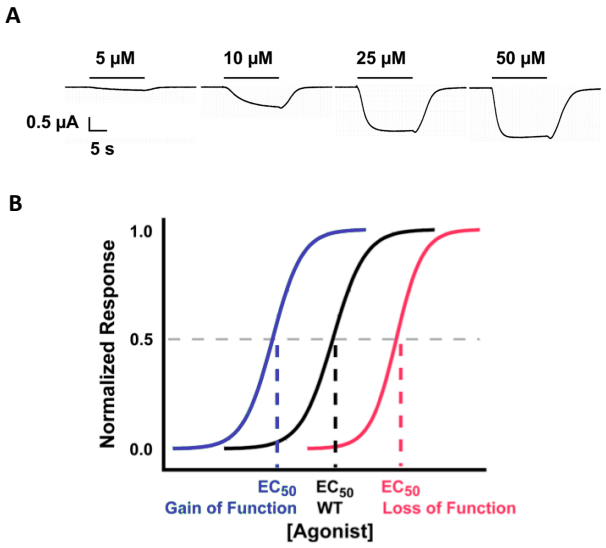

Figure 1.9 Agonist dose-response curves. (A) Increasing current in response to increasing concentrations of agonist observed by electrophysiology. (B) Dose-response plot fit to the Hill equation showing the effect of gain and loss of function mutations.

Cys-loop receptors are often capable of being activated by many ligands. However, not all of these ligands are equally capable of triggering the conformational change that links ligand binding with channel opening. Thus, two agonists, each at its saturating concentration or I_{max}, acting on the same number of receptors, may result in different absolute changes in current (Figure 10). This difference is reflected in the relative efficacy (R_{max} or ε). This measure is a ratio of the maximal currents elicited by an agonist with respect to that of the endogenous agonist. Ligands that produce roughly the same current are called full agonists, those that produce less are partial agonists, and those that produce more are super agonists.

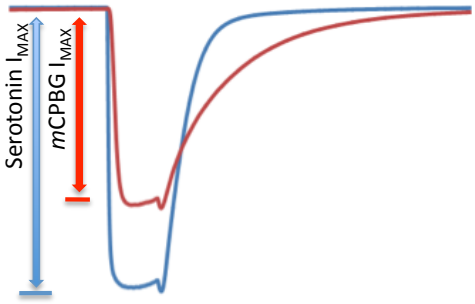

Figure 1.10 Electrophysiology traces showing maximal currents for the endogenous agonist serotonin and and the partial agonist mCPBG at the 5-HT_3A receptor.

It is also possible to study ligands that deactivate ion channels, or antagonists. As electrophysiology is only sensitive to the open state, antagonist activity is measured in the presence of agonists. Increasing amounts of antagonist are added to a constant amount of agonist and current drops from the stable initial level observed in the absence of antagonist down to levels indistinguishable from baseline noise (Figure 11A). A dose-response relationship from this experiment can also be plotted and fit to the Hill equation, yielding a measure called the IC_{50} (Figure 11B). This corresponds to the concentration of antagonist that produces half maximal receptor deactivation. As with the EC_{50}, mutations that change the IC_{50} reflect changes in the sensitivity of the receptor to the ligand.

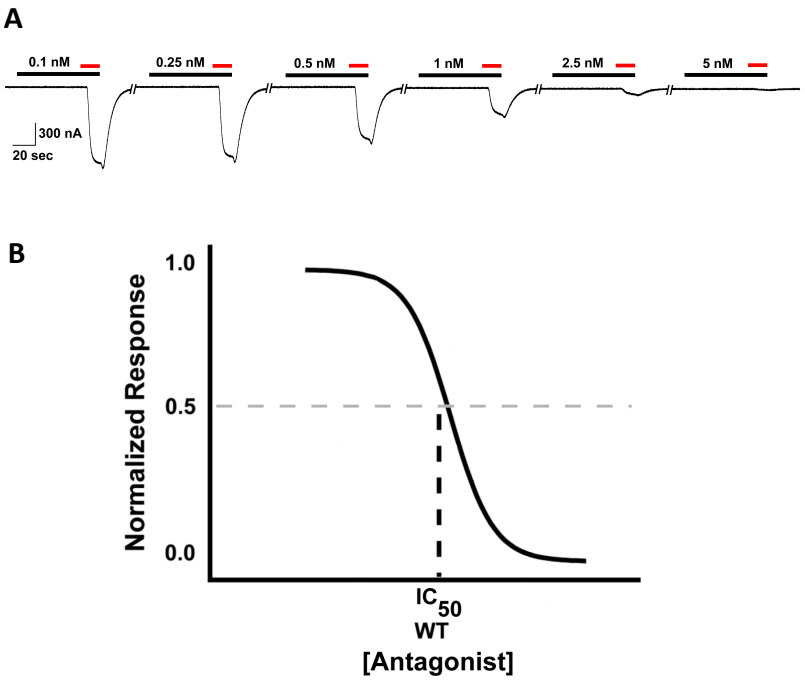

Figure 1.11 Antagonist dose-response curves. (A) Electrophysiology traces showing decreasing response to constant agonist as increasing antagonist is applied. (B) Dose-response plot fit to the Hill equation.

1.4.2 Fluorescence Microscopy

The discovery and optimization of genetically-encodable fluorescent proteins that are modular, cover a wide spectral range, and require no cofactor has transformed the study of molecular biology in the past twenty years. Fusions of fluorescent proteins and proteins of interest have allowed not only for the study of protein expression and sub-cellular localization, but also of dynamic changes in protein conformation and oligomeric state.

These latter findings are made possible by the study of Förster's resonance energy transfer or FRET. FRET is the process by which a fluorophore, when excited, may undergo energy transfer to the excited state of another fluorophore from which it may fluoresce as it relaxes to the ground state. This process requires spectral overlap between

the emission profile of the donor fluorophore and the excitation profile of the acceptor fluorophore and is highly dependent on the distance between the two fluorophores, with a $1/r^6$ dependence. Thus FRET efficiency has been widely used as a molecular ruler.

While there are several methods for determining FRET efficiency, the method used here is called donor recovery after acceptor photobleaching, or DRAP. This method relies on the ability of destroy a fluorophore by exposing it to high intensity light at its excitatory wavelengths, and on the insight that every photon that undergoes FRET and emits from the acceptor is a photon that does not emit from the donor. Thus, on the population level, one can compare the donor fluorescence emission levels before and after destroying all the acceptors, and donors that undergo FRET more efficiently will show a greater photobleaching dependent increase in donor fluorescent emission.

This approach has many drawbacks. Fluorescent proteins are often quite large compared to the motions one wishes to observe, complicating or precluding their application to many interesting experimental questions (*22*). The DRAP method is also by its nature an ensemble methodology and incompatible with time-resolved systems. Thus the above methodology is best suited for studying relatively gross and static characteristics of proteins, such as stoichiometry.

1.5 Summary of Dissertation Work

This dissertation describes studies on the structure of serotonin type 3 (5-HT_3) receptors and how two agonists, serotonin (5-HT) and *m*-chlorophenyl biguanide (mCPBG), act on that structure. It also details efforts to expand the application of unnatural amino acid mutagenesis to a family of proteins called transcription factors.

Chapter 2 describes a study seeking to identify differences in the sensitivity of 5-HT and mCPBG to binding site organization. Through conventional and unnatural amino acid mutagenesis, we identify a structural element of the 5-HT_3A binding site that orients critical side chains for binding interactions with serotonin. We find that mCPBG behaves differently than 5-HT and, unlike 5-HT, lacks a cation-π interaction at TrpB.

Chapter 3 describes a study that utilizes fluorescent protein fusions of the 5-HT_3A and 5-HT_3B subunits to determine the stoichiometry of the heteromeric 5-HT_3AB receptor. Multiple FRET and other fluorescence experiments support an A_3B_2 stoichiometry at the plasma membrane with a likely subunit order of A-A-B-A-B.

Chapter 4 examines the actions of 5-HT and mCPBG at the heteromeric 5-HT_3AB receptor. Using conventional and unnatural amino acid mutagenesis, we find that while 5-HT acts only at the A-A binding site, mCPBG binds and activates the receptor at all five binding sites. We also show that mCPBG is capable of modulating the response of 5-HT from B subunit containing binding sites.

Chapter 5 describes efforts to expand the application of unnatural amino acid mutagenesis to a class of proteins called transcription factors. We have attempted to develop quantitative reverse-transcribed PCR experiments for the detection mRNA products of transcription factor activation in *Xenopus laevis* oocytes.

1.6 References

1. Green, T., Heinemann, S. F., and Gusella, J. F. (1998) Molecular neurobiology and genetics: investigation of neural function and dysfunction, *Neuron 20*, 427-444.
2. Gotti, C., Zoli, M., and Clementi, F. (2006) Brain nicotinic acetylcholine receptors: native subtypes and their relevance, *Trends Pharmacol Sci 27*, 482-491.

3. Jensen, A. A., Frolund, B., Liljefors, T., and Krogsgaard-Larsen, P. (2005) Neuronal nicotinic acetylcholine receptors: structural revelations, target identifications, and therapeutic inspirations, *J Med Chem 48*, 4705-4745.
4. Thompson, A. J., and Lummis, S. C. (2007) The 5-HT3 receptor as a therapeutic target, *Expert Opin Ther Targets 11*, 527-540.
5. Thompson, A. J., Lester, H. A., and Lummis, S. C. (2010) The structural basis of function in Cys-loop receptors, *Q Rev Biophys 43*, 449-499.
6. Millar, N. S. (2003) Assembly and subunit diversity of nicotinic acetylcholine receptors, *Biochem Soc Trans 31*, 869-874.
7. Xiu, X., Puskar, N. L., Shanata, J. A., Lester, H. A., and Dougherty, D. A. (2009) Nicotine binding to brain receptors requires a strong cation-pi interaction, *Nature 458*, 534-537.
8. Tavares Xda, S., Blum, A. P., Nakamura, D. T., Puskar, N. L., Shanata, J. A., Lester, H. A., and Dougherty, D. A. (2012) Variations in binding among several agonists at two stoichiometries of the neuronal, alpha4beta2 nicotinic receptor, *J Am Chem Soc 134*, 11474-11480.
9. Lester, H. A., Xiao, C., Srinivasan, R., Son, C. D., Miwa, J., Pantoja, R., Banghart, M. R., Dougherty, D. A., Goate, A. M., and Wang, J. C. (2009) Nicotine is a selective pharmacological chaperone of acetylcholine receptor number and stoichiometry. Implications for drug discovery, *Aaps J 11*, 167-177.
10. Nys, M., Kesters, D., and Ulens, C. (2013) Structural insights into Cys-loop receptor function and ligand recognition, *Biochem Pharmacol 86*, 1042-1053.
11. Rucktooa, P., Smit, A. B., and Sixma, T. K. (2009) Insight in nAChR subtype selectivity from AChBP crystal structures, *Biochem Pharmacol 78*, 777-787.
12. Van Arnam, E. B., and Dougherty, D. A. (2014) Functional Probes of Drug-Receptor Interactions Implicated by Structural Studies: Cys-Loop Receptors Provide a Fertile Testing Ground, *J Med Chem*.
13. Unwin, N. (2005) Refined structure of the nicotinic acetylcholine receptor at 4A resolution, *J Mol Biol 346*, 967-989.
14. Hibbs, R. E., and Gouaux, E. (2011) Principles of activation and permeation in an anion-selective Cys-loop receptor, *Nature 474*, 54-60.
15. Zhong, W., Gallivan, J. P., Zhang, Y., Li, L., Lester, H. A., and Dougherty, D. A. (1998) From ab initio quantum mechanics to molecular neurobiology: a cation-pi binding site in the nicotinic receptor, *Proc Natl Acad Sci U S A 95*, 12088-12093.
16. Chin, J. W. (2012) Molecular biology. Reprogramming the genetic code, *Science 336*, 428-429.
17. Rodriguez, E. A., Lester, H. A., and Dougherty, D. A. (2007) Improved amber and opal suppressor tRNAs for incorporation of unnatural amino acids in vivo. Part 1: minimizing misacylation, *Rna 13*, 1703-1714.
18. Rodriguez, E. A., Lester, H. A., and Dougherty, D. A. (2007) Improved amber and opal suppressor tRNAs for incorporation of unnatural amino acids in vivo. Part 2: evaluating suppression efficiency, *Rna 13*, 1715-1722.
19. Wang, L., Xie, J., and Schultz, P. G. (2006) Expanding the genetic code, *Annu Rev Biophys Biomol Struct 35*, 225-249.
20. Nowak, M. W., Gallivan, J. P., Silverman, S. K., Labarca, C. G., Dougherty, D. A., and Lester, H. A. (1998) In vivo incorporation of unnatural amino acids into

ion channels in Xenopus oocyte expression system, *Methods Enzymol 293*, 504-529.

21. Millar, N. S. (2009) A review of experimental techniques used for the heterologous expression of nicotinic acetylcholine receptors, *Biochem Pharmacol 78*, 766-776.
22. Shaner, N. C., Steinbach, P. A., and Tsien, R. Y. (2005) A guide to choosing fluorescent proteins, *Nat Methods 2*, 905-909.

Chapter 2

A Coupled Array of Noncovalent Interactions Impacts the Function of the 5-HT_3A Receptor in an Agonist-Specific Way*

2.1 ABSTRACT

The serotonin type 3A (5-HT_3A) receptor is a Cys-loop (pentameric) neurotransmitter-gated ion channel found in the central and peripheral nervous systems and implicated in numerous diseases. In previous studies with the endogenous agonist serotonin, we identified two interactions critical for receptor function: a cation-π interaction with W183 in loop B (TrpB) and a hydrogen bond to E129 in loop A. Here we employ mutant cycle analyses utilizing conventional and unnatural amino acid mutagenesis to demonstrate that a third residue, D124 of loop A, forms two functionally important hydrogen bonds to the backbone of loop B. We also show that these three interactions, the cation-π interaction, the backbone hydrogen bonds, and the E129 hydrogen bond, are tightly coupled to each other, suggesting that they function as a single unit. We also identify key functional differences between serotonin and the competitive partial agonist *m*-chlorophenyl biguanide (mCPBG) at these residues. mCPBG displays

---

* *This chapter is adapted with permission from:* Miles, T. F.; Bower, K. S.; Lester, H. A.; Dougherty, D. A. A Coupled Array of Noncovalent Interactions Impacts the Function of the 5-HT_3A Serotonin Receptor in an Agonist-Specific Way. *ACS Chem. Neurosci.* **2012**; 3: 753-760. © American Chemical Society. *This work was done in collaboration with Dr. Kiowa Bower, who collected the data concerning the action of mCPBG at W183 in the 5-HT_3A receptor.*

no cation-π at TrpB and extreme sensitivity to the positioning of E129, on which it is reliant for initiation of channel gating.

2.2 INTRODUCTION

The serotonin type 3 receptor (5-HT_3) is a Cys-loop (pentameric) neurotransmitter-gated ion channel whose activation elicits fast excitatory responses. (1, 2) The 5-HT_3 receptor is expressed in both the central and peripheral nervous systems and is known to be involved in multiple psychiatric and neurological disorders. (3) Five distinct subunits of the 5-HT_3 receptor have been identified, (4) but only the A subunit forms functional homomeric receptors. These subunits, consisting of a large N-terminal extracellular domain, four transmembrane helices (M1–4), and a large intracellular loop (M3–M4), arrange into a symmetrical pentamer around a central pore.

As with other pentameric receptors, the ligand binding domain is located at the interface between the extracellular domains of two adjacent subunits. More specifically, the binding site is composed of six loops from both the principle (A–C) and complementary (D–F) faces. Agonist binding leads to an opening of the channel gate at the M2 helix, over 60 Å distant.

In previous studies of the 5-HT_3A receptor, we identified critical roles for two residues. W183 on loop B (termed TrpB) makes a cation−π interaction to serotonin, (5) playing the same role as the aligning residue in most nicotinic acetylcholine receptors (nAChR). (6-8) E129 on loop A of the 5-HT_3 receptor makes a hydrogen bond that is critical to receptor function. (9) We proposed that the hydrogen bond occurs with the OH of the agonist, serotonin. The aligning residue of nAChRs is Y93 (TyrA) (Figure 2.1).

	Loop A										Loop B				
	121									130	181				185
Mouse 5-HT_3A	W	V	P	D	I	L	I	N	E	F	T	S	W	L	H
Human 5-HT_3A	W	V	P	D	I	L	I	N	E	F	T	S	W	L	H
Torpedo nACh α1	W	L	P	D	L	V	L	–	Y	N	G	I	W	T	Y
Human nACh α7	W	K	P	D	I	L	L	–	Y	N	G	S	W	S	Y
Lymnaea AChBP	W	V	P	D	L	A	A	–	Y	N	G	S	W	T	H

Figure 2.1 Alignment of loops A and B from the mouse and human 5-HT_3A subunits, the *Torpedo* nACh α1 subunit, the human nACh α7 subunit, and the *Lymnaea* AChBP. Residues contributing significant interactions through their side chains are shaded in gray. The numbering is that of the mouse 5-HT_3A subunit.

In the present work, we evaluate the role of a second residue on loop A that is very highly conserved across the entire Cys-loop family of neurotransmitter-gated ion channels, D124 of the 5-HT_3A receptor. In the nAChR family, the aligning residue, D89, makes a number of hydrogen bonds to loop B, positioning the key TrpB residue (10-12). This role was suggested by crystal structures of acetylcholine binding proteins (AChBP) and confirmed by extensive mutagenesis studies. We also find interesting differences between the 5-HT_3 receptor and the nAChR with respect to the role of D124. Mutant cycle analyses reveal a collection of interactions in which hydrogen bonds between D124 and loop B serve to position W183, W183 makes the key cation−π interaction, and E129 makes binding interactions with serotonin (Figure 2.2). Triple mutant cycle analysis shows that these three interactions are tightly coupled to each other, such that disrupting any one interaction destroys the coupling between the other two. In addition, we find that the natural agonist serotonin and the potent orthosteric agonist mCPBG are affected differently by mutations in this region of the receptor.

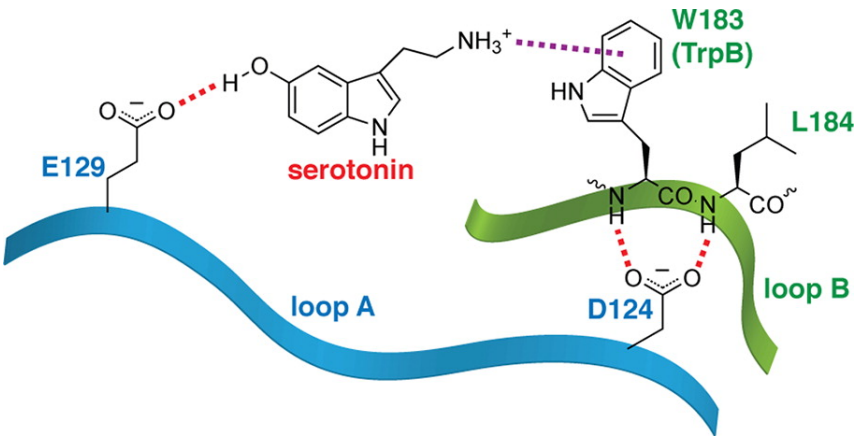

Figure 2.2 Schematic of the collection of interactions being probed here. Dashed red lines are hydrogen bonds. Purple dashed line is a cation-π interaction.

2.3 RESULTS AND DISCUSSION

2.3.1 Serotonin

The 5-HT_3A receptor differs from other members of the Cys-loop (pentameric) neurotransmitter-gated ion channel family in that one of the members of the canonical binding site aromatic box (TyrA) is missing (Figure 2.1). Alignment of loop A across the Cys-loop family is challenging, (9) but our previous functional studies suggested that the side chain of E129 points in toward the agonist binding site, making it the residue that corresponds to TyrA. In particular, we suggested that E129 forms a critical hydrogen bond with the 5-hydroxyl of serotonin. We have now further probed the role of E129 and established a collection of binding interactions that impact receptor function.

Here we propose that another residue on loop A, D124, forms hydrogen bonds with both of the backbone nitrogens flanking the TrpB side chain (Figure 2.2). Based on the AChBP structures and mutagenesis studies of the nAChR, loop A of the 5-HT_3A receptor in the vicinity of D124 lies "behind" loop B, such that the D124 side chain can hydrogen bond to the backbone of loop B in the vicinity of W183. The functional

significance of this conserved aspartate has long been appreciated, in that the D-to-N mutation very significantly impedes receptor function in Cys-loop receptors. (11) Not shown in Figure 2.2 is Ser182, the side chain of which could also contribute to this hydrogen bond network. However, as in studies of the nAChR, (12) we find that the S182A mutation has a negligible effect on receptor function (Table 2.1), and so we will not further consider hydrogen bonding interactions involving the side chain of S182.

agonist	mutation[b]	EC_{50} (μM)	fold shift	Hill	R_{max}	N
5-HT	WT	1.9 ± 0.1		2.7 ± 0.3		7
	W183Wah	27 ± 1	14	2.4 ± 0.3		6
	L184Lah	13 ± 1	6	2.8 ± 0.2		23
	E129Q	88 ± 7	46	1.5 ± 0.1		17
	E129D	2.5 ± 0.3	1	1.6 ± 0.2		7
	S182A	2.6 ± 0.1	1.4	2.3 ± 0.2		7
	D124N	140 ± 10	70	2.6 ± 0.2		6
	E129Q L184Lah	46 ± 10	24	1.5 ± 0.4		9
	E129Q W183Wah	80 ± 10	41	1.8 ± 0.3		7
	D124N L184Lah	61 ± 2	31	2.5 ± 0.1		6
	D124N W183Wah	160 ± 10	85	4.1 ± 0.4		6
	D124N E129Q	490 ± 60	255	3.2 ± 1.0		6
	L184Lah E129Q D124N	230 ± 40	118	3.1 ± 1.3		8
	T6′S	1.8 ± 0.2	0.9	2.3 ± 0.3		6
	T6′S E129Q	6.0 ± 0.5	3	1.4 ± 0.1		6
5-FT	WT	18 ± 1		2.2 ± 0.2	0.60 ± 0.03	6
	W183Wah	*c*				8
	L184Lah	36 ± 4	2	3.2 ± 0.9	0.03 ± 0.01	10
	E129Q	*c*				8
mCPBG	WT	0.61 ± 0.03		2.2 ± 0.2	0.73 ± 0.02	7
	W183Wah	*c*				8
	L184Lah	*c*				8
	E129Q	*c*				8
	E129D	0.12 ± 0.01	0.2	1.1 ± 0.1	0.10 ± 0.01	11
	S182A	0.15 ± 0.01	0.2	3.0 ± 0.4	0.74 ± 0.04	7
	D124N	15 ± 1	24	3.4 ± 0.3	1.09 ± 0.07	6
	D124N L184Lah	55 ± 2	90	3.5 ± 0.3	0.87 ± 0.04	6
	D124N W183Wah	*c*				8
	W183−4-F-W	0.47 ± 0.03	0.8	1.5 ± 0.1	0.44 ± 0.03	6
	W183−4,7-F_2-W	0.34 ± 0.03	0.6	1.4 ± 0.1	*d*	19
	W183−5−F-W	5.8 ± 0.1	10	2.1 ± 0.1	0.11 ± 0.01	8
	W183−5,7-F_2−W	2.8 ± 0.1	5	1.9 ± 0.1	0.38 ± 0.03	8
	W183−5,6,7-F_3-W	9.7 ± 0.3	16	2.4 ± 0.1	0.57 ± 0.03	11
	W183−4,5,6,7-F_4−W	7.3 ± 0.3	12	2.1 ± 0.2	0.59 ± 0.01	8
	W183−5-Br-W	20 ± 2	33	2.5 ± 0.4	0.06 ± 0.01	8
mCPG	WT	0.61 ± 0.03		2.2 ± 0.2	0.73 ± 0.02	7
	E129Q	*c*				8
	E129D	*c*				8
	W183−4-F-W	2.7 ± 0.4	0.8	2.4 ± 0.8	0.23 ± 0.03	7
	W183−4,7-F_2-W	*e*				8
	W183−5-F-W	13 ± 2	4	2.2 ± 0.4	0.09 ± 0.01	7
	W183−5-Br-W	42 ± 3.4	12	1.9 ± 0.3	0.02 ± 0.01	8

Table 2.1 Agonist dose-response data. All values are reported as mean ± SEM. Fold shift >1 indicates loss of function; fold shift < 1 indicates gain of function. *b*, Xah = α-hydroxy X. *c*, No response (I_{max} < 20 nA). *d*, Not determined. *e*, Small response (I_{max} < 100 nA).

The key potential hydrogen bonding interactions involving D124 are to a pair of backbone NHs on loop B, contributed by W183 and L184. Using nonsense suppression methodology, (13, 14) we can perturb the loop B backbone by replacing W183 and L184 with their corresponding α-hydroxy acids (Wah and Lah; ah standing for α-hydroxy) (Figure 2.3). This subtle mutation deletes the hydrogen bond donor but leaves nearly all other aspects of the receptor intact. The functional effects of these mutations are determined by constructing dose-response curves of the agonist-induced currents (Figure 2.4).

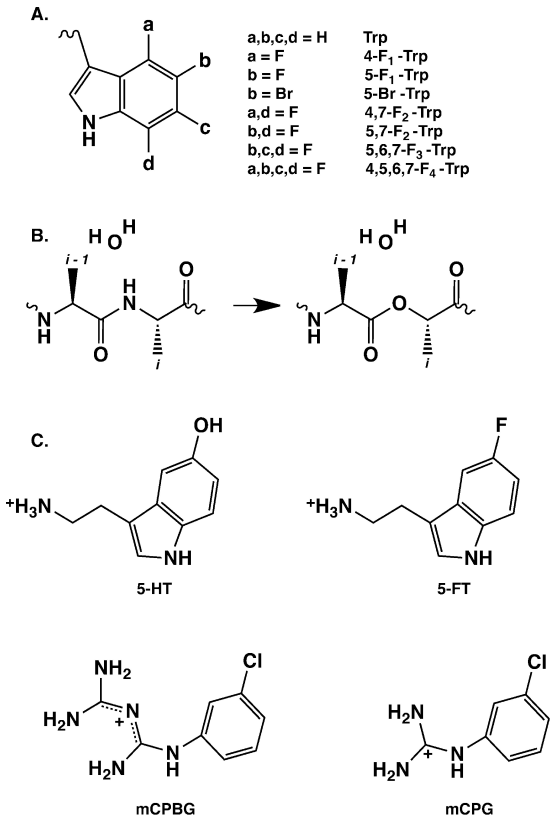

Figure 2.3 (A) Structures of unnatural amino acids considered here. Unless specified, a, b, c, and d are H. (B) The α-hydroxy acid strategy for probing backbone hydrogen bonding interactions. (C) Structures of agonists considered here.

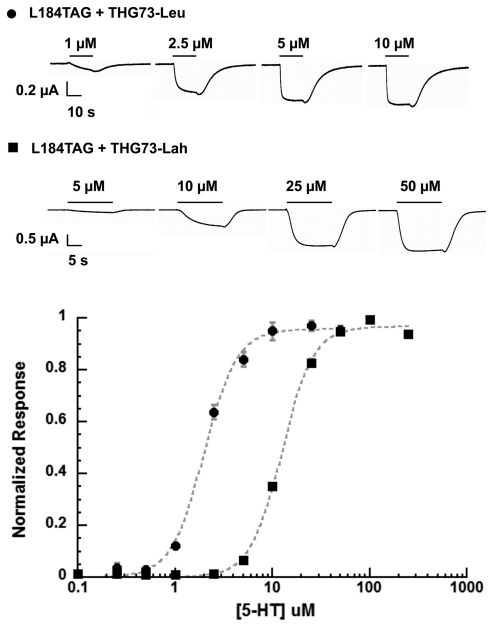

Figure 2.4 Examples of responses for 5-HT on receptors in which a nonsense mutation (TAG) at L184 is suppressed by THG73 tRNA bearing either leucine (wild-type recovery) or α-hydroxy leucine expressed in *Xenopus* oocytes and their corresponding concentration–response curves. Circles correspond to L184TAG + THG73-Leu; squares correspond to L184TAG + THG73-Lah. Each data point represents the mean ± SEM (n = 7–23).

As shown in Figure 2.5 and Table 2.1, both backbone mutations in loop B cause partial loss of function (rise in EC_{50}) with serotonin as agonist. The magnitudes of the perturbations are similar for the two backbone mutations, but they are markedly less than what is seen for the D124N mutation. It is interesting that although these hydrogen bonding interactions were first highlighted in structures of the acetylcholine binding protein (AChBP), comparable backbone mutations of the nAChR did not have strong effects on receptor function. (12)

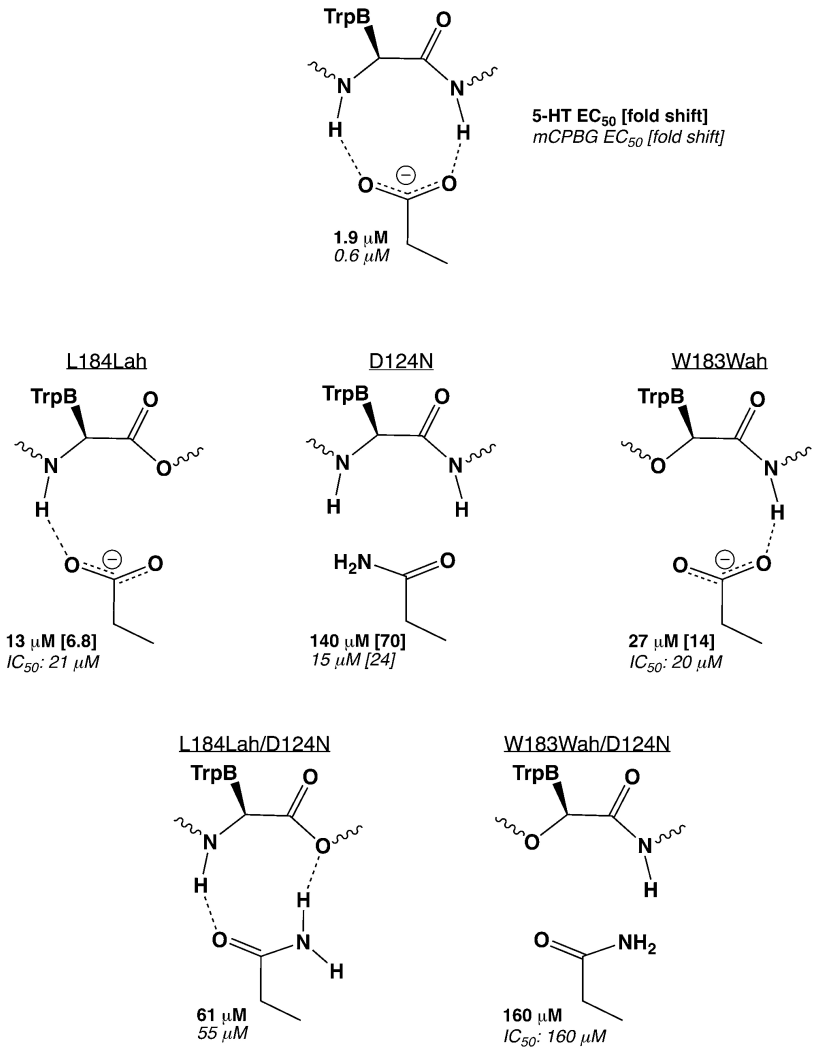

Figure 2.5 Results of select mutagenesis studies.

To establish that the backbone mutations are indeed influencing a hydrogen bond to D124, we performed double mutant cycle analyses (15, 16) with the D124N mutation. We consider a $\Delta\Delta G° > 0.65$ kcal/mol (i.e., a 3-fold deviation from additivity) to represent a meaningful interaction energy. For both the W183Wah and the L184Lah mutations, a significant interaction energy is seen when paired with the D124N mutation (Table 2.2). The magnitude of the interaction is consistent with a hydrogen bond.

mutant pair[a]	background	Ω^b	$\Delta\Delta G°$ (kcal/mol)
W183Wah, D124N		0.080	1.5
W183Wah, E129Q		0.064	1.6
L184Lah, D124N		0.064	1.6
L184Lah, D124N	E129Q	0.90	0.062
L184Lah, E129Q		0.076	1.5
L184Lah, E129Q	D124N	0.93	0.043
E129Q, D124N		0.076	1.5
E129Q, D124N	L184Lah	0.94	0.037
L184Lah, 5-HT/5-FT		0.29	0.73
E129Q, T6′S		0.072	1.6

Table 2.2 Serotonin mutant cycle analyses. *a*, Xah = α-hydroxy X. *b*, Coupling coefficient.

Because of the key role of TrpB (W183) in making a cation-π interaction to agonists, it seems reasonable to think of the loop A aspartate as positioning loop B through the hydrogen bonds just probed. However, given our earlier findings (9) of a key role for a second loop A residue (E129), we considered the reverse scenario: that loop B positions two key residues on loop A (Figure 2.2). If this were so, one expects that disruption of the hydrogen bonding interactions between D124 and W183/L184 would impact E129. We find that this is indeed the case. Both the W183Wah and the L184Lah

mutations are coupled via mutant cycle analysis to the E129Q mutation (Table 2.2), and the magnitude of the coupling is comparable to that measured for couplings to D124N.

These results implied a collection of interactions: the loop B backbone NHs interact with loop A via D124; this in turn positions E129 on loop A properly for interaction with the agonist OH, and the agonist protonated amine makes a cation-π interaction to W183 back on loop B (Figure 2.2). This suggested experiments that constitute a triple mutant cycle analysis, combining D124N, E129Q, and L184Lah (protein expression for W183Wah mutants was too low to consider triple mutant studies). Such an analysis is best described by a cube, as in Figure 2.6. The wild type is in the front lower left corner, and the triple mutant is in the back upper right corner. Each face of the cube is a double mutant cycle analysis. Both the front and back faces, for example, depict the D124N/L184Lah double mutant cycle, but in the background of the wild type or the E129Q mutant, respectively (i.e., all four corners of the back face contain the E129Q mutation). As noted above, $\Delta\Delta G$ for the front face is 1.6 kcal/mol. However, $\Delta\Delta G$ for the back face is 0.06 kcal/mol. That is, the coupling between D124N and L184Lah is completely absent if we include the E129Q mutation. The coupling between D124 and L184 (backbone) depends on the presence of the E129 side chain. The difference between the $\Delta\Delta G$ values for the front and back faces produces a $\Delta\Delta\Delta G$, the extent to which the three mutations all influence each other. In the present system, $\Delta\Delta\Delta G$ is 1.5 kcal/mol. The value for $\Delta\Delta\Delta G$ can also be obtained by subtracting $\Delta\Delta G$ values for the left and right faces or the top and bottom faces; the same $\Delta\Delta\Delta G$ value is always obtained. Interestingly, any double mutant cycle analysis that includes the wild-type receptor, the front, left, and bottom faces, shows a significant $\Delta\Delta G$ of 1.5 kcal/mol. However, the

remaining three faces, all of which have one of the three mutations present in all four corners, show $\Delta\Delta G$ values of 0. Having any one of the three mutations completely decouples the other two, suggesting a very tight interaction among the three.

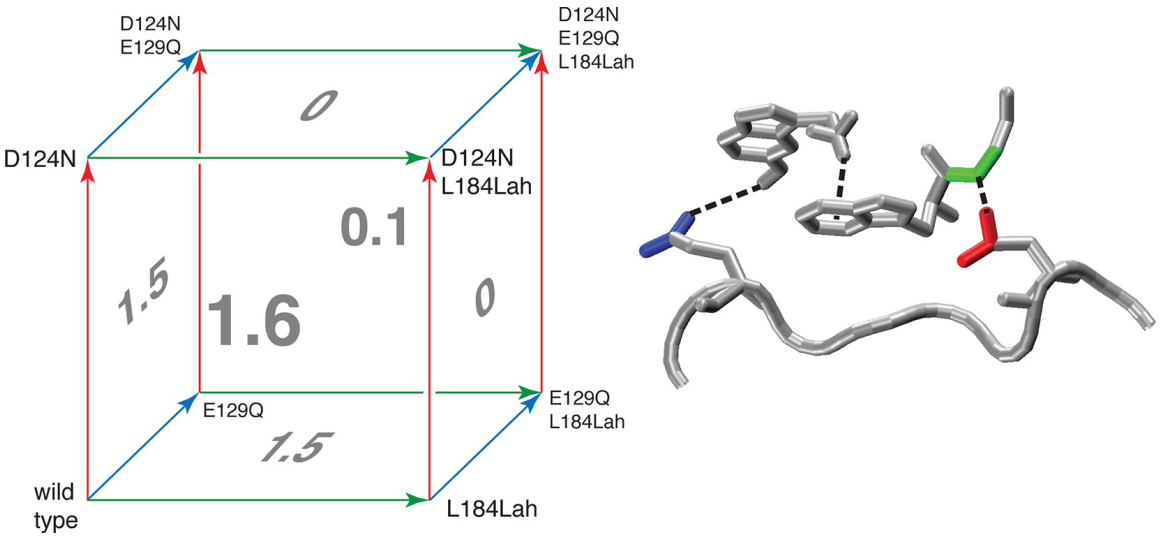

Figure 2.6 Triple mutant cycle analysis. $\Delta\Delta G$ values (kcal/mol) are given on each face of the cube. $\Delta\Delta\Delta G$ for the diagonal from lower left front to upper right back is 1.5 kcal/mol. The structural image is a simple docking of 5-HT into a previously described (9) homology model of the receptor and is for illustrative purposes only. See text for a full description and analysis.

If the proposed model of E129 making a hydrogen bond to the OH of serotonin is correct, we expect that mutations that influence E129 would impact this interaction. We previously showed that 5-FT (Figure 2.3) has a potency 10-fold lower than 5-HT and acts as a partial agonist with a relative efficacy (R_{max}) of 0.64. (17) Assuming 5-FT binds in essentially the same manner as serotonin, the F of 5-FT would be near the side chain of E129 but cannot make a hydrogen bond. The high relative efficacy of 5-FT compared with that of tryptamine (serotonin without the OH; R_{max} = 0.15) suggests that 5-FT retains a steric or electrostatic interaction at the 5 position that contributes to receptor function.

Interestingly, when we introduce the E129Q mutation, 5-FT becomes an antagonist, with an IC_{50} value comparable to its EC_{50} in the wild-type receptor (Table 2.3). As expected, given their strong coupling to E129, the W183Wah and L184Lah backbone mutations behave similarly, strongly disrupting the ability of 5-FT to gate the receptor. W183Wah converts 5-FT to a weak antagonist, while the efficacy of 5-FT relative to serotonin decreases to three percent in the background of L184Lah. This weak agonism allows consideration of serotonin/5-FT as one component of a double mutant cycle analysis. When the agonist pair is coupled to the L184Lah backbone mutation, the $\Delta\Delta G$ value (0.73 kcal/mol) is smaller than others we have seen but clearly meaningful, bolstering the interpretation that the backbone NHs and E129 are linked.

mutation[b]	antagonist	IC_{50} (μM)	Hill	N
L184Lah	mCPBG	21 ± 1	−2.1 ± 0.2	12
W183Wah	mCPBG	20 ± 1	−1.8 ± 0.1	7
	5-FT	140 ± 20	−1.6 ± 0.3	11
W183Wah D124N	mCPBG	160 ± 10	−2.6 ± 0.3	7
E129Q	mCPBG	0.28 ± 0.03	−1.6 ± 0.1	6
	mCPG	0.32 ± 0.08	−1.2 ± 0.3	7
	5-FT	8.6 ± 2.7	−0.8 ± 0.2	7
E129D	mCPG	0.0094 ± 0.0024	−0.9 ± 0.1	11

Table 2.3 Dose-response data for mutations in which the ligand is converted to an antagonist. All values are reported as mean and SEM. *b*, Xah = α-hydroxy X.

In the model that we are proposing (Figure 2.2), two of the interactions considered, the cation-π interaction to TrpB and the hydrogen bond between E129 and the OH of serotonin, involve direct binding between the receptor and the drug. Two others, the hydrogen bonds to the backbone of loop B, occur within the receptor itself. It

may be that these various interactions impact different aspects of the receptor activation process.

The metric we use to evaluate receptor function is EC_{50}, the effective concentration of agonist needed to induce half-maximal response. This is a functional measure of agonist potency. The actual process of activating the 5-HT_3A receptor and related molecules is complex, involving multiple equilibria reflecting drug binding to and coming off the receptor, conformational changes of the protein, and "gating" equilibria between the open and closed states of the channel. It is important to acknowledge the ambiguity that a change in EC_{50} could reflect a change in "binding" or a change in "gating". Certainly there is value in knowing which step(s) in the gating process is impacted by a particular mutation, but this requires much more detailed studies, typically at the single channel level; such studies are further complicated in the present case by the low single-channel conductance of the 5-HT_3A receptor. An alternative strategy would be to determine K_i values for various ligands at mutant receptors. The standard strategy for 5-HT_3 receptors is displacement of tritiated granisetron. However, it has been reported that various mutants at E129, including E129Q, show no binding of granisetron. (18) A further complication with the determination of binding constants is the large amount of receptor required, quantities greater than what can typically be produced with unnatural amino acid mutagenesis. In light of these limitations, we do not believe binding studies would be feasible on the most interesting of the mutants studied here.

An alternative way to evaluate the role a particular residue plays is through employing a different type of mutant cycle analysis. In previous studies of the nAChR, we have often introduced a mutation in the transmembrane domain, quite far from the

agonist binding site, that facilitates gating and thereby lowers EC_{50} in a general way (19, 20). Typically, such transmembrane mutations show simple additivity when paired with a second mutation in the agonist binding site ($\Delta\Delta G = 0$). However, meaningful coupling between the two sites can be observed when the agonist binding site mutation significantly impacts gating. We considered a similar strategy here, using a mutation in M2 termed T6′S (21), where 6′ denotes the sixth amino acid from the cytoplasmic end of the transmembrane helix. As noted earlier, the E129Q mutation is strongly perturbing, producing a high EC_{50} of 88 μM (46-fold shift from wild type) for serotonin (Table 2.1). With the addition of the T6′S mutation, EC_{50} drops 15-fold to 6.0 μM, following a pattern we have seen with other mutations of this sort. However, the same effect is not seen in the otherwise wild-type receptor; the T6′S single mutant shows an EC_{50} of 1.8 μM, indistinguishable from wild-type. Of course, this means that the T6′S and E129Q mutations are coupled, and a mutant cycle analysis gives a large $\Delta\Delta G$ of 1.6 kcal/mol (Table 2.2). Since the T6′S mutation presumably affects channel gating, the coupling seen here suggests that the proposed hydrogen bond between E129 and the 5-hydroxyl of serotonin contributes to the initiation of channel gating.

The observed lack of effect on EC_{50} upon introduction of the T6'S mutation to the wild type receptor strays from our original model for employing a long-range reporter of gating (Figure 2.7, A) (20). This simplified kinetic model for activation leads to an expression for EC_{50}, where A is the agonist; R_C and R_O denote the closed and open states of the receptor; k_1 and k_{-1} are forward and reverse rate constants for agonist binding; K_D is the dissociation constant for the agonist; and Θ is the gating equilibrium constant, given by the ratio of the channel opening rate, β, to the channel closing rate, α. At

regions of low Θ, the K_D is invariant to small changes in Θ. At higher (and more physiologically relevant) values of Θ, there is a linear relationship between K_D and Θ with negative slope. Thus, a reporter mutation that affects the gating equilibrium should display a marked gain of function by EC_{50}.

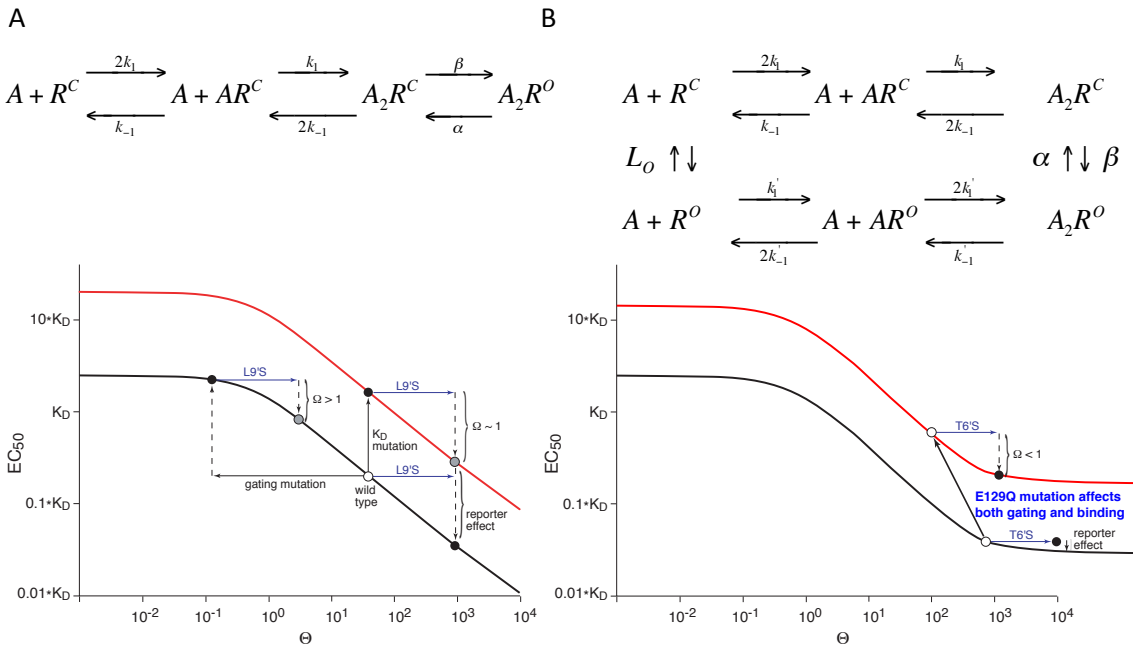

Figure 2.7 Models of receptor activation. (A) A simple receptor activation model and resultant relationship between EC_{50} and Θ. (B) A receptor activation model that includes agonist disassociation from open receptors and its resultant relationship between EC50 and Θ. In both panels the lines show the relationship between EC_{50} and Θ, with the red line corresponding to a larger K_D than the black line. For both plots, in the negative slope region changes in Θ produce significant changes in EC_{50}, as shown when the reporter effect is added to the wild-type receptor. However, when beginning with Θ in either plateau region, a much smaller shift in EC_{50} occurs for equivalent shifts in Θ. Figure adapted from Gleitsman, K.R. *et al.* (2009) *Biophys. J.* (20)

The EC_{50} of mutations that purely affect gating will slide along this function (black curve). Mutations that affect ligand binding directly however will result in a vertical shifting of the entire function (red curve). As the receptor would reside in the same horizontal region of the function in a purely binding mutation, the effect of the reporter will be purely additive. In contrast, a purely gating mutation may push the

receptor into the horizontal region where EC_{50} is invariant with respect to Θ, thereby leading to non-additivity and functional coupling. This model captures all necessary phenomena for application in numerous nicotinic receptors, however, it clearly fails to explain the current mutation in the 5-HT_3A receptor.

A slightly more complex (and naturalistic) model may be constructed, however, that accounts for the response of the T6'S mutant (Figure 2.7, B). When rates are included for the dissociation of ligand from open receptors without channel closure, a third region in the relationship between K_D and Θ emerges. At Θ of 10^3-10^4 the function again plateaus. The dynamic between binding and gating mutations and their (non-)additivity from the prior model, however, remain intact for other regions. Thus, if the serotonin receptor were to have a markedly higher Θ than typical for nicotinic receptors, a reporter mutation might access this region. While the low single channel conductance of the wild type 5-HT3A receptor precludes direct determination of Θ, recent studies using a high conductance variant have suggested that the 5-HT3A Θ does indeed lie within the predicted region of the high Θ plateau (22).

2.3.2 mCPBG

In addition to the endogenous ligand serotonin, the 5-HT_3A receptor is capable of being gated by many structurally diverse molecules, including the potent orthosteric agonist mCPBG. The biguanide mCPBG (Figure 2.3) (23) is an agonist at 5-HT_3 receptors with a potency comparable to that of serotonin and a relative efficacy of 0.74. The structures of 5-HT_3 and mCPBG are different enough that it seemed possible that the two might interact differently with the receptor. Along with a clearly different shape and size (Figure 2.8), mCPBG displays a weak and diffuse positive electrostatic potential

across its biguanide moiety compared with the primary amine of serotonin. The chlorine atom of mCPBG may provide some steric and electronegative interactions of the sort shown to be important for 5-FT gating but without the hydrogen bonding ability of the serotonin OH. We have probed all the mutations discussed above using mCPBG as the agonist, with intriguing results. As with serotonin, the D124N mutation produces marked loss of function.

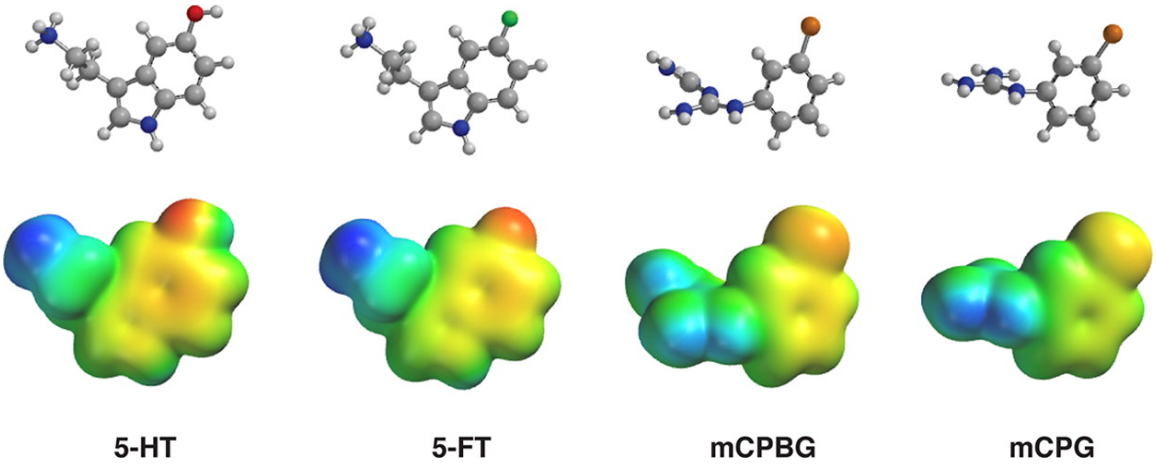

Figure 2.8 Structures and electrostatic potential surfaces for agonists considered here. Structures and surfaces were generated at the HF 3-21G* level. Electrostatic potentials are plotted with blue most positive and red least positive over a range from 0 to +750 kJ/mol. For the individual molecules, the electrostatic potentials span the following ranges: 5-HT, 13–733; 5-FT, 47–745; mCPBG, 116–636; mCPG, 152–698.

A surprising result is seen with both of the backbone mutations: when either W183Wah or L184Lah is introduced, mCPBG becomes an *antagonist*, with a comparable IC_{50} for both mutants (Table 2.3). Remarkably, restoring the hydrogen bond between L184 and D124 by pairing a D124N mutation with a backbone ester at L184 rescues the ability of mCPBG to gate the receptor, with significant loss-of-function but a relative efficacy of 0.87 (Figure 2.5). The W183Lah/D124N receptor still shows mCPBG as an

antagonist, with a further elevated IC_{50}, suggesting that the two backbone mutants may assume different geometries. We cannot do mutant cycle analyses on these systems, because one cannot meaningfully mix EC_{50} and IC_{50} values. The functional necessity of the hydrogen bonds linking loops A and B suggests that proper positioning of E129 is critical for mCPBG channel gating.

There are two other important ways in which mCPBG responds to mutations in a qualitatively distinct way from serotonin. First, the single mutation E129Q also converts mCPBG into an antagonist. Second, activation or block by mCPBG is not affected by fluorination of the W183 side chain, although serotonin and many agonists at other Cys-loop receptors are affected by such fluorination. (5) Substituting W183 with 5-F-Trp does produce a 10-fold increase in EC_{50}, but further fluorination does not produce the progressive increases in EC_{50} that are indicative of a cation-π interaction. This suggests that the 5-F-Trp effect could reflect a steric interaction, so we incorporated 4-F-Trp (Figure 2.3). This should produce an equivalent response if we are probing a cation-π interaction but a different response if steric interactions are important. The EC_{50} value for 4-F-Trp was close to wild-type. Increased fluorination, avoiding the 5 position, also resulted in near wild-type behavior. Greatly increasing the steric bulk at the 5 position via 5-Br-Trp led to a larger increase in EC_{50}, further supporting the idea of a steric interaction. This lack of fluorination effect could be due to a slight positioning difference, or it could be that the positive charge of mCPBG is so diffuse that it cannot pick up an energetically significant electrostatic interaction with the side chain of W183.

2.3.3 mCPG

The guanide analogue of mCPBG, termed mCPG (Figure 2.3, 2.8), is also an

agonist at 5-HT_3 receptors with an efficacy relative to serotonin of 0.31. Compared with mCPBG, the smaller mCPG contains a less delocalized positive electrostatic potential that would seemingly be more capable of forming a cation−π interaction. As with the biguanide however, mCPG shows wild-type behavior with the 4-F-Trp mutant at W183 and increasing losses of function as increasing steric bulk is introduced at the 5 position.

mCPG also forms a crucial interaction at E129. Mutation to glutamine results in the conversion of mCPG to an antagonist with an IC_{50} comparable to that of mCPBG. mCPG behaves uniquely in one regard, however (Table 2.3). E129D, which is only mildly disruptive for both serotonin and mCPBG, converts mCPG to an antagonist with an IC_{50} in the low nanomolar range, or 100-fold stronger inhibition than that observed for any other converted agonist.

2.3.4 Conclusions

Together these results suggest an interesting cycle of interactions that mutually reinforce each other. The essential role of TrpB for the natural agonist serotonin is clear, making a cation-π interaction to the positive charge of the neurotransmitter. Loop A residue D124 makes two hydrogen bonds to loop B that no doubt serve to position TrpB, an effect that has been seen in the nAChR. Also on loop A, E129 interacts strongly with serotonin, and we propose that this interaction is a hydrogen bond to the OH of the agonist. The interconnectedness of these interactions suggested in Figure 2.2 is supported by mutant cycle analyses. Several pairwise interactions are significant, and the triple mutant cycle analysis of Figure 2.6 is especially compelling. In particular, we find that mutating any one of the trio of residues D124, E129, or L184 (backbone) decouples the other two from each other. This suggests that this cyclic array acts as a single unit, with

an important functional role in the 5-HT_3 receptor.

We have also found that the structurally distinct agonist mCPBG displays some differences from serotonin. In particular, activating the 5-HT_3A receptor, the cation-π interaction to TrpB that is seen for serotonin and many other agonists at Cys-loop receptors is not present for mCPBG.

2.4 METHODS

2.4.1 Mutagenesis and Preparation of cRNA and Oocytes

Mutant 5-HT_3A receptor subunits, within the complete coding sequence for the mouse 5-HT_3A receptor subunit (accession number Q6J1J7), were cloned into pcDNA3.1 (Invitrogen, Abingdon, U.K.). Mutagenesis reactions were performed using the QuikChange mutagenesis kit (Stratagene) and confirmed by DNA sequencing. For unnatural mutagenesis, a stop codon, TAG, was made at the site of interest. Harvested stage V–VI *Xenopus* oocytes were washed in four changes of Ca^{2+}-free OR2 buffer (82.5 mM NaCl, 2 mM KCl, 1 mM $MgCl_2$, 5 mM HEPES, pH = 7.5), defolliculated in 1 mg/mL collagenase for approximately 1 h, washed again in four changes of Ca^{2+}-free OR2 and transferred to ND96 (96 mM NaCl, 2 mM KCl, 1.8 mM $CaCl_2$, 1 mM $MgCl_2$, 5 mM HEPES, pH = 7.5) supplemented with 0.28 mg/mL pyruvate, 0.05 mg/mL Gentamicin, and 0.12 mg/mL theophylline. Oocytes were injected with 5–25 ng of mRNA produced by *in vitro* transcription using the mMESSAGE mMACHINE kit (Ambion, Austin, Texas, USA) from cDNA subcloned into pGEMHE as previously described. (13) For unnatural amino acid experiments, a 1:1 mixture of mRNA and THG73 tRNA charged with an unnatural amino acid was injected (5–25 ng each).

Electrophysiological measurements were performed after incubation for 24–72 h postinjection at 18 °C. Wild-type recovery experiments (injection of tRNA appended to the natural amino acid) were performed to evaluate the fidelity of the unnatural suppression experiments. The 76-mer THG73 was also injected with mRNA as a control.

2.4.2 Synthesis of tRNA and dCA Amino Acids

This was as described previously. (13) Briefly, unnatural amino acids were chemically synthesized as nitroveratryloxycarbonyl (NVOC)-protected cyanomethyl esters and coupled to the dinucleotide dCA, which was then enzymatically ligated to 74-mer THG73 $tRNA_{CUA}$. Immediately prior to coinjection with cRNA, aminoacyl tRNA was deprotected by photolysis. Typically 5–10 ng of total cRNA was injected with 25–50 ng of tRNA-aa in a total volume of 50 nL. For a control, cRNA was injected with THG 76-mer tRNA (no unnatural amino acid attached).

2.4.3 Characterization of Mutant Receptors

Agonist-induced currents were recorded at 22–25 °C from individual oocytes using the OpusXpress system (Molecular Devices Axon Instruments, Union City, CA). 5-HT, *m*-chlorophenylbiguanide (mCPBG), *m*-chlorophenylguanide (mCPG), and 5-fluorotryptamine (5-FT) (Sigma) were stored as 25 mM aliquots at −20 °C, diluted in Ca-free ND96 buffer (96 mM NaCl, 2 mM KCl, 1 mM $MgCl_2$, 5 mM HEPES, pH = 7.5) and delivered to cells via the automated perfusion system of the OpusXpress. Glass microelectrodes were backfilled with 3 M KCl and had a resistance of 1 MΩ. The holding potential was −60 mV. Agonist doses in Ca^{2+}-free ND96 were applied for 15 s followed by a 116 s wash with the running buffer. Dose-response data were obtained for ≥8 agonist concentrations on ≥6 cells. To determine EC_{50} values, concentration-response

data were fitted to the four-parameter logistic equation, $I = I_{max}/[1 + (EC_{50}/[A])^{nH}]$ where I_{max} is the maximal response plateau, [A] is the log concentration of agonist, and nH is the Hill coefficient, using KaleidaGraph v3.6 software (Synergy Software, Reading, PA). A detailed error analysis of nonsense suppression experiments shows that data are reproducible to ±50% in EC_{50}. (24) Relative efficacies (ε) of the partial agonists mCPBG, mCPG, and 5-fluorotryptamine (5-FT) are reported as $\varepsilon = I_{max\text{-}drug}/I_{max\text{-}5\text{-}HT}$. Efficacy was calculated for individual cells and then averaged and reported as mean ± SEM.

The coupling coefficient, Ω, is defined as

$$\frac{EC_{50}(wt,wt) * EC_{50}(mut,mut)}{EC_{50}(wt,mut) * EC_{50}(mut,wt)}$$

and the coupling energy of the double mutation, $\Delta\Delta G = RT \ln(\Omega)$.

For receptor antagonist experiments, antagonist doses in Ca^{2+}-free ND96 were applied to the oocyte for 15 s and incubated for a further 45 s. An identical dose of antagonist was then applied in a concentration of serotonin equal to 2-fold the mutant EC_{50} for 15 s before a 124 s wash with the running buffer. To ensure that current decreases result from antagonist alone, consistency of cell responses was determined by applying serotonin of concentration equal to 2-fold mutant EC_{50} for 15 s followed by a 124 s wash with the running buffer prior to the first antagonist dose and following a 5 min washout with running buffer after every fourth subsequent antagonist dose. Dose–response data were obtained for ≥8 agonist concentrations on ≥6 cells. To determine IC_{50} values, concentration–response data were fitted to the four-parameter logistic equation, $I = I_{max}/[1 + (IC_{50}/[A])^{nH}]$ where I_{max} is the maximal response plateau, [A] is the log concentration of agonist, and nH is the Hill coefficient, using KaleidaGraph v4.1.2 software (Synergy Software, Reading, PA).

2.4.4 Computation

Calculations were performed with the program SPARTAN. (25)

2.5 ACKNOWLEDGEMENTS

We thank Dr. Sarah Lummis (Cambridge) for helpful discussions and Noah Duffy for the preparation of 4,7-F_2-Trp.

2.6 REFERENCES

1. Thompson, A. J., Lester, H. A., and Lummis, S. C. (**2010**) The structural basis of function in Cys-loop receptors *Q. Rev. Biophys.* 43, 449– 499
2. Cederholm, J. M., Schofield, P. R., and Lewis, T. M. (**2009**) Gating mechanisms in Cys-loop receptors *Eur. Biophys. J.* 39, 37– 49
3. Thompson, A. J. and Lummis, S. C. (**2007**) The 5-HT_3 receptor as a therapeutic target *Expert Opin. Ther. Targets* 11, 527– 540
4. Jensen, A. A., Davies, P. A., Brauner-Osborne, H., and Krzywkowski, K. (**2008**) 3B but which 3B and that's just one of the questions: the heterogeneity of human 5-HT_3 receptors *Trends Pharmacol. Sci.* 29, 437– 444
5. Beene, D. L., Brandt, G. S., Zhong, W., Zacharias, N. M., Lester, H. A., and Dougherty, D. A. (**2002**) Cation-pi interactions in ligand recognition by serotonergic (5-HT_3A) and nicotinic acetylcholine receptors: The anomalous binding properties of nicotine *Biochemistry* 41, 10262– 10269
6. Zhong, W., Gallivan, J. P., Zhang, Y., Li, L., Lester, H. A., and Dougherty, D. A. (**1998**) From *ab initio* quantum mechanics to molecular neurobiology: A cation-π binding site in the nicotinic receptor *Proc. Natl. Acad. Sci. U.S.A.* 95, 12088– 12093
7. Puskar, N. L., Xiu, X., Lester, H. A., and Dougherty, D. A. (**2011**) Two neuronal nicotinic acetylcholine receptors, α4β4 and α7, show differential agonist binding modes *J. Biol. Chem.* 286, 14618– 14627
8. Xiu, X., Puskar, N. L., Shanata, J. A. P., Lester, H. A., and Dougherty, D. A. (**2009**) Nicotine binding to brain receptors requires a strong cation-π interaction *Nature* 458, 534– 537
9. Price, K. L., Bower, K. S., Thompson, A. J., Lester, H. A., Dougherty, D. A., and Lummis, S. C. (**2008**) A hydrogen bond in loop A is critical for the binding and function of the 5-HT_3 receptor *Biochemistry* 47, 6370– 6377
10. Celie, P. H. N., van Rossum-Fikkert, S. E., van Dijk, W. J., Brejc, K., Smit, A. B., and Sixma, T. K. (**2004**) Nicotine and carbamylcholine binding to nicotinic acetylcholine receptors as studied in AChBP crystal structures *Neuron* 41, 907– 914

11. Lee, W. Y. and Sine, S. M. (**2004**) Invariant aspartic acid in muscle nicotinic receptor contributes selectively to the kinetics of agonist binding *J. Gen. Physiol.* 124, 555– 567
12. Cashin, A. L., Torrice, M. M., McMenimen, K. A., Lester, H. A., and Dougherty, D. A. (**2007**) Chemical-scale studies on the role of a conserved aspartate in preorganizing the agonist binding site of the nicotinic acetylcholine receptor *Biochemistry* 46, 630– 639
13. Nowak, M. W., Gallivan, J. P., Silverman, S. K., Labarca, C. G., Dougherty, D. A., Lester, H. A., and Conn, P. M. (**1998**) In vivo incorporation of unnatural amino acids into ion channels in Xenopus oocyte expression system, *Methods in Enzymology*, pp 504– 529, Academic Press, San Diego, CA.
14. Dougherty, D. A. (**2000**) Unnatural amino acids as probes of protein structure and function *Curr. Opin. Chem. Biol.* 4, 645– 652
15. Horovitz, A. (**1996**) Double-mutant cycles: A powerful tool for analyzing protein structure and function *Folding Des.* 1, R121– 126
16. Niesler, B., Walstab, J., Combrink, S., Moller, D., Kapeller, J., Rietdorf, J., Bonisch, H., Gothert, M., Rappold, G., and Bruss, M. (**2007**) Characterization of the novel human serotonin receptor subunits 5-HT_3C, 5-HT_3D, and 5-HT_3E *Mol. Pharmacol.* 72, 8– 17
17. Bower, K. S., Price, K. L., Sturdee, L. E., Dayrell, M., Dougherty, D. A., and Lummis, S. C. (**2008**) 5-Fluorotryptamine is a partial agonist at 5-HT_3 receptors, and reveals that size and electronegativity at the 5 position of tryptamine are critical for efficient receptor function *Eur. J. Pharmacol.* 580, 291– 297
18. Sullivan, N. L., Thompson, A. J., Price, K. L., and Lummis, S. C. R. (**2006**) Defining the roles of Asn-128, Glu-129 and Phe-130 in loop A of the 5-HT_3 receptor *Mol. Membr. Biol.* 23, 442– 451
19. Shanata, J. A., Frazier, S. J., Lester, H. A., and Dougherty, D. A. (**2012**) Using mutant cycle analysis to elucidate long-range functional coupling in allosteric receptors *Methods Mol. Biol.* 796, 97– 113
20. Gleitsman, K. R., Shanata, J. A., Frazier, S. J., Lester, H. A., and Dougherty, D. A. (**2009**) Long-range coupling in an allosteric receptor revealed by mutant cycle analysis *Biophys. J.* 96, 3168– 3178
21. Barnes, N. M., Hales, T. G., Lummis, S. C., and Peters, J. A. (**2009**) The 5-HT_3 receptor--the relationship between structure and function *Neuropharmacology* 56, 273– 284
22. Corradi, J., Gumilar, F., and Bousat, C. (**2009**) Single-channel kinetic analysis for activation and desensitization of homomeric 5-HT_3A receptors. *Biophys. J.* 97, 1335-1345
22. Kilpatrick, G. J., Butler, A., Burridge, J., and Oxford, A. W. (**1990**) 1-(m-Chlorophenyl)-biguanide, a potent high affinity 5-HT_3 receptor agonist *Eur. J. Pharmacol.* 182, 193– 197
23. Torrice, M. M. (**2009**) Chemical-scale studies of nicotinic and muscarinic acetylcholine receptors, *Chemistry and Chemical Engineering*, California Institute of Technology, Pasadena, CA.
24. SPARTAN, Wavefunction, Inc., Irvine, CA.

Chapter 3

The 5-HT_3AB Receptor Shows an A_3B_2 Stoichiometry at the Plasma Membrane*

3.1 ABSTRACT

The 5-HT_3AB receptor is the best-characterized heteropentameric 5-HT_3 receptor. Under conditions of heterologous expression, the 5-HT_3AB receptor shows a single functionally resolvable population, suggesting the presence of a unique subunit stoichiometry; however, conflicting previous reports have suggested two different possible stoichiometries. Here we isolate plasma membrane sheets containing assembled receptors from individual HEK293T cells. We then determine the stoichiometry of 5-HT_3AB receptors on the plasma membrane by fluorescence methods, employing meCFP- and meYFP-labeled A and B subunits. Over a wide range of cDNA transfection ratios, fluorescence intensity ratios are closest to values that correspond to a subunit ratio of A_3B_2. Förster resonance energy transfer (family FRET) efficiencies provide minor corrections (3–6%) to the subunit ratios and provide independent support for a predominantly A_3B_2 stoichiometry on the plasma membrane sheets. Twin FRET efficiencies support these data, also suggesting that the two B subunits are nonadjacent in most of the heteropentamers. The high-frequency variant HTR3B p.Y129S (c.386A>C, rs11767445), linked to psychiatric disease, also forms A_3B_2 receptors on the plasma membrane. The 5-HT_3B Y129S subunit incorporates in a slightly (11–14%) more

---

This chapter is adapted with permission from:* Miles, T.F.; Dougherty, D. A.; Lester, H. A. The 5-HT_3AB Receptor Shows an A_3B_2 Stoichiometry at the Plasma Membrane. *Biophys. J.* **2013; 105; 887-898. © Biophysical Society.

efficient manner than the common variant. For the wild type and mutant receptors, most expressed subunits reside within the cell, rather than on the surface. In contrast to the findings for the plasma membrane, the relative abundances and FRET characteristics of intracellular subunits depend strongly on the transfection ratio. The straightforward and unambiguous combination of plasma membrane-sheet isolation, fluorescence intensity ratios, and FRET is a generally promising procedure for determining stoichiometry of proteins on the plasma membrane.

3.2 INTRODUCTION

Recognition of serotonin (5-HT) is accomplished by the various proteins (including enzymes, transporters, and receptors) that regulate its fundamental role in neurotransmission. Among the seven families of serotonin receptor, only one is an ion channel. The 5-HT_3 receptor, as a member of the Cys-loop superfamily of ligand-gated ion channels, is composed of five subunits that arrange symmetrically around a central pore (1 and 2). Found in both the peripheral and central nervous systems, 5-HT_3 receptors have been implicated in numerous salutary and pathological processes including emesis, nociception, cognition, and depression (3 and 4).

Once believed to consist of only one member (5-HT_3A), the known 5-HT_3 receptor family has recently been expanded by identification of four additional subunits (B–E) (4, 5, and 6). Unlike 5-HT_3A, which is capable of forming functional homopentameric receptors, the B–E subunits convey function only in the presence of the A subunit as heteromers. The best studied of these, 5-HT_3AB, differs greatly from the homomeric receptor (7). For 5-HT, the AB receptor shows an increased EC_{50} and rate of

desensitization coupled with decreased cooperativity, inward rectification, and calcium permeability (5, 8, 9, and 10). Major differences in pharmacological selectivity at allosteric sites have also been observed (7, 11, and 12). Moreover, only the markedly higher conductance of the 5-HT_3AB receptor agrees with that observed in native tissue (13, 14, 15, and 16). Heteromeric receptors containing 5-HT_3C, D, or E subunits, on the other hand, are as yet functionally indistinguishable from the homomeric receptor (17 and 18).

As heteropentamers, functional 5-HT_3AB receptors may exhibit numerous potential subunit stoichiometries. Unlike other members of the Cys-loop superfamily, however, the 5-HT_3AB receptor shows a single functionally resolvable population in heterologous expression systems. In an early study aimed at determining the stoichiometry of this population, purified 5-HT_3AB receptors were antibody-labeled at epitope tags specific to the A and B subunits (19). AFM was then used to observe the angle between adjacent antibodies. For the 5-HT_3AB receptor, two inter-antibody angles were observed: one that is unique to the heteromer and one that is also seen in the homomer. Based on the pattern of these angles, the authors proposed that receptors are composed of two A subunits and three B subunits arranged B-B-A-B-A.

Because the orthosteric ligand-binding site of Cys-loop receptors spans the interface of two adjoining subunits, this finding suggested that the B subunit must successfully contribute to the gating of 5-HT_3AB receptors. Recent studies, however, have called this conclusion into question. While conversion of critical A subunit residues to the corresponding residue of the B subunit is strongly deleterious to orthosteric ligand binding, the analogous mutations from B to A exhibit no effect (20). Furthermore,

introduction of double cysteine mutants (placed one per face on a potential binding site) in the A subunit displayed no response in either homo- or heteromeric receptors until exposed to a reducing agent. Finally, it was shown that cysteine labeling near the postulated AB orthosteric site hinders ligand binding only for A subunit residues (21). Together these findings suggested, contrary to the AFM data (19), the presence of at least one A-A subunit interface in the 5-HT_3AB receptor.

In this study, we have sought to resolve the stoichiometry of functional membrane 5-HT_3AB receptors using various fluorescence methods on isolated membrane sheets from whole cells expressing fluorescent protein fusions of the 5-HT_3A and B subunits.

3.3 MATERIALS AND METHODS

3.3.1 Materials

The pcDNA3.1(+) expression vector and fetal bovine serum reagents were purchased from Invitrogen (Carlsbad, CA). TransIT transfection reagent was purchased from Mirus (Madison, WI). Penicillin/streptomycin (100×) solution was purchased from Mediatech (Herndon, VA). Culture dishes (35 mm, with 14 mm, No. 0 thickness, glass coverslip microwells) were purchased from Mattek (Ashland, MA). Coverslips (25 mm, No. 1 thickness glass) were purchased from VWR (Radnor, PA). Other tissue-culture plasticware was purchased from Greiner Bio-One (Monroe, CA).

3.3.2 Molecular Biology

Monomeric-enhanced (me) CFP and YFP were introduced in frame into the M3-M4 loops of the human $5HT_3$A and $5HT_3$B subunits, taking care to avoid known signaling and trafficking motifs. The forward primer

5′-AAG ACT GAT GAC TGC TCA GCC ATG GGA AAC CAC TGC AGC CAC ATG GGA GCT GGC GCC ATG GTG AGC AAG GGC GAG GAG-3′

and the reverse primer

5′-GGG AGG GCT ACA TCT GTC CCT CGG GCT CTT CTC GAA GTC CTG GGG TCC GGC GCC TGC CTT GTA CAG CTC GTC CAT GCC-3′

were used in PCR to add overlapping regions homologous to the M3-M4 region of h5-HT_3A to meCFP and meYFP. The forward primer

5′- GCT AAG TCC ATC GTG TTG GTC AAA TTC CTC CAT GAT GAG CAG CGT GGT GCT GGC GCC ATG GTG AGC AAG GGC GAG GAG-3′

and the reverse primer

5′-GGT TCC TGG CTG GGC CAG GTG CTC TCC ATA CAG CGA GGA CTC TGT TAC GGC GCC TGC CTT GTA CAG CTC GTC CAT GCC-3′

were used in PCR to add overlapping regions homologous to the M3-M4 region of h5-HT_3B to meCFP and meYFP. These products were then isolated and used as inserts in a second PCR reaction with the corresponding full-length subunit to generate the receptor subunit-fluorescent protein fusion constructs. The fluorescent protein insertion point for the A subunit is between Gly-421 and Gly-422. The insertion point for the B subunit is between Gly-333 and Gly-334. All constructs were verified by sequencing.

3.3.3 Cell Culture and Transfection

Human embryonic kidney (HEK) 293T cells, bearing T-antigen, were maintained on 100 mm culture plates at 37°C and 5% CO_2 in a humidified atmosphere. They were cultured in Dulbecco's modified Eagle's medium/nutrient mix F12 (1:1) with GlutaMAX I media (Invitrogen) containing 10% fetal calf serum and

penicillin/streptomycin. Cells at 60–80% confluency within 35 mm dishes were transfected with a total of 2 μg of plasmid DNA using the TransIT transient transfection kit (Mirus). For FlexStation studies (Molecular Devices, Eugene, OR), cells were transfected and then plated in 96 well plates. Cells were incubated 1–2 days before assay. For whole-cell fluorescence studies, cells were plated in 35 mm glass-bottomed dishes and imaged one day after transfection. For membrane isolation studies, cells were prepared four days after transfection.

3.3.4 Flexstation Analysis

The FlexStation (Molecular Devices) analysis technique uses fluorescent voltage-sensitive dyes to detect changes in the membrane potential. It has been used to examine various ion channels, including those of the 5-HT_3 receptors (22). In brief, fluorescent membrane potential dye (Molecular Devices) was diluted in the Flex buffer (10 mM HEPES, 115 mM NaCl, 1 mM KCl, 1 mM $CaCl_2$, 1 mM $MgCl_2$, and 10 mM glucose, pH = 7.4) and added to transfected cells grown on a 96 well plate. The cells were incubated at room temperature for 30 min and then fluorescence was measured in a FlexStation (Molecular Devices) at 2 s intervals for 200 s. Serotonin (5-HT) was added to each well after 20 s. The percentage change in fluorescence was calculated as

$$\frac{(F - F_{\min})}{F_{\max}},$$

where F is peak fluorescence for the current agonist dose, F_{max} is peak fluorescence at saturating agonist, and F_{min} is baseline fluorescence at 20 s.

To determine EC_{50} values, concentration-response data were fitted to the four-parameter logistic equation,

$$I = \frac{I_{\max}}{\left[1 + \left(\frac{\mathrm{EC}_{50}}{[\mathrm{A}]}\right) n_{\mathrm{H}}\right]},$$

where I_{max} is the maximal response plateau, [A] is the log concentration of agonist, and n_H is the Hill coefficient, using KaleidaGraph v3.6 software (Synergy Software, Reading, PA).

3.3.5 Membrane Isolation

When one performs ensemble measurements of integral membrane proteins on the plasma membrane, it is important to restrict the pool of observed subunits to only those that reside on the plasma membrane. To isolate this restricted population, membrane was mechanically removed from the rest of the cell as described previously in Perez et al. (23).

This is achieved by bathing HEK293T cells 72–96 h posttransfection in deionized water to induce swelling. After 1 min, a No. 1 coverslip, sterilized by sequential 20 min 6 M KOH and acetone baths with sonication and stored in 20 μm filtered deionized water, was placed on top of the cells. Pressure was applied to the coverslip with a pipette tip for 3 min, ensuring contact with the cell membrane. The coverslip was then removed, bringing adhered membrane with it, and thoroughly rinsed with phosphate-buffered saline (PBS) to remove remaining intracellular contents. To ensure complete intracellular removal, all samples subjected to this preparation were transfected with DsRed2-ER, which labels endoplasmic reticulum (ER).

The membrane-attached side of the coverslip was then covered in filtered deionized water, inverted to create a hanging drop, and imaged by confocal microscopy

as detailed below, using a 63×, 1.2 NA violet-corrected Plan Apochromatic water-immersion objective (Nikon Instruments, Melville, NY).

3.3.6 Confocal Microscopy

Live cells grown on 14 mm glass-bottomed 35 mm dishes (Mattek) precoated with poly-d-lysine were washed with PBS and observed in the same solution. Imaging was performed at room temperature on an Eclipse C1si laser-scanning confocal microscope (Nikon Instruments) equipped with a 63×, 1.4 NA, violet-corrected plan Apochromatic oil objective and a multianode photomultiplier tube with 32 channels (both by Nikon Instruments). The meCFP, meYFP, and DsRed2 fluorescence signals were acquired by 439, 514, and 561 nm excitation, respectively. Where required, images were linearly unmixed with the EZ-C1 software (Nikon Instruments) for the emission spectra of the fluorophores of interest, using reference spectra individually compiled for each fluorophore expressed in the same cell type.

3.3.7 Donor Recovery After Acceptor Photobleach FRET

A series of λ-stack X-Y images were collected with the Eclipse C1si laser-scanning confocal microscope (Nikon Instruments). Dequenching of meCFP fluorescence during incremental photobleaching of meYFP was performed and analyzed as described previously in Son et al. (24) and Nashmi et al. (25). Donor recovery after acceptor photobleach (DRAP) Förster resonance energy transfer (FRET) efficiency (E) was calculated as

$$E = 1 - \left(\frac{I_{DA}}{I_D}\right). \qquad \text{(Equation 3.1)}$$

Here, I_{DA} represents the normalized fluorescence intensity of meCFP (100%) in the presence of nonbleached acceptor. I_D represents the normalized fluorescence intensity of meCFP after 100% photobleach of I_A, the acceptor meYFP. The I_D value was extrapolated from a scatter plot of the percentage increase of meCFP fluorescence versus the percentage decrease of meYFP fluorescence for each cell (as seen later in Figures 3.4 and 3.6, *C*) (25).

3.3.8 Fluorescence Intensity Ratio

First described by Zheng and Zagotta (26) in 2004, fluorescence intensity ratios (FIR) allow the pairwise determination of the relative abundance of proteins (27 and 28). This is achieved by labeling both proteins of interest with each of two fluorescent reporters. Given reporter requirements for complete and stoichiometric labeling and the desire to minimize fluorophore-specific changes in target expression, fluorescent protein fusions utilizing the highly homologous meCFP and meYFP are typically chosen.

In FIR, all of the photophysical particularities of the instrumental setup and the chosen fluorescent proteins reside within a coefficient (C) that relates observed fluorescence intensities to the relative abundance of the receptor subunits to which they are fused.

For AmeCFP BmeYFP, this relationship is

$$k_1 = \frac{I_{\text{meCFP}}}{I_{\text{meYFP}}} = C \times \left(\frac{[A]}{[B]}\right), \qquad \text{(Equation 3.2)}$$

and for AmeYFP BmeCFP this relationship is

$$k_2 = \frac{I_{\text{meCFP}}}{I_{\text{meYFP}}} = \frac{C}{\left(\frac{[A]}{[B]}\right)}. \qquad \text{(Equation 3.3)}$$

Having determined the fluorescence intensity ratios for fluorescent protein-receptor subunit fusion pairs, one rearranges the above equations to yield both [A]/[B] and C as follows:

$$\left(\frac{[A]}{[B]}\right) = \sqrt{\frac{k_1}{k_2}}, \qquad \text{(Equation 3.4)}$$

$$C = \sqrt{k_1 \times k_2}. \qquad \text{(Equation 3.5)}$$

One complication resides in the ability of meCFP and meYFP to FRET. However, as a ratiometric method, donor intensity loss via FRET is expected to affect FIR only to the extent that FRET efficiency differs between the two fluorescent protein fusion pairs. When such a difference in FRET efficiency occurs, and before the acceptor is photobleached, a correction factor (d_0) to predict the direction and degree of change in subunit ratio can be calculated by Equations 3.6 and 3.7, where E_1 is the FRET efficiency for $A_{\text{meCFP}}B_{\text{meYFP}}$ and E_2 is that for $A_{\text{meYFP}}B_{\text{meCFP}}$:

$$d_0 = \sqrt{\frac{\left(1/1 - E_2\right)}{\left(1/1 - E_1\right)}}, \qquad \text{(Equation 3.6)}$$

$$\text{Corrected}\left(\frac{[A]}{[B]}\right)_0 = d_0 \times \left(\left(\frac{[A]}{[B]}\right)_0\right). \qquad \text{(Equation 3.7)}$$

To calculate FIR, we always used the acceptor intensity at the beginning of the experiment, before any acceptor photobleaching (shown later in Tables 3.4 and 3.5, $I_{meYFP} = 1$). Note that these later-appearing tables, Tables 3.4 and 3.5, contain experimental values for d_0. Figures 3.4 and 3.6, *B*, also shown later, provide examples of this progression.

The constant C varied by ±20% among our experiments performed on different days. This was determined both through calculation of C in FIR measurements and tests of the predictive power of that value, including one using equal mole fractions of 5-HT_3A-meYFP and 5-HT_3A-meCFP cDNA and unlabeled 5-HT_3B, and another using unlabeled 5-HT_3A and equal mole fractions of 5-HT_3B-meYFP and 5-HT_3B-meCFP cDNA. Possible bases for this variation include small, uncontrolled changes in oxygenation, temperature, or the cell cycle, any of which may change the fraction of immature (i.e., dark) fluorophores.

3.4 RESULTS

Fusion constructs of the human 5-HT_3A and 5-HT_3B subunits with fluorescent proteins were generated. Both meCFP and meYFP were individually added to the 5-HT_3A and 5-HT_3B subunits, allowing both combinations of the two fluorescent proteins to be probed. As with previous Cys-loop receptor subunits, the fluorescent protein was introduced into the M3-M4 intracellular loop, taking care to avoid known phosphorylation and trafficking motifs (2, 25, and 29). These constructs were then transiently expressed in HEK293T cells, and their functional response to serotonin was assayed using a voltage-sensitive dye. The 5-HT_3AB receptors formed from the

fluorescent protein fusion constructs show maximal responses, EC_{50} values, and Hill coefficients essentially equivalent to the unlabeled receptor (Figure 3.1; Table 3.1). This suggests that neither fluorescent label perturbs the expression level or function of the hetero-pentameric 5-HT_3 receptor. The characteristic shifts in EC_{50} and Hill coefficient between the homo- and heteromeric receptors would betray mixed populations of receptor by generating a biphasic dose-response relationship. An equal mole ratio of transfected 5-HT_3A and 5-HT_3B subunit DNA, however, yielded a pure population of heteromeric receptors.

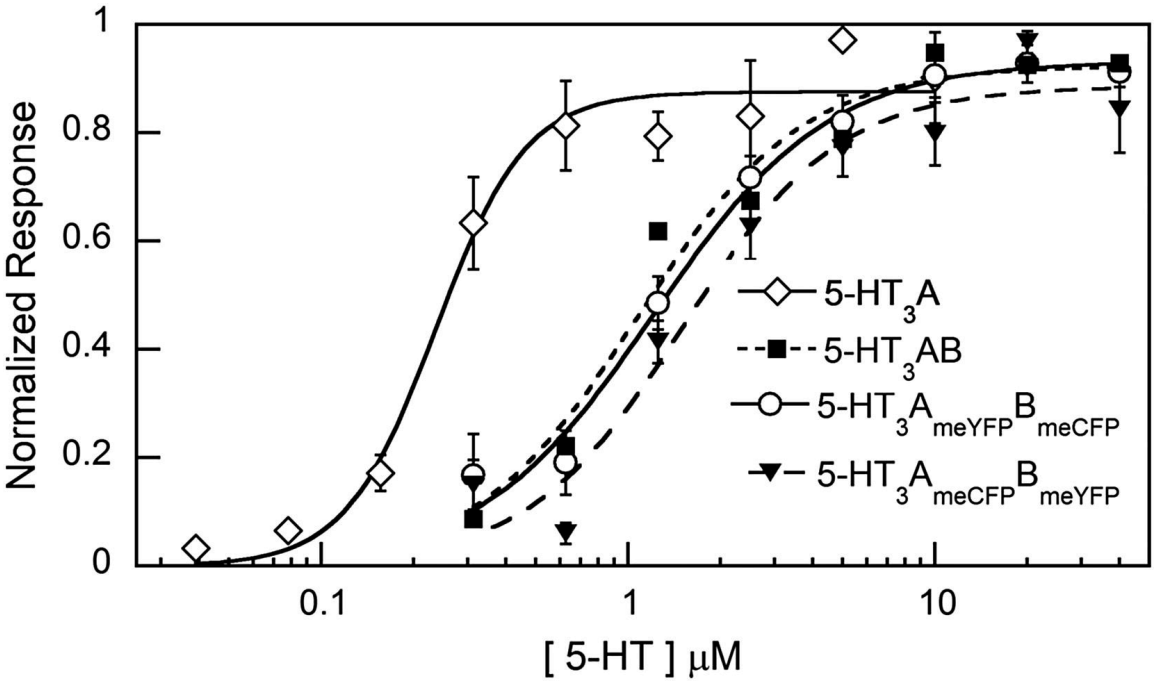

Figure 3.1 5-HT_3 receptor agonist dose-response relations are not changed by labeling the fluorescent labels on the subunits. Receptors expressed in HEK293T cells were assayed with a voltage-sensitive dye. All heteromeric receptors were transfected with a 1:1 ratio of A/B subunit cDNA.

	Maximal response (AU)	5-HT EC_{50} (μM)	Hill coefficient (n_H)	*N*
5-HT_3A	667 ± 28	0.24 ± 0.02	3.0 ± 0.6	16
5-HT_3AB	616 ± 23	1.1 ± 0.2	1.8 ± 0.3	6
5-$HT_3A_{meYFP}B_{meCFP}$	574 ± 31	1.2 ± 0.1	1.5 ± 0.2	6
5-$HT_3A_{meCFP}B_{meYFP}$	571 ± 54	1.5 ± 0.3	1.7 ± 0.4	6
5-HT_3AB_{Y129S}	526 ± 23	1.3 ± 0.1	1.8 ± 0.3	6

Table 3.1 5-HT_3 Receptor agonist dose-response data. All values are reported as mean ± standard error.

Transfected fluorescent 5-HT_3 receptor and ER marker showed extensive colocalization, demonstrating marked ER retention of the component receptor subunits, thereby obscuring the plasma membrane population of assembled functional receptors (Figure 3.2). The ER retention seen with transfected cells may be partially due to the addition of the large GFP proteins. To isolate plasma membrane-embedded receptors, plasma membranes were allowed to adhere to a coverslip before being mechanically sheared away from the cell body by removal of that coverslip. Extensive rinsing in PBS removed residual intracellular contents. Subsequent imaging of the coverslip reveals much lower ER marker fluorescence while retaining fragments bearing fluorescent 5-HT_3 receptor with shallow z-axis signatures. We term these “membrane sheets”.

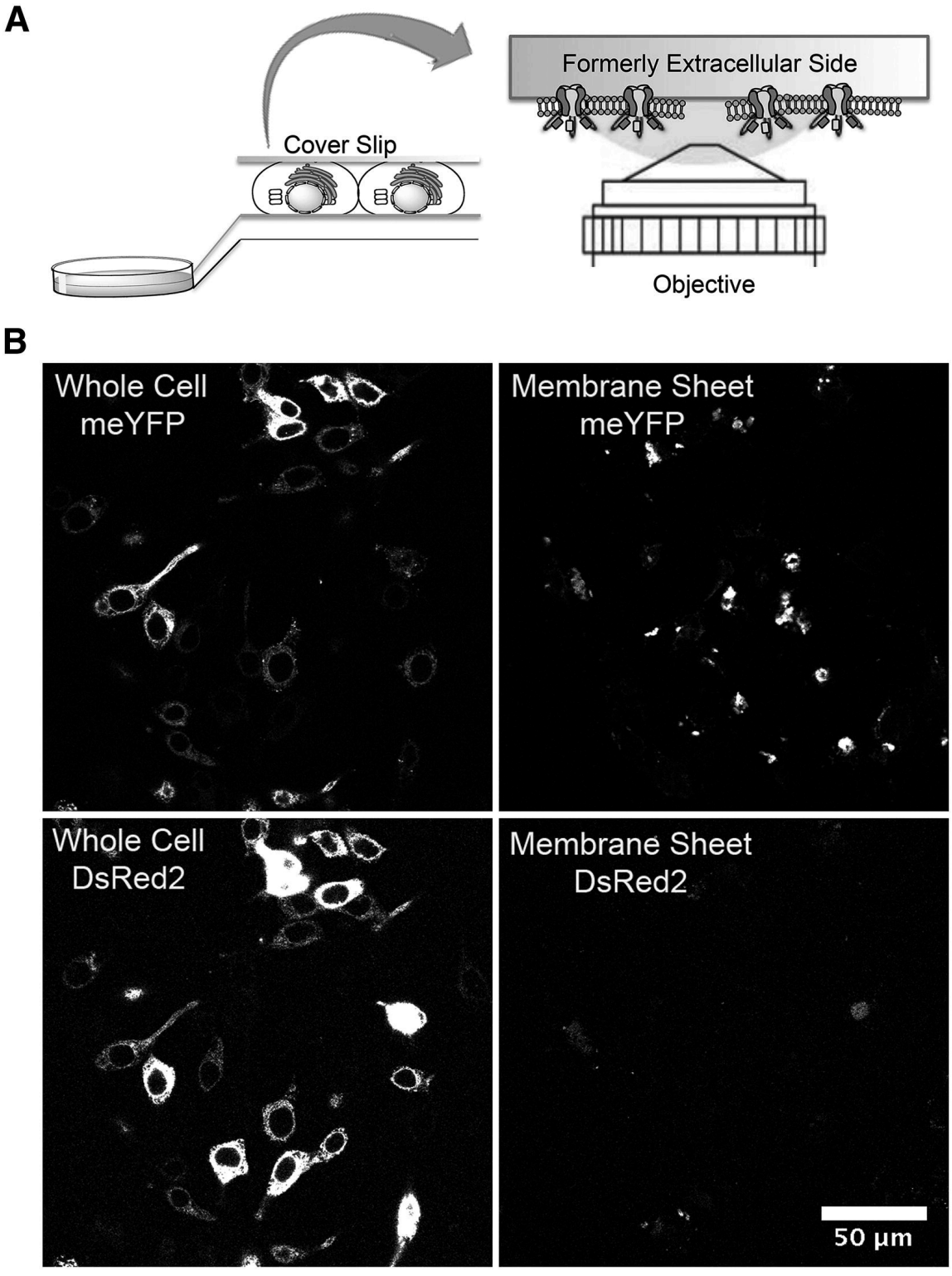

Figure 3.2 Fluorescence imaging of whole cells and isolated membrane sheets. (A) Illustration of membrane-sheet preparation method. (B) HEK293T cells transfected with 5-HT_3A_{meYFP} and DsRed2-ER

3.4.1 FIR Measurements Show A_3B_2 Subunit Ratios

FIR measurements provide direct determination of subunit ratios. As will be shown below, these measurements required only minimal correction for FRET. FIR were determined for membrane sheets containing both labeling patterns (5-HT_3A-meYFP/5-HT_3B-meCFP and 5-HT_3A-meCFP/5-HT_3B-meYFP). Fluorescence intensity ratios for individual membrane sheets display tight bunching, as demonstrated in Figure 3.3. The average FIR for both pairings of subunit and fluorescent protein were then related by Equation 3.4 to yield the relative concentration of A to B subunits (Table 3.2). The membrane-sheet/subunit ratio revealed by FIR shows a slight dependence on the cDNA transfection ratio, but in all cases strongly suggests three A subunits for every two B subunits (Figure 3.4).

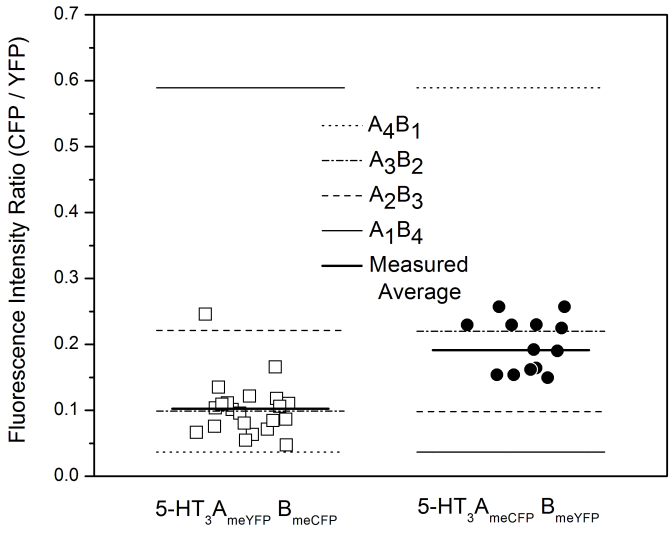

Figure 3.3 Fluorescence intensity ratio (FIR) on 5-HT_3AB membrane sheets: support for the A_3B_2 subunit ratio. Heteromers were expressed from a 1:9 ratio of A subunit to B subunit cDNA. Each point corresponds to a single membrane sheet's FRET corrected FIR. Expected average values for various stoichiometries were calculated using C as determined by Equation 3.5. These data provide one of the data points in Figure 3.4 and Table 3.2.

Mole fraction 5-HT$_3$A		Mole fraction 5-HT$_3$B		FRET	Fluorescence intensity		
meCFP	meYFP	meCFP	meYFP	efficiency (%)	ratio (meCFP/meYFP)	[A]/[B]	*N*
0.5			0.5	26.1 ± 0.7	0.273 ± 0.023	1.93 ± 0.29	22
	0.5	0.5		30.8 ± 0.4	0.073 ± 0.009		16
0.25			0.75	27.6 ± 0.6	0.231 ± 0.015	1.57 ± 0.17	44
	0.25	0.75		32.7 ± 0.8	0.094 ± 0.008		40
0.1			0.9	25.2 ± 0.6	0.190 ± 0.015	1.37 ± 0.15	13
	0.1	0.9		33.9 ± 1.4	0.102 ± 0.009		21

Table 3.2 Fluorescence data, membrane sheets. All values are reported as mean ± standard error.

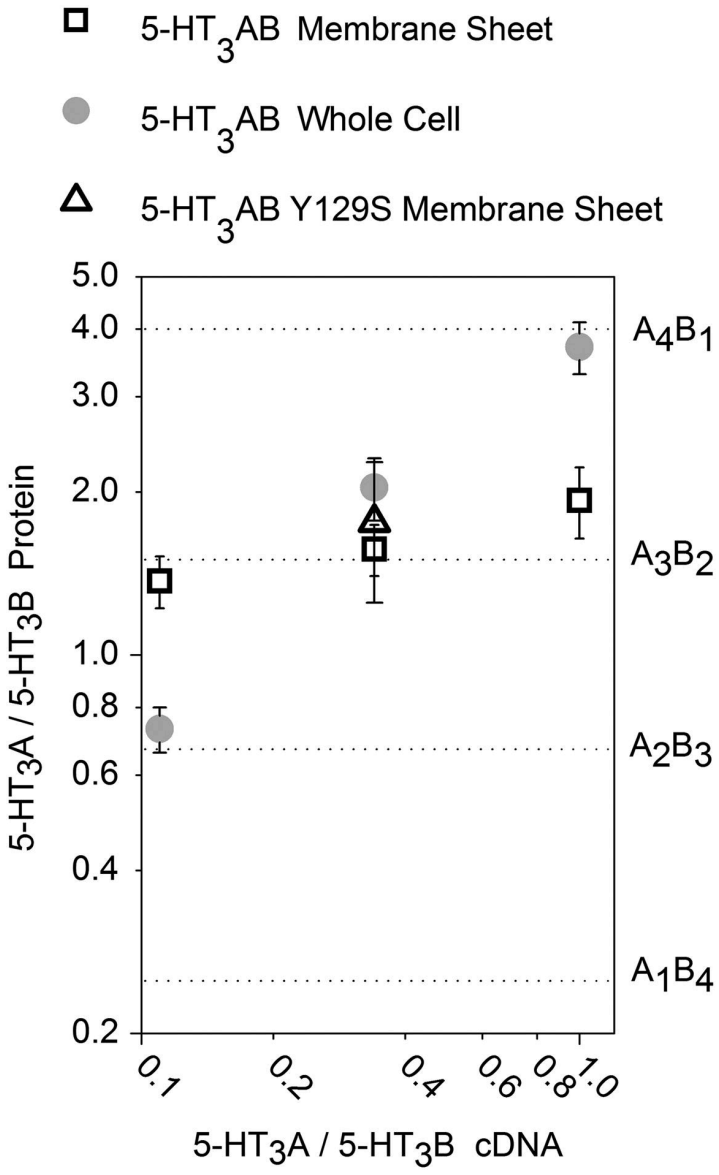

Figure 3.4 5-HT$_3$AB receptor subunit ratio is 3:2 on the plasma membrane, as calculated by FIR at various subunit cDNA transfection ratios. Both axes are shown on a logarithmic scale. (see Table 2). Error bars depict the standard error.

Clearly, the ratio of subunit cDNA transfected did not strongly influence the ratio of subunit protein expressed in the plasma membrane sheets. When similar analyses were performed on intact cells, we found a markedly different pattern. Although 2–3 day incubations were required for satisfactory fluorescence signals in the membrane-sheet samples, strong fluorescence was observed within 24 h of transfection for whole cells. In identically treated samples transfected with 0.75 mol fraction 5-HT_3B, the whole cell fluorescence intensity corresponding to the A subunit increased 7.5 ± 1.2 fold from membrane-sheet levels. The fluorescence intensity corresponding to the B subunit increased only 3.5 ± 0.5 fold. The subunit ratios calculated by FIR were strongly dependent on the relative amount of subunit cDNA transfected. Whereas the membrane-sheet subunit ratios all suggest a single receptor subunit ratio, in whole cells every condition points toward a different ratio (Figure 3.4; Table 3.3).

Mole fraction 5-HT_3A		Mole fraction 5-HT_3B		FRET	Fluorescence intensity		
meCFP	meYFP	meCFP	meYFP	efficiency (%)	ratio (meCFP/meYFP)	[A]/[B]	*N*
0.5			0.5	15.7 ± 0.5	0.618 ± 0.047	3.71 ± 0.41	23
	0.5	0.5		57.8 ± 5.0	0.045 ± 0.003		24
0.25			0.75	26.8 ± 1.2	0.424 ± 0.025	2.04 ± 0.27	25
	0.25	0.75		47.5 ± 2.2	0.102 ± 0.012		17
0.1			0.9	32.5 ± 0.7	0.135 ± 0.011	0.73 ± 0.07	20
	0.1	0.9		21.7 ± 1.2	0.252 ± 0.017		24

Table 3.3 Fluorescence data, whole cells. All values are reported as mean ± standard error.

3.4.2 Family FRET measurements provide minor corrections to FIR and support for A3B2 stoichiometry

Previous work with other heteromeric Cys-loop receptors, especially α4β2 nicotinic receptors, has shown that fluorescently labeled heteromeric receptors of

differing stoichiometries can display differences in FRET efficiencies (24 and 30). The FIR experiments described in Figure 4.4 provide a family FRET experiment: all the A subunits bear donor fluorophores, and all the B subunits bear acceptor fluorophores (or vice versa). To evaluate family FRET efficiencies, DRAP time courses were determined (Figure 3.5, *A–C*). Donor fluorescence at complete acceptor photobleach is extrapolated from this time course, allowing for the calculation of FRET efficiency by Equation 3.1. This procedure was performed for both pairings of subunit and fluorescent protein within the heteromeric receptor at various transfected mole ratios of 5-HT_3A and 5-HT_3B subunit cDNA (Table 3.2). The stoichiometry of donor fluorophores to acceptor fluorophores is different in the two pairings of subunit and fluorescent protein. This causes changes in the measured FRET efficiencies of CFP- and YFP-labeled 5-HT_3AB receptors in the membrane sheets.

In a first application of these family FRET measurements, we employed them in Equations 3.6 and 3.7 to calculate the correction factor (d_0) to the FIR measurements.

In a second application of these family FRET measurements, their comparative amplitudes provide independent support for our conclusions about subunit stoichiometry.

A satisfactory theory for family FRET measurements must account for several factors, including the subunit order, dipole orientation, departures from pentameric symmetry, and coplanarity of the fluorophores within the M3-M4 loops (24 and 30). These parameters are not known for any heteromeric Cys-loop receptor. Importantly, a reasonable range of assumptions about these parameters predict that FRET for two donor subunits and three acceptor subunits exceeds that for a receptor with three donor subunits and two acceptor subunits (24 and 30). The theory accounts for published data on

transfected cells in which α4β2 stoichiometries were manipulated in one of three ways:

1. By varying fluorescent subunit cDNA ratios;
2. By treating with pharmacological chaperone; or
3. By mutations that change the stoichiometry (30 and 31)

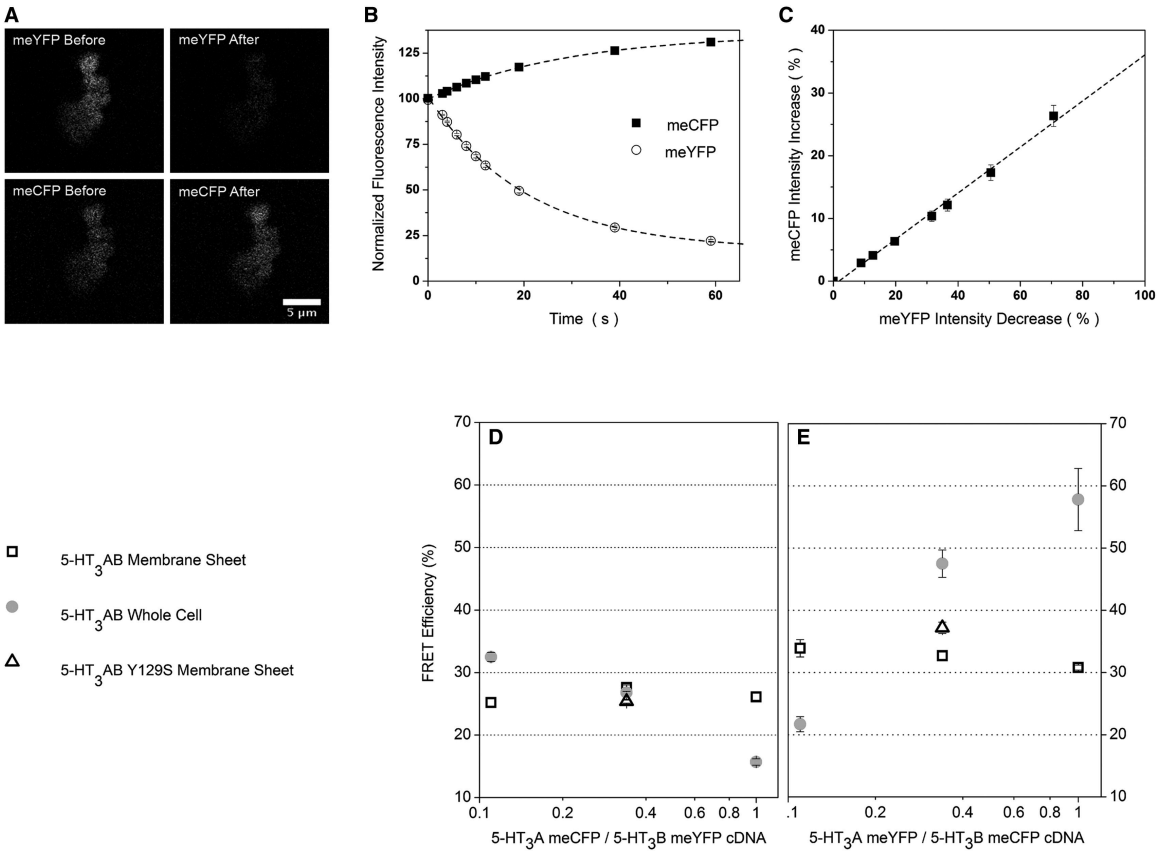

Figure 3.5 Family FRET measurements are consistent with A_3B_2 stoichiometry. Donor recovery after acceptor photobleaching (DRAP) on 5-HT_3AB membrane sheets. (A) Representative membrane-sheet images before and after photobleaching for $A_{meCFP}B_{meYFP}$ transfected with a 1:1 ratio of A/B subunit cDNA. (B) The corresponding plot of fluorescence during the acceptor photobleaching time course. (C) Extrapolation of the photobleaching time course in B to donor fluorescence intensity at complete acceptor bleach. (D) FRET efficiency of 5-$HT_3A_{meYFP}B_{meCFP}$ at various subunit cDNA transfection ratios. The X-axis is shown on a logarithmic scale. (E) FRET efficiency of 5-$HT_3A_{meCFP}B_{meYFP}$ at various subunit cDNA transfection ratios. The X-axis is shown on a logarithmic scale (see Table 3.2). Error bars depict the standard error.

These experiments on 5-HT_3AB showed the pattern expected from the FIR data (24 and 30). 5-HT_3AB receptors thought to have two donors/three acceptors from the FIR data had greater FRET than those with three donors/two acceptors. When the A subunit was labeled with the acceptor (meYFP) and the B subunit with the donor (meCFP), FRET efficiency was 1.18–1.34 times that with the opposite pairing when evaluating membrane sheets. The FRET efficiency was also independent of cDNA transfection ratio. These data are consistent with the view of a receptor with an A_3B_2 stoichiometry on the plasma membrane. In contrast, the FRET efficiencies for whole cells were strongly dependent on cDNA transfection ratio (Figure 3.5, *D* and *E*; Table 3.3).

In the absence of a correction for the higher FRET efficiency when the A subunit has meYFP, the ratio of A/B subunits derived from FIR (detailed previously) varies at different degrees of acceptor photobleaching. Furthermore, if both measures are exclusively the result of assembled receptors, the difference in FRET efficiencies should predict the direction and degree of change in the subunit ratio, according to Equations 3.6 and 3.7. For membrane sheets, the changes in subunit ratios derived from FIR during photobleaching agree with the corrected FIR at all cDNA transfection ratios (Table 3.4).

Mole fraction 5-HT_3B	$I_{meYFP} = 1$	$I_{meYFP} = 0.6$	$I_{meYFP} = 0.25$	$I_{meYFP} = 0$	d_0	$I_{meYFP} = 1$ corrected by d_0
0.5	1.96 ± 0.31	1.95 ± 0.29	1.97 ± 0.28	1.93 ± 0.29	0.97	1.90
0.75	1.60 ± 0.19	1.58 ± 0.19	1.56 ± 0.17	1.57 ± 0.17	0.96	1.54
0.9	1.41 ± 0.20	1.38 ± 0.18	1.36 ± 0.15	1.37 ± 0.15	0.94	1.33

Table 3.4 Effect of acceptor photobleaching on subunit ratio, membrane sheets. All values are reported as mean ± standard error.

For whole cells, the d_0-corrected subunit ratio is markedly different from that observed at complete acceptor photobleach for two of three transfection ratios

(Table 3.5). This indicates that additional complexities contribute to the FRET efficiencies and subunit ratios for whole cells.

Mole fraction 5-HT$_3$B	$I_{meYFP} = 1$	$I_{meYFP} = 0.6$	$I_{meYFP} = 0.25$	$I_{meYFP} = 0$	d_0	$I_{meYFP} = 1$ corrected by d_0
0.5	4.84 ± 0.68	4.09 ± 0.53	3.59 ± 0.50	3.71 ± 0.41	0.71	3.42
0.75	2.17 ± 0.37	2.09 ± 0.31	2.05 ± 0.27	2.04 ± 0.27	0.85	1.84
0.9	0.68 ± 0.07	0.71 ± 0.08	0.72 ± 0.08	0.73 ± 0.07	1.08	0.73

Table 3.5 Effect of acceptor photobleaching on subunit ratio, whole cells. All values are reported as mean ± standard error.

3.4.3 Twin FRET measurements support the inference of A_3B_2 stoichiometry

We also employed another FRET-based method for probing stoichiometry—twin FRET analysis—in which receptors are composed of one subunit subtype that is unlabeled and another that is an equal mixture of CFP and YFP constructs (24) (Figure 4.6, *A–D*). Previous theory and experiments show that twin FRET data for $(\alpha4)_3(\beta2)_2$ versus $(\alpha4)_2(\beta2)_3$ nAChRs are dominated by the fact that the former stoichiometry has two adjacent α4 subunits and no adjacent β2 subunits; but the latter stoichiometry has the contrasting pattern of adjacency. The differences arise from the steep distance-dependence of FRET (24).

Membrane sheets transfected with 0.75 mol fraction 5-HT$_3$B with the A subunit doubly labeled have a FRET efficiency of 33.2 ± 1.2% (N = 19) (Figure 3.6, *D*). This is generally compatible with a structure containing at least two A subunits. The rather high efficiency suggests that two of the A subunits are adjacent in most receptors; this is required if there are three A subunits in a pentamer.

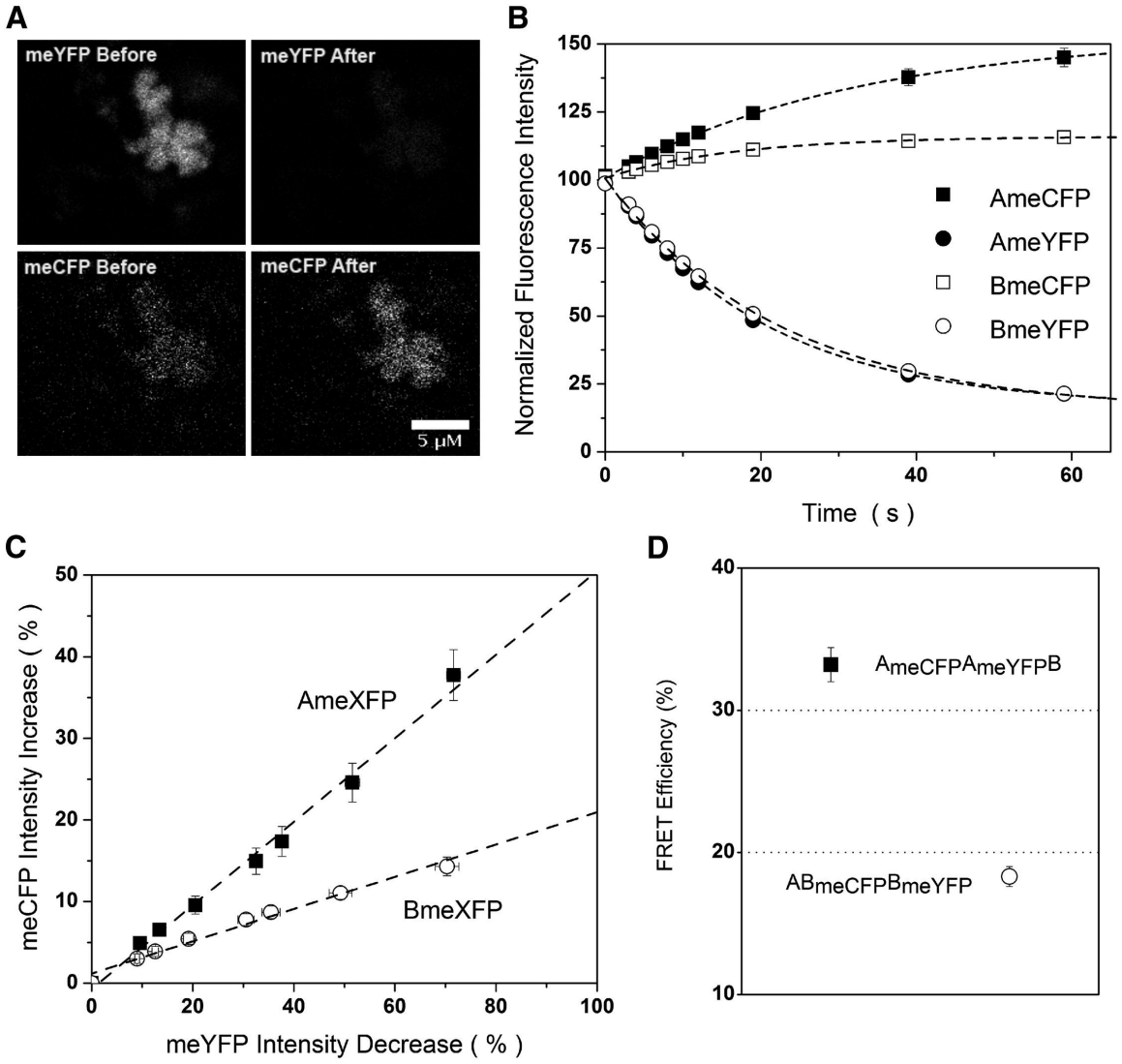

Figure 3.6 Twin FRET measurements are consistent with A_3B_2 stoichiometry and with nonadjacent B subunits. Donor recovery after acceptor photobleaching (DRAP) on 5-HT_3AB membrane sheets. (A) Representative membrane-sheet images before and after photobleaching for $A_{meCFP}A_{meYFP}B$ transfected with a 1:1:6 ratio of A_{meCFP}/A_{meYFP} to untagged B subunit cDNA. (B) Plot of fluorescence during the acceptor photobleaching time course for both tagged A or tagged B subunit 5-HT_3AB twin FRET experiments. (C) Extrapolation of the photobleaching time courses in B to donor fluorescence intensity at complete acceptor bleach. (D) Twin FRET efficiencies of tagged A or tagged B subunit 5-HT_3AB receptors. Error bars depict the standard error.

Twin FRET between the labeled B subunits is also detectable, at an efficiency of $18.3 \pm 0.7\%$ (N = 9) (Figure 3.6, *D*). This shows that there are also at least two B subunits. As discussed below, the lower FRET efficiency for the B subunits indicates

that there are probably only two nonadjacent B subunits in most receptors. Thus, these twin FRET experiments also support the conclusion of predominantly A_3B_2 stoichiometry.

3.4.4 The 5-HT$_3$B Y129S subunit assembles into receptors like the B subunit

The B subunit studied in the experiments above contains tyrosine at position 129. A single-nucleotide nonsynonymous polymorphism HTR3B p.Y129S (c.386A>C, rs11767445) has been associated with several diseases, including major depression and bipolar affective disorder (4, 32, 33, and 34). This residue is located on a β-strand beneath the orthosteric binding site, and the side chain is modeled to project into the inter-subunit interface. We constructed and studied Y129S subunits containing both fluorophores.

To investigate the possibility that Y129S might affect receptor assembly and stoichiometry, the subunit ratio determined by FIR was measured on membrane sheets transfected with 0.75 mol fraction 5-HT_3B_{Y129S}. The FRET efficiencies and subunit ratio calculated by FIR were largely unchanged from that of the Y129 B subunit (which we usually term B) receptor, suggesting a receptor stoichiometry of three A subunits and two B subunits for the variant receptor (Tables 3.2 and 3.6; Figure 3.4; Figure 3.5, *D* and *E*).

Mole fraction 5-HT_3A		Mole fraction 5-HT_3B_{Y129S}		Family FRET	Fluorescence intensity		
meCFP	meYFP	meCFP	meYFP	efficiency (%)	ratio (meCFP/meYFP)	[A]/[B_{Y129S}]	*N*
0.25			0.75	25.4 ± 0.3	0.309 ± 0.083	1.76 ± 0.51	13
	0.25	0.75		37.2 ± 0.9	0.100 ± 0.010		20

Table 3.6 5-HT_3AB_{Y129S} membrane-sheet fluorescence data for A and B subunits. All values are reported as mean ± standard error.

Because heterozygotes for the B subunit allele (one 129Y, one 129S) occur in >30% of many human populations (32), we investigated the relative efficiency of incorporating the two variant B subunits, when both are expressed simultaneously. In the conceptually simplest experiments (Table 3.7), we directly compared the plasma membrane subunit ratios of tagged Y129 B (also called simply B) subunits and tagged B_{Y129S} subunits when those cDNAs were transfected at equal amounts, along with labeled A subunit cDNAs. We found a [B]/B_{Y129S} ratio of 0.86 ± 0.12. Twin FRET efficiencies between coassembled B and B_{Y129S} subunits (17–19%) are near those between coassembled B and B subunits (18%) (Figure 3.6, *D* and Table 3.7).

Mole fraction 5-HT_3A		Mole fraction 5-HT_3B_{Y129S}		Family FRET	Fluorescence intensity		
meCFP	meYFP	meCFP	meYFP	efficiency (%)	ratio (meCFP/meYFP)	[A]/[B_{Y129S}]	*N*
0.25			0.375	12.4 ± 0.2	0.466 ± 0.049	2.66 ± 0.37	19
	0.25	0.375		36.0 ± 0.5	0.066 ± 0.006		20

Table 3.7 5-HT_3AB_{Y129S} membrane-sheet FIR data for A and B subunits. All values are reported as mean ± standard error. All conditions contain 0.375 mol fraction unlabeled 5-HT_3B.

In another experiment (Table 4.8), untagged B subunits and tagged B_{Y129S} subunits were expressed at equal cDNA amounts, along with tagged A subunits. We measured a plasma membrane [A]/B_{Y129S} subunit ratio of 2.66 ± 0.37, implying that B_{Y129S} subunits are 1.11 fold more abundant than the value of 3 expected if the two B subunit variants incorporated with equal efficiency in A_3B_2 receptors. Family FRET experiments gave additional information. With B_{Y129S}-meYFP as acceptor, we measured

a FRET efficiency of 12.4 ± 0.2%, as expected if each receptor has roughly half as many B-acceptors. With B_{Y129S}-meCFP as donor, we measured a FRET efficiency like that in previous experiments, suggesting that, as usual, each B subunit donor resides in a receptor with three A subunit acceptors.

Mole fraction 5-HT_3B		Mole fraction 5-HT_3B_{Y129S}		Twin FRET	Fluorescence intensity		
meCFP	meYFP	meCFP	meYFP	efficiency (%)	ratio (meCFP/meYFP)	[B]/[B_{Y129S}]	*N*
0.375			0.375	17.2 ± 0.3	0.104 ± 0.007	0.86 ± 0.10	16
	0.375	0.375		19.4 ± 0.5	0.140 ± 0.013		16

Table 3.8 5-HT_3A(BY129 and BS129) membrane-sheet fluorescence data. All values are reported as mean ± standard error. All conditions contain 0.25 mol fraction unlabeled 5-HT_3A.

Thus, the FIR experiments show a consistent pattern. When the two subunit variants are expressed simultaneously, the B_{Y129S} subunit incorporates into assembled plasma membrane 5-HT_3AB receptors in a manner slightly (1.11–1.14 fold) more efficient than that of the B subunit.

3.5 DISCUSSION

These measurements provide a robust determination of subunit stoichiometry for a Cys-loop receptor in the plasma membrane. The data arise from combining several techniques, including isolation of plasma membrane sheets (23), FIR measurements (26, 27, and 28), FRET measurements, and the placement of fluorescent proteins in the M3-M4 loop of Cys-loop receptors while conserving most aspects of receptor function (24 and 25). Heteromeric receptors formed from subunits containing fluorescent proteins display minimally perturbed serotonin EC_{50} values and Hill coefficients in HEK293T

cells (Figure 3.1; Table 3.1).

In whole cells, retention of the receptor subunits in the endoplasmic reticulum complicated the characterization of assembled receptors on the plasma membrane. In particular, subunit ratios determined by various approaches are strongly dependent on cDNA transfection ratios. This suggests that unassembled and partially assembled subunits in the ER dominate the calculation, as might be expected given the observed subunit ER retention (Figure 3.2). We also observe an overabundance of the A subunit relative to its cDNA proportion, which is likely due to the previously reported endoplasmic reticulum-associated degradation of the B subunit (35).

To circumvent this problem, the membrane was isolated by glass adhesion and mechanical shearing (Figure 3.2) (35 and 36). Following this procedure, the appearance of ER marker is sharply reduced, while patches of membrane-containing receptor termed "membrane sheets" remain. All efforts to characterize the stoichiometry of receptors employed membrane sheets.

FIR were constructed for each membrane sheet using FRET-corrected fluorescence intensities. Average values were calculated for each pairing of fluorescent protein and receptor subunit at each cDNA transfection ratio (Tables 3.2 and 3.3; Figure 3.4). The relative amount of each subunit was then extracted by Equation 3.4. Studies of membrane sheets are rather consistent in their support of an A_3B_2 subunit ratio (Figure 3.4). The FIR at 0.5 mol fraction 5-HT_3A is, however, significantly different from the expected value for this stoichiometry. There are two possible explanations:

1. This deviation could arise from a small population of homomeric 5-HT_3A

receptors. This is supported by the whole-cell subunit ratio at this transfection condition, which shows nearly four A subunits per B subunit expressed. While a monophasic dose-response curve for serotonin is seen at this transfection ratio (Figure 3.1), the markedly higher single channel conductance of the 5-HT_3AB receptor (16–30 pS versus sub-pS for 5-HT_3A) allows it to obscure even moderate proportions of homomeric receptor (7).

2. The membrane-sheet preparation could retain a small amount of intracellular receptors, perhaps in organelles, again distorting the measurements (Figure 3.1).

FIR measurements do not formally rule out the possibility that the data arise in part from isolated groups of A subunits and B subunits, because the groups would be separated by less than the resolution of the microscope. FRET measurements, however, present the advantage that the FRET efficiencies depend on donor-acceptor interactions within assembled pentamers.

The family FRET efficiencies between receptor subunits within these membrane sheets were determined for various ratios of transfected subunit cDNA by monitoring DRAP (Figure 3.5, *A–C*). Unlike those in whole cells, the FRET efficiencies in membrane sheets are nearly independent of subunit cDNA transfection ratio (Table 3.2; Figure 3.5, *D* and *E*). This supports the contention of the FIR measurements that membrane sheets are enriched in a single population of assembled membrane receptors.

The FRET efficiency of 5-$HT_3A_{meYFP}B_{meCFP}$ was 1.18–1.34 fold (average of 1.24 fold) greater than that for the opposite pairing of fluorescent protein and receptor

subunit. Previous theoretical and experimental studies on other members of the Cys-loop receptor family have determined that this difference in FRET efficiency is consistent with a receptor stoichiometry of A_3B_2 (Figure 3.7) (24 and 30).

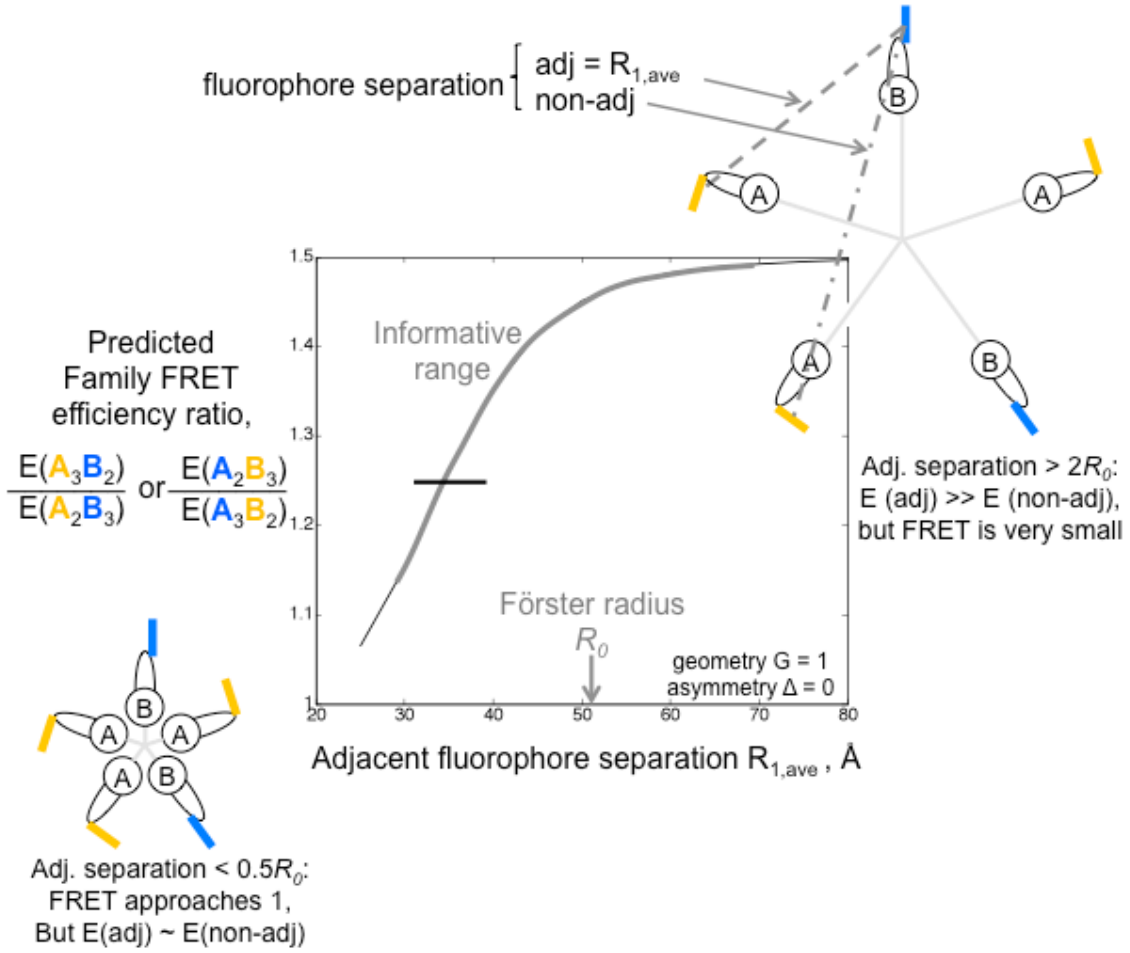

Figure 3.7 A schematic interpretation of family FRET measurements, based on the theory and simulations of Ref (30). The 5-HT_3AB receptor is depicted with A_3B_2 stoichiometry; the A_2B_3 stoichiometry is not depicted. Each A subunit has a **YFP** acceptor, and each B subunit has a **CFP** donor fused into the M3-M4 cytoplasmic loops. The average separation between adjacent (adj) fluorophores is termed $R_{1,ave}$ in Ref (30); this parameter varies along the X-axis. The Y-axis shows that family FRET efficiency, $E(A_{YFP}B_{CFP})$ for the A_3B_2 stoichiometry, always exceeds $E(A_{CFP}B_{YFP})$ for the A_3B_2 stoichiometry. The Förster radius R_0 is ~ 52 Å for this fluorophore pair.

These analyses depend on the ratio of donors/acceptors imposed by a pentameric receptor and the proportion of couplings between adjacent/nonadjacent receptor subunits. In its simplest form, the theory simulates a regular planar pentagon that has radially disposed fluorophore dipoles. Departures from this structure are described by parameters termed geometry/coplanarity G, and asymmetry Δ. Ref (30) presents simulations over ranges of G and Δ; for the simulations presented here, G and Δ are set to 1 and 0, respectively, to represent a regular planar pentagon.

For all reasonable values of $R_{1,ave}$, G and Δ, FRET efficiency for the A_3B_2 stoichiometry, $E(A_{YFP}B_{CFP})$, exceeds that for A_2B_3, $E(A_{YFP}B_{CFP})$, by a factor of 1.1 to 1.4. For fluorophore separations < $0.5R_0$, E approaches 1, but E for an adjacent pair only slightly exceeds E for a non-adjacent pair; this vitiates accurate measurements. For fluorophore separations > $2R_0$, E for an adjacent pair >> E for a non-adjacent pair, but the E values become unmeasurably small. This again vitiates accurate data. Therefore FRET measurements can distinguish the two stoichiometries, if $0.6R_0$ < the fluorophore separation < $1.4R_0$. The structures of cytoplasmic loops are not known. Structural data for the extracellular binding domains and transmembrane domains of Cys-loop receptor shows that homologous residues on adjacent subunits are separated by 5 to 40 Å. Fluorescent proteins have a diameter of 25 Å, precluding a closer approach of the fluorophores. Because we do not know G and Δ, more specific inferences cannot be made about the size / shape of the M3-M4 loops, or about the fluorophore separation $R_{1,ave}$.

The heavy horizontal line in Figure 4.7 shows the average ratio determined in this study, 1.24 (Figure 3.5). Because this value exceeds 1, the data are compatible with a stoichiometry of A_3B_2. This compatibility, not a value for the fluorophore separation, is

the major conclusion of this section.

The FRET measurements present the disadvantage that conclusions cannot be made about the actual physical distance between the fluorophores, because one does not know many factors, including the subunit order, dipole orientation, departures from pentameric symmetry, and coplanarity of the fluorophores within the M3–M4 loops. The measured FRET efficiencies would be compatible with a wide range of assumptions about these parameters, if adjacent subunits have a fluorophore separation of 30–45 Å. This distance is broadly consistent with known Cys-loop receptor structures (30).

Further support that the membrane sheets correspond to purified plasma membrane containing assembled receptors is found by analyzing the effect of acceptor photobleaching on the calculated subunit ratios. The observed difference in FRET efficiencies between the two pairs of fluorescent proteins and receptor subunits described earlier can be used to generate a correction factor, d_0 (Equation 3.6). The value d_0 can then be used to predict the direction and magnitude of the change in calculated subunit ratio upon acceptor photobleaching (Equation 3.7). This prediction will fail if loose or partially assembled subunits sway the subunit ratio without FRET, or if they contribute inordinately to FRET by aggregating, as is observed in whole cells (Table 3.4). In membrane sheets the correction factor correctly predicts subunit ratios under every condition (Table 3.5).

Additional information about stoichiometry and subunit order is found in twin FRET experiments on membrane sheets (Figure 3.6). With this technique, the FRET between two subunits of the same subtype is monitored. The existence of twin FRET between A subunits, and in another preparation between B subunits, is consistent with a

receptor stoichiometry containing at least two A subunits and at least two B subunits. The markedly higher efficiency of the FRET between A subunits, compared to that between B subunits, suggests that most individual 5-HT_3AB receptor molecules have an A-A subunit interface but no adjacent B subunits. Pentameric receptors with an A_3B_2 stoichiometry, as suggested by FIR and FRET experiments, must contain at least one A-A subunit interface.

We can provide a more-quantitative interpretation of the twin FRET efficiencies in light of previous theoretical and experimental studies on $\alpha_4\beta_2$ nicotinic acetylcholine receptors (24). In $\alpha_4\beta_2$ receptors, known subunit stoichiometries and known subunit orders on the plasma membrane can be generated by varying cDNA transfection ratios. In a receptor with two α_4 subunits, they are nonadjacent, and in a receptor with two β_2 subunits, they too are nonadjacent. The twin FRET ratio between adjacent and nonadjacent subunits is 1.80 ± 0.21, nearly identical to that found here (1.81 ± 0.10) for A twin FRET versus B twin FRET efficiencies. The agreement between these two analogous experiments on Cys-loop receptors suggests that the 5-HT_3AB receptor has subunit order of A-A-B-A-B, that is, one lacking a B-B interface and analogous to an α4-α4-β2-α4-β2 nAChR. This order, in which A-B assembly precludes B-B interactions, is intuitively consistent with previous knowledge that B subunits assemble and traffic to the membrane only upon coexpression with the A subunit.

A synonymous polymorphism in the HTR3B gene results in either the more common allele, encoding tyrosine 129, or a modestly less common allele encoding serine. The serine allele is linked to several disorders, including major depression and bipolar affective disorder (32, 33, and 34). While the serine allele increases 5-HT-induced

responses by extending the duration of channel opening (32, 33, and 34), its complete effects on channel function remain poorly defined. Because the polymorphic residue lies on a β-strand just below the proposed orthosteric ligand-binding site where it may project into the inter-subunit space, we considered the possibility that the side chain affects heteromeric receptor assembly. The 5-HT_3AB receptors containing only the B_{Y129S} subunit, however, display a subunit ratio and FRET efficiencies consistent with those observed for the more common B subunit variant (Figure 3.4; Figure 3.5, *D* and *E*). Thus, the B_{Y129S} subunit's profoundly altered gating characteristics (32, 33, and 34) occur within the usual A_3B_2 receptor structure.

Heterozygotes for the B subunit common allele (one 129Y, one 129S) occur in >30% of many human populations (32), prompting additional experiments to study the 5-HT_3AB receptors that would be produced in a heterozygote. We directly compared the efficiency of incorporation of the common and minor variant B subunit by transfecting cells with the A subunit cDNA plus a mixture of cDNAs for these two B subunits. Under the conditions of our experiments, two types of FIR data show that 5-HT_3B-Y129S subunit incorporates slightly (1.11–1.14 fold) more efficiently than the 5-HT_3B-Y129 subunit (Table 3.4). In an individual pentamer containing both B subunit alleles, FRET efficiencies between the two B subunits suggest that this heterozygote pentamer has the same stoichiometry and subunit order as a pentamer containing only major alleles of the B subunit (Figure 3.6, *D* and Table 3.7).

Our experiments perform a quantitative analysis of heteropentameric receptors with only two types of subunits. They require modest equipment and minimal assumptions. The methods do require moderately high levels of plasma membrane

protein density, probably >100/μm^2. In future studies, the membrane-sheet isolation procedure will allow more precise information on Cys-loop receptors with more complex compositions in the plasma membrane; such receptors would include nAChR, $GABA_A$, and some invertebrate Cys-loop receptors. This can be accomplished through the accumulation of pairwise subunit relative abundances or through employing modern available fluorophores, and modern spectrally resolved microscopes, that enable one to detect three fluorophores in a given membrane sample. One can readily permute fluorophores among three subunit types, leading to six FIR experiments. This would provide redundant, consistent determinations of subunit ratios.

Previous reports have shown how pairwise family FRET experiments provide qualitative proof that individual pentameric receptors contain three types of nAChR subunits (α4β2β3, α4α6β2, α6β2β3) or four types of nAChR subunits (α4, α6, β2, β3) (37). In twin FRET experiments, the β3 subunit, where present, displays near-zero twin FRET and therefore exists as only one copy per pentamer. In contrast, the other tested subunits have >1 copy in at least some individual nAChR molecules (37). It would therefore be possible to determine subunit ratios, stoichiometry, and order in pentameric Cys-loop receptors containing three, four, or even five (38) subunit types. Thus, the straightforward combination of membrane-sheet isolation, FIR, family FRET, and twin FRET is a generally promising procedure for determining subunit ratios, stoichiometry, and subunit order of proteins on the plasma membrane.

3.5.1 Conclusions

Previous reports have supported two different possible stoichiometries for the 5-HT_3AB receptor. In this work, we have utilized a method to isolate plasma membrane

sheets containing assembled receptors and used this to determine the stoichiometry of the 5-HT_3AB receptor by fluorescence methods: FIR, family FRET, and twin FRET. Our strongest, non-model-dependent conclusion arises from FIR, which shows an A_3B_2 subunit ratio. Family FRET and twin FRET efficiencies are also consistent with an A_3B_2 stoichiometry.

3.6 ACKNOWLEDGEMENTS

The authors thank Rahul Srinivasan, Kristina N. Daeffler, and Ethan B. Van Arnam for technical assistance and helpful discussion.

This work was supported by grants (No. NS034407, No. DA017279, and No. AG033954) from the National Institutes of Health, Bethesda, MD.

3.7 REFERENCES

1. Lummis, S. C. 2012. 5-HT_3 receptors. J. Biol. Chem. 287:40239– 40245.
2. Thompson, A. J., H. A. Lester, and S. C. Lummis. 2010. The structural basis of function in Cys-loop receptors. Q. Rev. Biophys. 43:449–499.
3. Walstab, J., G. Rappold, and B. Niesler. 2010. 5-HT_3 receptors: role in disease and target of drugs. Pharmacol. Ther. 128:146–169.
4. Jensen, A. A., P. A. Davies, . , K. Krzywkowski. 2008. 3B but which 3B, and that's just one of the questions: the heterogeneity of human 5- HT_3 receptors. Trends Pharmacol. Sci. 29:437–444.
5. Davies, P. A., M. Pistis, . , E. F. Kirkness. 1999. The 5-HT_3B subunit is a major determinant of serotonin-receptor function. Nature. 397:359–363.
6. Niesler, B., J. Walstab, . , M. Brüss. 2007. Characterization of the novel human serotonin receptor subunits 5-HT_3C,5-HT_3D, and 5-HT_3E. Mol. Pharmacol. 72:8–17.
7. Thompson, A. J., and S. C. Lummis. 2013. Discriminating between 5-HT_3A and 5-HT_3AB receptors. Br. J. Pharmacol. 169:736–747.
8. Hapfelmeier, G., C. Tredt, . , G. Rammes. 2003. Co-expression of the 5-HT_3B serotonin receptor subunit alters the biophysics of the 5-HT_3 receptor. Biophys. J.

84:1720–1733.
9. Stewart, A., P. A. Davies, . , T. G. Hales. 2003. Introduction of the 5- HT_3B subunit alters the functional properties of 5-HT_3 receptors native to neuroblastoma cells. Neuropharmacology. 44:214–223.
10. Hu, X. Q., and R. W. Peoples. 2008. The 5-HT_3B subunit confers spontaneous channel opening and altered ligand properties of the 5-HT_3 receptor. J. Biol. Chem. 283:6826–6831.
11. Das, P., and G. H. Dillon. 2003. The 5-HT_3B subunit confers reduced sensitivity to picrotoxin when co-expressed with the 5-HT_3A receptor. Brain Res. Mol. Brain Res. 119:207–212.
12. Baptista-Hon, D. T., T. Z. Deeb, . , T. G. Hales. 2012. The 5-HT_3B subunit affects high-potency inhibition of 5-HT_3 receptors by morphine. Br. J. Pharmacol. 165:693–704.
13. Kelley, S. P., J. I. Dunlop, . , J. A. Peters. 2003. A cytoplasmic region determines single-channel conductance in 5-HT_3 receptors. Nature. 424:321–324.
14. Livesey, M. R., M. A. Cooper, . , J. A. Peters. 2008. Structural determinants of Ca^{2+} permeability and conduction in the human 5-hydroxytryptamine type 3A receptor. J. Biol. Chem. 283:19301–19313.
15. Peters, J. A., M. A. Cooper, . , J. J. Lambert. 2010. Novel structural determinants of single channel conductance and ion selectivity in 5-hydroxytryptamine type 3 and nicotinic acetylcholine receptors. J. Physiol. 588:587–596.
16. Maricq, A. V., A. S. Peterson, . , D. Julius. 1991. Primary structure and functional expression of the $5HT_3$ receptor, a serotonin-gated ion channel. Science. 254:432–437.
17. Holbrook, J. D., C. H. Gill, . , M. J. Gunthorpe. 2009. Characterization of 5-HT_3C, 5-HT_3D and 5-HT_3E receptor subunits: evolution, distribution and function. J. Neurochem. 108:384–396.
18. Kapeller, J., D. Mo¨ller, . , B. Niesler. 2011. Serotonin receptor diversity in the human colon: expression of serotonin type 3 receptor sub- units 5-HT_3C, 5-HT_3D, and 5-HT_3E. J. Comp. Neurol. 519:420–432.
19. Barrera, N. P., P. Herbert, . , J. M. Edwardson. 2005. Atomic force microscopy reveals the stoichiometry and subunit arrangement of 5-HT_3 receptors. Proc. Natl. Acad. Sci. USA. 102:12595–12600.
20. Lochner, M., and S. C. Lummis. 2010. Agonists and antagonists bind to an A-A interface in the heteromeric 5-HT_3AB receptor. Biophys. J. 98:1494–1502.
21. Thompson, A. J., K. L. Price, and S. C. Lummis. 2011. Cysteine modification reveals which subunits form the ligand binding site in human heteromeric 5-HT_3AB receptors. J. Physiol. 589:4243–4257.
22. Price, K. L., and S. C. Lummis. 2005. FlexStation examination of 5-HT_3 receptor function using Ca^{2+}- and membrane potential-sensitive dyes: advantages and potential problems. J. Neurosci. Methods. 149:172–177.
23. Perez, J. B., K. L. Martinez, . , H. Vogel. 2006. Supported cell-membrane sheets for functional fluorescence imaging of membrane proteins. Adv. Funct. Mater. 16:306–312.
24. Son, C. D., F. J. Moss, . , H. A. Lester. 2009. Nicotine normalizes intracellular subunit stoichiometry of nicotinic receptors carrying mutations linked to autosomal

dominant nocturnal frontal lobe epilepsy. Mol. Pharmacol. 75:1137–1148.
25. Nashmi, R., M. E. Dickinson, . , H. A. Lester. 2003. Assembly of a4b2 nicotinic acetylcholine receptors assessed with functional fluorescently labeled subunits: effects of localization, trafficking, and nicotine-induced upregulation in clonal mammalian cells and in cultured midbrain neurons. J. Neurosci. 23:11554–11567.
26. Zheng, J., and W. N. Zagotta. 2004. Stoichiometry and assembly of olfactory cyclic nucleotide-gated channels. Neuron. 42:411–421.
27. Staruschenko, A., E. Adams, . , J. D. Stockand. 2005. Epithelial Na^+ channel subunit stoichiometry. Biophys. J. 88:3966–3975.
28. Grasser, E., B. Steinecker, . , W. Schreibmayer. 2008. Subunit stoichiometry of heterologously expressed G-protein activated inwardly rectifying potassium channels analyzed by fluorescence intensity ratio measurement. Pflugers Arch. 455:1017–1024.
29. Massoura, A. N., T. J. Dover, . , N. M. Barnes. 2011. The identification of N-glycosylated residues of the human 5-HT_3B receptor subunit: importance for cell membrane expression. J. Neurochem. 116:975–983.
30. Srinivasan, R., C. I. Richards, . , H. A. Lester. 2012. Förster resonance energy transfer (FRET) correlates of altered subunit stoichiometry in Cys-loop receptors, exemplified by nicotinic α4β2. Int. J. Mol. Sci. 13:10022–10040.
31. Srinivasan,R. ,R. Pantoja, . , H. A. Lester. 2011. Nicotine up-regulates α4β2 nicotinic receptors and ER exit sites via stoichiometry-dependent chaperoning. J. Gen. Physiol. 137:59–79.
32. Krzywkowski, K., P. A. Davies, . , A. A. Jensen. 2008. High-frequency HTR3B variant associated with major depression dramatically augments the signaling of the human 5-HT3AB receptor. Proc. Natl. Acad. Sci. USA. 105:722–727.
33. Hammer, C., S. Cichon, . , B. Niesler. 2012. Replication of functional serotonin receptor type 3A and B variants in bipolar affective disorder: a European multicenter study. Transcult. Psychiatry. 2:e103.
34. Walstab, J., C. Hammer, . , B. Niesler. 2008. Naturally occurring variants in the HTR3B gene significantly alter properties of human heteromeric 5-hydroxytryptamine-3A/B receptors. Pharmacogenet. Genomics. 18:793–802.
35. Boyd, G. W., P. Low, . , C. N. Connolly. 2002. Assembly and cell surface expression of homomeric and heteromeric 5-HT_3 receptors: the role of oligomerization and chaperone proteins. Mol. Cell. Neurosci. 21:38–50.
36. Ilegems, E., H. M. Pick, . , H. Vogel. 2004. Noninvasive imaging of 5-HT_3 receptor trafficking in live cells: from biosynthesis to endocytosis. J. Biol. Chem. 279:53346–53352.
37. Drenan, R. M., R. Nashmi, ., H. A. Lester. 2008. Subcellular trafficking, pentameric assembly, and subunit stoichiometry of neuronal nicotinic acetylcholine receptors containing fluorescently labeled α6 and β3 subunits. Mol. Pharmacol. 73:27–41.
38. Boulin, T., M. Gielen, ., J. L. Bessereau. 2008. Eight genes are required for functional reconstitution of the *Caenorhabditis elegans* levamisole-sensitive acetylcholine receptor. Proc. Natl. Acad. Sci. USA. 105:18590–18595.

Chapter 4

Allosteric Activation of the 5-HT_3AB Receptor by mCPBG*

4.1 ABSTRACT

The 5-HT_3AB receptor contains three A and two B subunits, likely in an A-A-B-A-B order. However serotonin function at the 5-HT_3AB receptor has been shown to depend solely on the A-A interface present in the homomeric receptor. Using mutations at sites on both the primary (E122) and complementary (Y146) faces of the B subunit, we demonstrate that mCPBG, a 5-HT_3 selective agonist, is capable of binding and activating the 5-HT_3AB receptor at all five subunit interfaces of the heteromer. Further, mCPBG is capable of allosterically modulating the activity of serotonin from these sites. While these five binding sites appear functionally degenerate in terms of mCPBG EC_{50}, we uncover subtle differences in heteromeric binding site sensitivity to mutation. We also find that the A-A interface appears to contribute disproportionately to the efficacy of 5-HT_3AB receptor activation. We also investigate a potential cation-π interaction between mCPBG and F226 of the B subunit in the 5-HT_3AB receptor.

4.2 INTRODUCTION

5-HT_3 receptors are excitatory ligand-gated ion channels of the Cys-loop (pentameric) receptor super-family that also includes nicotinic acetylcholine (nAChR), glycine and $GABA_A$ receptors (1). The 5-HT_3 family is principally composed of

---

** This work was done in collaboration with Matthew Davis, who performed computations to generate interaction energies between guanidinium and fluorinated benzenes.*

homomeric 5-HT_3A, and heteromeric receptors containing some combination of the A subunit and either B, C, D, or E subunits (2-4). The best studied heteromeric receptor is 5-HT_3AB. In addition to contributing to the fundamental role of 5-HT_3 in the gut, the 5-HT_3AB receptor is widely expressed in the brain and has been implicated in numerous salutary and pathological processes (5, 6).

As ligand binding occurs at the interface of adjacent subunits, heteromeric receptors present the opportunity for novel ligand binding sites. This potential complexity might afford one signaling molecule, serotonin (5-HT), the ability to elicit diverse responses depending on the repertoire of receptors present (7). The 5-HT_3AB receptor contains three A and two B subunits, likely in an A-A-B-A-B order (8). Thus, there are three potential types of binding sites in the 5-HT_3AB receptor: I., the single A-A interface also found in the homomeric receptor, II., the two heteromeric binding sites with the B subunit as the primary face, and III., the two heteromeric binding sites with the B subunit as the complementary face (Figure 1).

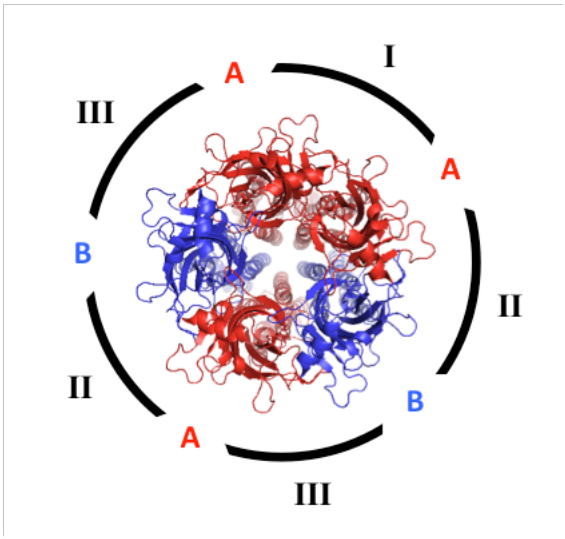

Figure 4.1 Top-down view of 5-HT_3AB receptor based on GluCl crystal structure (PDB: 3RHW). Three types of binding sites are present in the heteromeric receptor: I., A subunit as both principal and complementary faces, II., B subunit as principal and A subunit as complementary, and III., A subunit as principal and B subunit as complementary.

However, serotonin function at the 5-HT_3AB receptor depends solely on the type I binding site present in the homomeric receptor (9-11). Multiple studies have capitalized on the wealth of mutagenic data on homomeric receptors to identify crucial, non-conserved residues at both the principal and complementary faces of the B subunit that impact 5-HT function (9, 11). Combined, these studies demonstrate that only one serotonin molecule binds to and activates the 5-HT_3AB receptor, a finding predicted by modeling of receptor kinetic parameters (12). This makes the 5-HT_3AB receptor unusual in the Cys-loop super-family, where multiple binding sites predominate.

m-chlorophenyl biguanide (mCPBG) is a 5-HT_3 selective agonist (13). Unlike 5-HT, whose amine forms a cation-π interaction at W178 (human subunit numbering, akin to W183 in the mouse numbering of Chapter 1, and aligning with TrpB in the nAChR) (14) and whose hydroxyl forms a hydrogen bond at E124 (E129 in mouse numbering, and aligning with TyrA in the nAChR) (15), a satisfactory binding model of mCPBG has not been enumerated. While mCPBG forms no interaction at W178, it does rely upon E124 for the initiation of channel gating (16). In the face of this relative paucity of binding information, it is not readily apparent that mCPBG should be incapable of acting at type II and type III binding sites. Indeed, a molecule has already been identified that is functional at type III binding sites (17, 18).

Here we demonstrate that, unlike serotonin, mCPBG is capable of binding and activating the 5-HT_3AB receptor at all three types of binding site present in the heteromer. Through mutagenesis, we identify crucial residues on the B subunit, corresponding to both principle and complementary faces, and thus bind site types II and III, on which this activity is dependent. Further, we show that mCPBG is capable of

allosterically modulating the activity of serotonin from type II binding sites, demonstrating the potential for future development of 5-HT_3AB ligands with benzodiazapine-like properties.

4.3 RESULTS & DISCUSSION

4.3.1 5-HT and mCPBG behave differently at wild type 5-HT_3AB receptors

Serotonin activates 5-HT_3A receptors with a 3.4 μM EC_{50} and a high Hill coefficient (n^H), indicating a high level of cooperativity (Table 4.1). Though it need not be the case, this measure of cooperativity has tracked with the level of ligand binding in other Cys-loop receptors (19, 20). At the heteromeric AB receptor, both the EC_{50} and Hill coefficient markedly change, with a 7 fold decrease in ligand sensitivity and a loss of cooperativity reflected in a decreased Hill coefficient from 2.8 to 1.1 (Figure 4.2A). These data are consistent with the finding that 5-HT likely acts at only the single type I binding site in the AB receptor.

mCPBG has a similar potency to 5-HT (3.8 μM) at the homomeric receptor along with a similarly high Hill coefficient (n^H = 3.0) (Table 4.2). Unlike 5-HT, both of these measures remain practically unchanged in the AB receptor (EC_{50} = 2.8μM, n^H = 2.5), suggesting that mCPBG may retain the ability to bind the receptor at type II and type III binding sites (Figure 4.2B). Meanwhile, the relative efficacy (ε) of mCPBG surges from 0.85 to 2.75, as it transitions from a strong partial agonist to a super-agonist (Table 4.3; Figure 4.2C). This is consistent with a drop in the absolute efficacy of 5-HT due to its reduction to a single binding site in the heteromeric receptor.

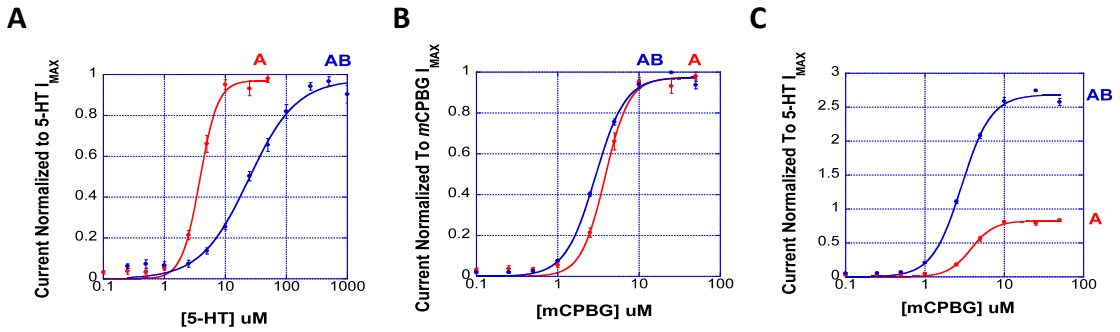

Figure 4.2 5-HT and mCPBG dose-response data for wild type 5-HT$_3$A and 5-HT$_3$AB receptors. (A) 5-HT dose-response data for wild type 5-HT$_3$A and 5-HT$_3$AB receptors with current normalized to the maximum elicited 5-HT current. (B) mCPBG dose-response data for wild type 5-HT$_3$A and 5-HT$_3$AB receptors with current normalized to the maximum elicited mCPBG current. (C) mCPBG dose-response data for wild type 5-HT$_3$A and 5-HT$_3$AB receptors with current normalized to the maximum elicited 5-HT current. 5-HT$_3$A data are shown in red and 5-HT$_3$AB data are shown in blue.

4.3.2 The 5-HT$_3$B subunit contributes to mCPBG activation of the 5-HT$_3$AB receptor

E124 of loop A on the principle side of the 5-HT$_3$A binding site plays a critical role in mCPBG activation. Mutation of E124 to glutamine has been shown to selectively ablate the ability of mCPBG to activate the 5-HT$_3$A receptor, converting mCPBG to a competitive antagonist (16). However, we find that the E124Q mutation in the A subunit of the heteromeric receptor, while highly deleterious, does not eliminate the ability of mCPBG to activate the 5-HT$_3$AB receptor (Figure 4.3). Relative efficacy drops sharply to 0.35 (Figure 4.3A, Table 4.3) and the Hill coefficient falls precipitously from 2.6 to 1.2 (Figure 4.3B, Tables 4.2), suggesting the elimination of functional ligand binding sites. As this mutation disrupts type I and type III binding sites, this remaining activation by mCPBG suggests that mCPBG acts at type II binding sites.

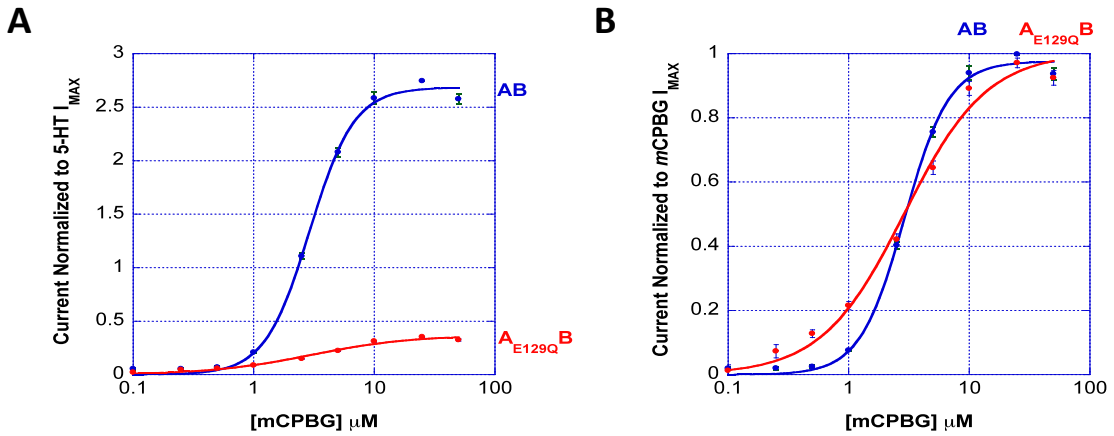

Figure 4.3 mCPBG dose-response data for 5-HT$_3$AB receptors bearing the E124Q mutation in the A subunit. (A) mCPBG dose-response data normalized to the maximum elicited 5-HT current. (B) mCPBG dose-response data normalized to the maximum elicited mCPBG current. 5-HT$_3$A data are shown in red and 5-HT$_3$AB data are shown in blue.

To determine if this difference in response between the A and AB receptors was due to ligand binding at the type II binding sites or to allosteric effects of the B subunit on the type I binding site, an experiment in which both agonists were applied was devised. First, an I_{max} dose of 5-HT was applied to AB receptors bearing the E124Q mutation in the A subunit. After 5-HT maximally opened the channel and saturated its binding sites, mCPBG was co-applied at its EC_{50}. Upon mCPBG addition a second wave of receptor opening corresponding to an additional 60 % beyond the 5-HT I_{max} was observed (ΔI_{max} = +60 ± 9 %, n = 18) (Figure 4.4A). This effect is only possible if mCPBG binds allosterically, increasing 5-HT efficacy. When the same experiment is performed with an I_{max} concentration of mCPBG, upon co-application the current sharply declines to approximately the relative efficacy of mCPBG alone (ΔI_{max} = -72 ± 2 %,

n = 20) (Figure 4.4B). This is consistent with mCPBG displacement of 5-HT at the type I binding site at higher concentrations.

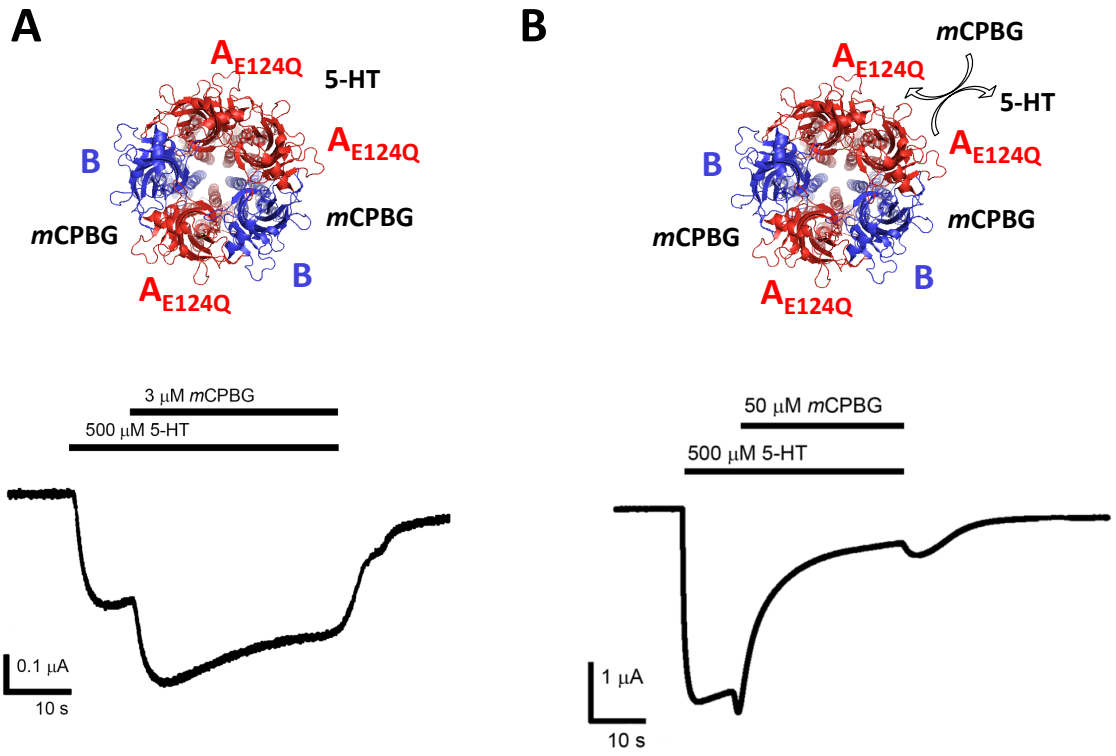

Figure 4.4 Dual Agonist Experiment on 5-HT$_3$AB receptors bearing the E124Q mutation in the A subunit. (A) Model of receptor binding by 5-HT and mCPBG and representative electrophysiology trace showing maximal 5-HT response followed by an additional 60 ± 9 % (n = 18) response upon addition of EC_{50} mCPBG. (B) Model of receptor ligation by 5-HT and mCPBG and representative electrophysiology trace showing maximal 5-HT response followed by a reduction in current by 72 ± 2 % (n = 20) upon addition of saturating mCPBG, whereupon mCPBG outcompetes 5-HT for binding at the A-A interface.

A Subunit	B subunit	EC_{50} (μM)	Fold Shift	n^H	# Cells
WT	-	3.4 ± 0.1	-	2.8 ± 0.1	10
E124Q	-	165 ± 9	48.5	1.9 ± 0.1	6
Y148A	-	185 ± 14	54.4	2.4 ± 0.3	5
WT	WT	24.1 ± 2.9	-	1.1 ± 0.1	7
E124Q	WT	141 ± 16	5.9	1.6 ± 0.2	6
Y148A	WT	300 ± 14	12.4	1.8 ± 0.1	7
WT	E122Q	15.5 ± 1.6	0.6	1.2 ± 0.1	5
WT	E122A	16.1 ± 2.5	0.7	1.0 ± 0.1	5
WT	Y146A	14.9 ± 0.9	0.6	1.2 ± 0.1	5
WT	E122Q Y146A	8.2 ± 0.6	0.3	1.4 ± 0.1	6
E124Q	E122Q	117 ± 10	4.9	1.5 ± 0.1	5
E124Q	E122A	197 ± 3	8.2	1.9 ± 0.1	5
E124Q	Y146A	178 ± 8	7.4	1.5 ± 0.1	9
E124Q	F236 F_1-Phe	150 ± 3	6.2	1.8 ± 0.1	5
E124Q	F236 F_3-Phe	139 ± 5	5.8	2.2 ± 0.1	5

Table 4.1 Serotonin functional data for 5-HT_3A and 5-HT_3AB receptors. Hill coefficient (n^H). Values are reported as mean ± standard error. Wild type (WT). No subunit supplied (-). Fold shift is reported relative to the wild type receptor of the same subunit composition.

A Subunit	B subunit	EC_{50} (μM)	Fold Shift	n^H	# Cells
WT	-	3.8 ± 0.2	-	3.0 ± 0.4	5
E124Q	-	NR			12
Y148A	-	24.7 ± 0.9	6.5	1.9 ± 0.1	6
WT	WT	2.8 ± 0.1	-	2.5 ± 0.3	7
E124Q	WT	3.0 ± 0.7	1.1	1.0 ± 0.2	10
Y148A	WT	11.2 ± 0.6	4	2.8 ± 0.4	7
WT	E122Q	2.3 ± 0.1	0.8	2.6 ± 0.4	5
WT	E122A	2.4 ± 0.1	0.9	2.2 ± 0.2	5
WT	Y146A	4.3 ± 0.3	1.5	2.1 ± 0.2	5
WT	F226 F_3-Phe	3.5 ± 0.3	1.3	1.6 ± 0.2	10
WT	E122Q Y146A	3.5 ± 0.1	1.3	2.2 ± 0.2	6
E124Q	E122Q	2.4 ± 0.4	0.9	1.2 ± 0.2	5
E124Q	E122A	SR			5
E124Q	Y146A	4.8 ± 0.7	1.7	1.5 ± 0.3	9
E124Q	F226 F_1-Phe	3.8 ± 0.2	1.4	1.5 ± 0.1	5
E124Q	F226 F_2-Phe	3.7 ± 0.3	1.3	1.5 ± 0.1	5
E124Q	F226 F_3-Phe	4.4 ± 0.3	1.6	1.4 ± 0.1	4

Table 4.2 mCPBG functional data for 5-HT_3A and 5-HT_3AB receptors. Hill coefficient (n^H) , Small Response (SR) refers to I_{max} < 100nA. No Response (NR) refers to I_{max} < 30nA. Values are reported as mean ± standard error. Wild type (WT). No subunit supplied (-). Fold shift is reported relative to the wild type receptor of the same subunit composition.

A Subunit	B Subunit	ε	# Cells
WT	-	0.85 ± 0.17	10
E124Q	-	< 0.01	10
Y148A	-	3.79 ± 0.37	7
WT	WT	2.75 ± 0.19	22
E124Q	WT	0.36 ± 0.04	10
Y148A	WT	10.6 ± 0.9	14
WT	E122Q	1.94 ± 0.12	19
WT	E122A	1.60 ± 0.14	11
WT	Y146A	2.18 ± 0.17	13
WT	F226 F_3-Phe	1.74 ± 0.23	12
WT	E122Q Y146A	1.58 ± 0.09	13
E124Q	E122Q	0.24 ± 0.02	13
E124Q	E122A	< 0.01	8
E124Q	Y146A	0.18 ± 0.03	9
E124Q	F226 F_1-Phe	0.13 ± 0.05	10
E124Q	F226 F_2-Phe	0.06 ± 0.01	5
E124Q	F226 F_3-Phe	0.05 ± 0.02	10

Table 4.3 5-HT_3A and 5-HT_3AB receptor relative efficacies of mCPBG (ε). Values are reported as mean ± standard error. Wild type (WT). No subunit supplied (-).

4.3.3 mCPBG binds to all five interfaces of the 5-HT$_3$AB receptor

Given the ability of mCPBG to compete at the orthosteric type I binding site, it was presumed that allosteric binding occurs at the equivalent location on B subunit-containing type II and type III binding sites. To determine if the B subunit could functionally contribute to the principal, complementary, or both faces of the potential binding site, mutants found to disrupt function in A subunits were introduced at the corresponding sites in the B subunit. E122Q (equivalent to E124 in the A subunit) was chosen for the principal face to probe type II binding sites.

Unfortunately, fewer crucial ligand interactions to the complementary face to probe type III binding are known (21). Previous studies demonstrated that Y148 on loop E of the A subunit (Y153 in mouse subunit numbering) is critical for both serotonin binding and gating of the homomeric receptor (22). Mutation of Y148 to alanine displays a loss of function for mCPBG as well, though less than that observed for 5-HT (Tables 4.1 and 4.2). The relative efficacy of mCPBG increases over 4 fold, suggesting that while this mutation affects mCPBG, it is more deleterious for serotonin function (Table 4.3). 5-HT$_3$AB receptors bearing Y148A in the A subunits show a similar pattern of effects. In the B subunit, serotonin is oblivious to mutation, leaving only the perturbation of mCPBG function, if mCPBG acts at type III binding sites.

5-HT$_3$AB receptors containing type II or type III binding site disrupting mutations were then assessed with both 5-HT and mCPBG. As 5-HT is found to be largely insensitive to B subunit mutations (Table 4.1), serotonin response serves as a control for proper folding and trafficking of the receptors.

While mCPBG EC_{50} remains unchanged for both mutant receptors, relative efficacy is significantly affected. mCPBG remains a super-agonist of slightly lower efficacy, 1.94 for E122Q (Type II disrupted) and 2.18 for Y146A (Type III disrupted) (Figure 4.5; Table 4.3). The lack of effect on mCPBG EC_{50} is expected if the mutations completely disrupt the binding sites that contain them while mCPBG is capable of opening the receptor, though less effectively, through the unaffected binding sites that remain. It is also possible that the apparent agonist efficacy at the receptor is decreased because the fraction of the response corresponding to the disrupted binding sites is shifted outside the observable window for mCPBG. Unfortunately, this would not take an enormous loss of function, as mCPBG appears to be a quite effective open channel blocker at concentrations above 100 μM (12).

The decrease in relative efficacy for the two mutations indicates that the B subunit is capable of functionally contributing to both faces of heteromeric binding sites. The similarity of the magnitude of the effect is consistent with the loss of two out of five possible binding sites in each case. As the number of remaining binding sites in either mutant receptor would still outnumber that of serotonin, it might be expected that mCPBG remains a super-agonist at the mutant receptors.

5-HT_3AB receptors containing both mutations in its B subunits show a relative efficacy that is still further decreased to 1.66, demonstrating that the two mutations are additive (Figure 4.5; Table 4.3). mCPBG is still a super-agonist at this receptor however, suggesting either that function is not completely disrupted at the binding sites that contain the mutations, or that the presence of the B subunit allosterically improves the relative efficacy of mCPBG activation through the A-A interface. In either case, the disruption of

all four B subunit containing binding sites is nearly an order of magnitude less disruptive than the disruption of three binding sites including the A-A interface. This suggests that the five binding sites do not contribute equally to mCPBG efficacy and that the A-A interface has a special importance.

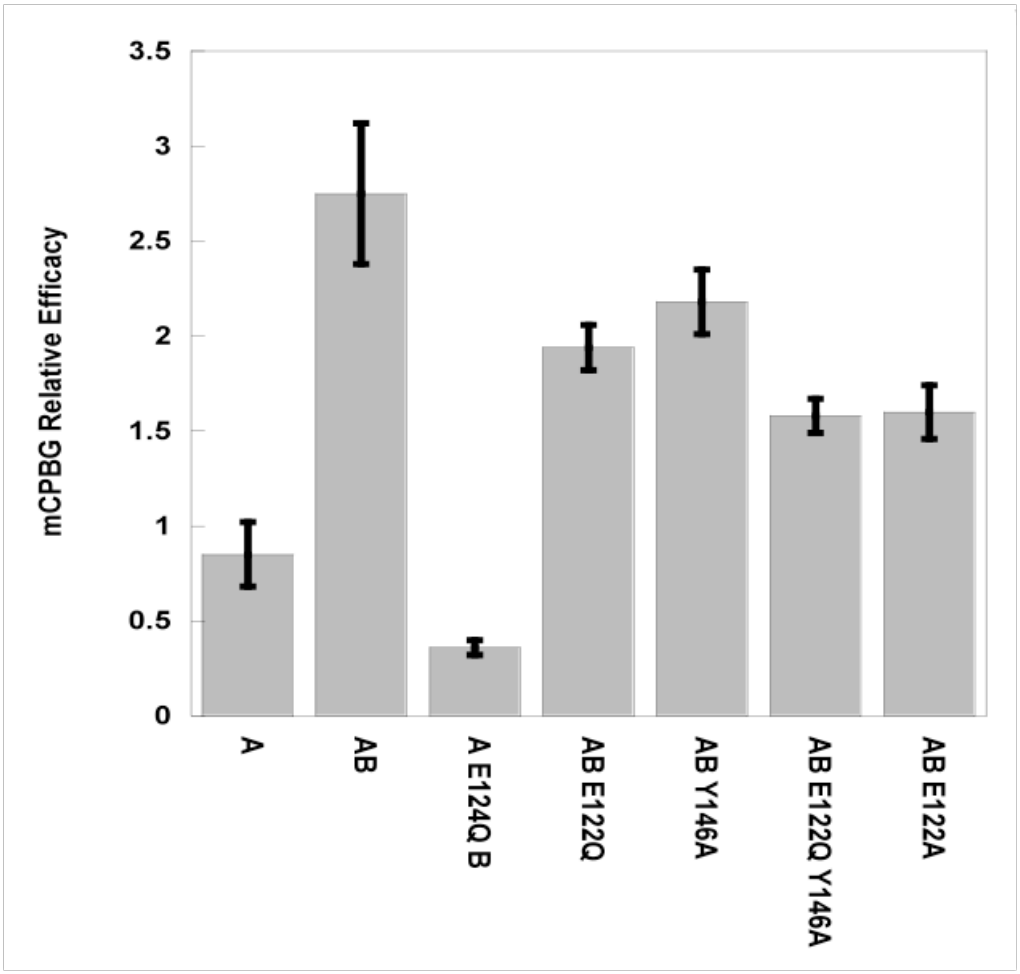

Figure 4.5 Relative Efficacies of mCPBG at 5-HT_3AB Receptor Mutants. All 5-HT_3AB receptors bearing mutations in the B subunits are significantly different ($p < 0.05$) than both the wild type receptor and 5-HT_3AB containing E124Q in the A subunit. 5-HT3AB bearing both E122Q and Y146A is significantly different ($p < 0.05$) from both single mutants. Values are depicted as the mean ± standard error.

4.3.4 Evidence for differences in heteromeric binding site organization

To test that the mutations are, in fact, completely disrupting function at the binding sites that contain them, heteromeric receptors in which the critical glutamate in every subunit (E124 in the A subunits and E122 in the B subunits) is mutated to glutamine were probed (disrupting all three binding site types). Unexpectedly, this quintuple mutant receptor is still responsive to mCPBG, with a relative efficacy only slightly worse than that of receptors with the mutation in the A subunit alone (disrupting types I and III) (Figure 4.6 and Table 4.3). Thus, it appears that there are subtle differences in the type II binding sites of the heteromeric receptor.

It may be puzzling why mutation to glutamine at E124 has such drastic effects, as glutamine retains a side chain oxygen capable of forming a hydrogen bond to the ligand. It may be that the glutamate to glutamine mutation has such drastic effects because the remaining side chain oxygen is pre-complexed with another residue in the homomeric receptor and thus unable to reposition to form ligand interactions. This might not be the case in a heteromeric receptor however, so the more drastic alanine mutation was made. 5-HT_3AB receptors with E122A in the B subunits (disrupting type I and type III binding sites) again showed no change in mCPBG EC_{50} but a large decrease in relative efficacy to 1.60, slightly worse than that for E122Q ($\varepsilon = 1.94$) (Figure 4.6; Tables 4.2 and 4.3). Heteromeric receptors bearing E124Q in the A subunits and E122A in the B subunits (disrupting all three binding site types) now show the expected destruction of mCPBG agonist activity ($\varepsilon < 0.01$), akin to E124Q mutation in the homomeric 5-HT_3A receptor (Figure 4.6; Table 4.3).

It appears that the type III binding site also behaves slightly differently with regard to mutation of E124. It would be expected based on the homomeric receptor that E124Q would destroy both the type I and type III binding sites. If so, the addition of Y146A in the B subunits (type III disrupting) should have no additional effect. This is not the case, however, as relative efficacy decreases from 0.36 to 0.18, suggesting that E124Q in the A subunit is not completely destroying the type III binding sites (Figure 4.6; Table 4.3).

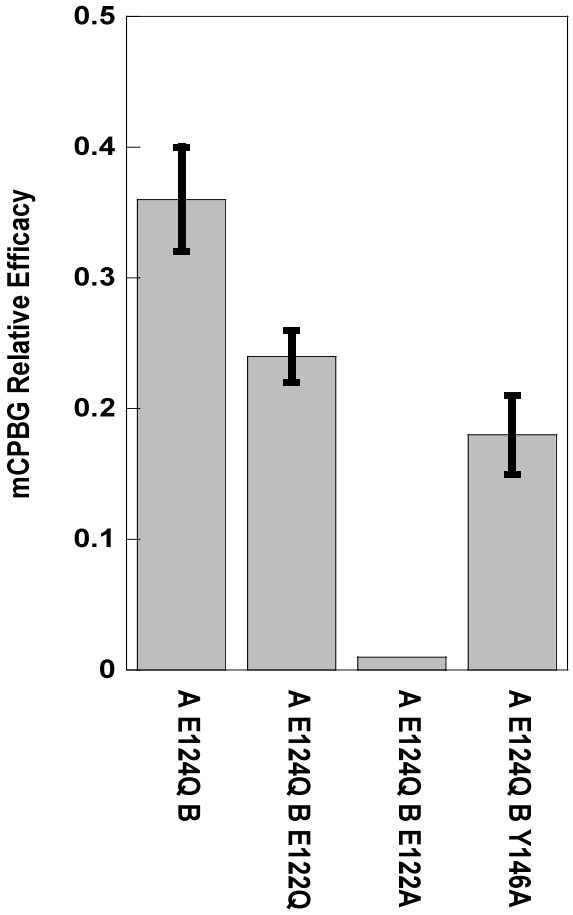

Figure 4.6 Relative efficacies of 5-HT_3AB receptors bearing mutations in both subunits. Addition of E122Q, E122A, or Y146A mutations to the B subunits show significant ($p < 0.05$) reductions in relative efficacy. Values are depicted as the mean ± standard error.

4.3.5 F226 of the B subunit (TyrC2) is important for mCPBG activation

mCPBG differs from serotonin in its interactions with the 5-HT_3A receptor. Unlike serotonin, it forms no cation-π interaction with W178 (TrpB) (16). Thus, it is not surprising that, unlike serotonin, mCPBG is not negatively affected by the absence of TrpB in the B subunit (I176). Given the ability of mCPBG to bind effectively at B subunit containing interfaces, the B subunit was scanned for residues capable of binding the positive charge of mCPBG. Of the five residues that constitute the "aromatic box" in the binding site of the prototypical Cys-loop receptor, only two remain in the B subunit: those that align with TrpD (W83) and TyrC2 (F226). As TrpD aromaticity has been found not to contribute to mCPBG or serotonin activation in the homomeric receptor, efforts were focused on TyrC2 (23).

F226 of the B subunit was considered promising, as previous studies of the 5-HT_3A receptor had suggested that TyrC2 (Y228) aromaticity was important for ligand binding; however, steric effects at the 4-position of the residue complicated interpretation (22). It was hoped that the phenylalanine present in the B subunit would simplify interpretation.

Fluorination of aromatic amino acids results in the depletion of electron density from the face of the side chain that may weaken or ablate the ability to form aromatic interactions (24). 5-HT_3AB receptors containing wild type A subunits and highly fluorinated phenylalanine residues at F226 of the B subunits show a loss of relative efficacy (ε = 1.74) and cooperativity (n^H = 1.6) as strong as that for any single mutation of the B subunit, including E122A (Table 4.2 and 4.3).

In order to simplify analysis, the E124Q mutation was introduced to the A subunit of the 5-HT_3AB receptor so that the intact binding sites would consist solely of B-A. Surprisingly, increasing fluorination of F226 does not affect mCPBG EC_{50}, suggesting that the site is not necessary for ligand binding (Table 4.2). Relative efficacy, however, is responsive to fluorination at F226, with F_1-Phe showing a large loss in efficacy ($\varepsilon = 0.13$) that is further weakened in F_2- and F_3-Phe, which are equivalent to each other ($\varepsilon = 0.06$; $\varepsilon = 0.05$, respectively) (Figure 4.7; Table 4.3). This loss of relative efficacy suggests that this site is important for activation of the receptor. This role is consistent with the residue's location on loop C, whose dynamics are thought to be critical for receptor activation (25, 26).

Unfortunately the lack of effect in EC_{50}, and the lack of further effect progressing from F_2- to F_3-Phe, is inconsistent with the trend in cation-π interaction energies computed using sodium as the positive charge (27). It may be that the large delocalized positive biguanide moiety of mCPBG behaves differently than sodium with regard to the changing electron density of the ring system upon higher fluorination, however, it is also possible that the effects observed are not electrostatic in nature.

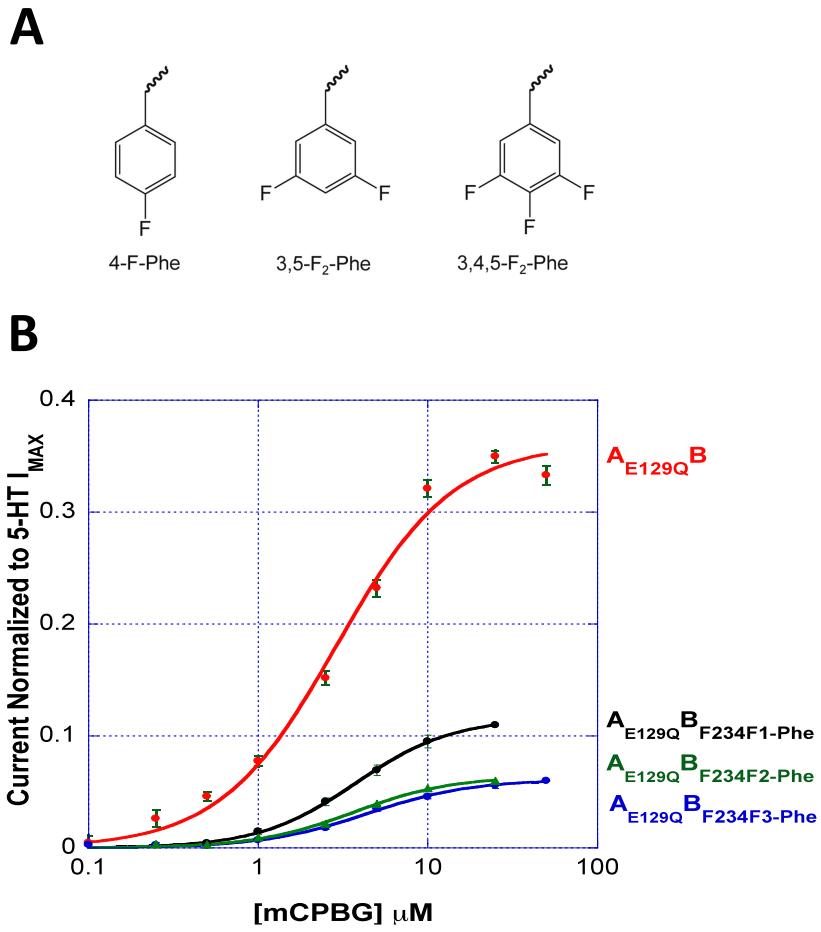

Figure 4.7 F226 (aligning with TyrC2) on the B subunit is important for mCPBG activation of 5-HT_3AB receptor. (A) Structures of the unnatural amino acids incorporated at F226 of the B subunit. (B) mCPBG dose-response data for sequential fluorination of F226 in the B subunit of 5-HT_3AB receptors containing the E124Q mutation in the A subunit and normalized to the maximal elicited 5-HT current.

Ab initio calculations of cation-π interaction energies between fluorinated benzenes and guanidinium were performed. Interpretation of the resulting interaction energies was precluded, however, as it became apparent that, unlike sodium, the guanidinium ion repositions itself to form direct interactions with the fluorine substituents (Figure 4.8).

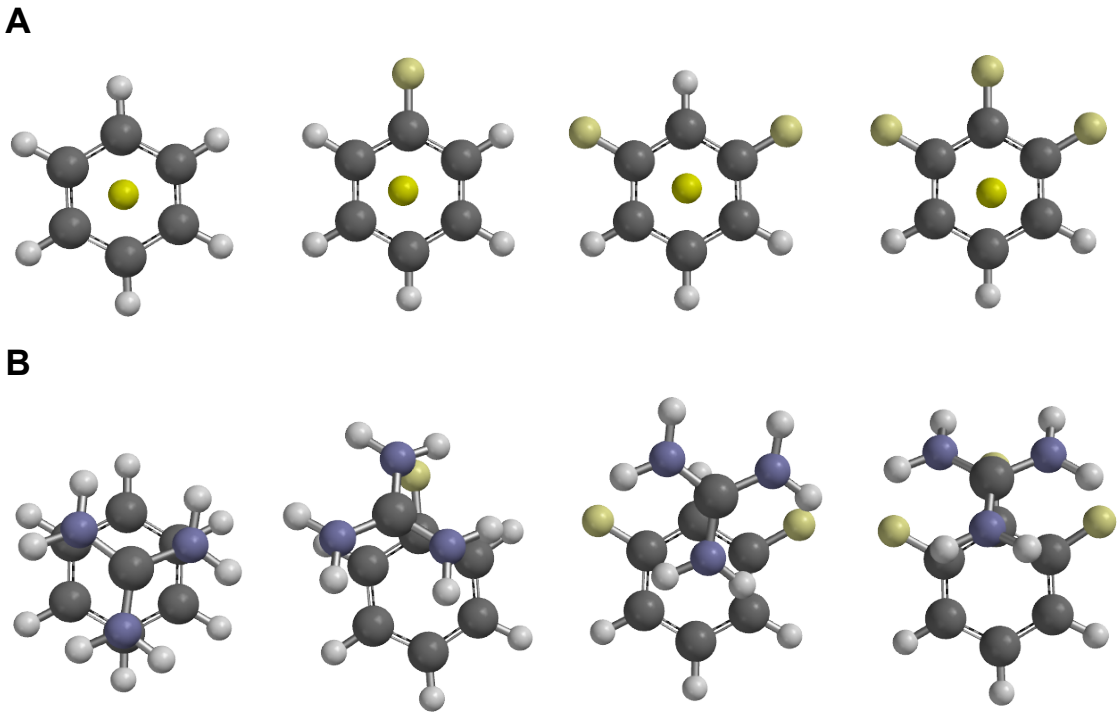

Figure 4.8 *Ab initio* calculations of benzene fluorination effects on sodium and guanidinium ions. (A) Top-down view of the geometry-minimized stacked binding pose of sodium and benzene or its fluorinated analogues. (B) Top-down view of the geometry-minimized stacked binding pose of guanidinium and benzene or its fluorinated analogues. Structures and were generated at HF 6-31G** and MP2/6-311+G** levels, with similar results (HF 6-31G** shown).

4.3.6 Conclusions

Unlike serotonin, which is only capable of activating 5-HT_3AB through its A-A interface, mCPBG is capable of binding the receptor at all five subunit interfaces. E124 (TyrA) and F226 (TyrC2) of the B subunit contribute to receptor activation in the principle face of the binding site and Y146 of Loop E contributes from the complementary face. mCPBG is capable of allosterically modulating the serotonin response through its binding at these additional interfaces. This highlights the potential

for the development of allosteric modulators of heteromeric 5-HT_3 receptors akin to the benzodiazepine actions at $GABA_A$ receptors.

4.4 METHODS

4.4.1 Mutagenesis and Preparation of cRNA and Oocytes

Mutant 5-HT_3A and 5-HT_3B receptor subunits, within the complete coding sequence for the human 5-HT_3A and 5-HT_3B receptor subunit (accession numbers P46098-1; NP_006019), were cloned into pGEMhe. Mutagenesis reactions were performed using the QuikChange mutagenesis kit (Stratagene), and confirmed by DNA sequencing. For unnatural mutagenesis, a stop codon, TAG, was made at the site of interest. Harvested stage V-VI *Xenopus* oocytes were washed in four changes of Ca^{2+}-free OR2 buffer (82.5 mM NaCl, 2 mM KCl, 1 mM $MgCl_2$, 5 mM HEPES, pH 7.5), de-folliculated in 1 mg/ml collagenase for approximately 1 h, washed again in four changes of Ca^{2+}-free OR2, and transferred to ND96 (96 mM NaCl, 2 mM KCl, 1.8 mM $CaCl_2$, 1 mM $MgCl_2$, 5 mM HEPES, pH 7.5) supplemented with 0.28 mg/ml pyruvate, 0.05 mg/ml Gentamicin, and 0.12 mg/ml theophylline. Oocytes were injected with 5-25 ng mRNA produced by *in vitro* transcription using the mMESSAGE MACHINE kit (Ambion, Austin, Texas, USA) from cDNA subcloned into pGEMhe as previously described (*28*). For unnatural amino acid experiments a 1:1 mixture of mRNA and tRNA was injected (5-25 ng each). Electrophysiological measurements were performed after incubation for 24 - 72 h post-injection at 18^o C. Wild-type recovery experiments (injection of tRNA appended to the natural amino acid) were performed to evaluate the fidelity of the unnatural suppression experiments. 76-mer THG73 was also injected with mRNA as a control.

4.4.2 Synthesis of tRNA and dCA amino acids

This was as described previously (*28*). Briefly, unnatural amino acids were chemically synthesized as nitroveratryloxycarbonyl (NVOC)-protected cyanomethyl esters and coupled to the dinucleotide dCA, which was then enzymatically ligated to 74-mer THG73 $tRNA_{CUA}$. Immediately prior to coinjection with cRNA, aminoacyl tRNA was deprotected by photolysis. Typically 5-10 ng total cRNA was injected with 25-50 ng of tRNA-aa in a total volume of 50 nl. For a control cRNA was injected with THG 76-mer tRNA (no unnatural amino acid attached).

4.4.3 Characterization of mutant receptors

Agonist-induced currents were recorded at 22-25^{o} C from individual oocytes using the OpusXpress system (Molecular Devices Axon Instruments, Union City, CA). 5-HT, and *m*-chlorophenylbiguanide (*m*CPBG) (Sigma) were stored as 25 mM aliquots at -20^{o} C, diluted in Ca^{2+}-free ND96 buffer (96 mM NaCl, 2 mM KCl, 1 mM $MgCl_{2,,}$ 5 mM HEPES, pH 7.5), and delivered to cells via the automated perfusion system of the OpusXpress. Glass microelectrodes were backfilled with 3 M KCl and had a resistance of ~1 MΩ. The holding potential was -60 mV. Agonist doses in Ca^{2+}-free ND96 were applied for 15 s followed by a 116 s wash with the running buffer. Dose-response data were obtained for ≥ 8 agonist concentrations on ≥ 5 cells. To determine EC_{50} values, concentration-response data were fitted to the four-parameter logistic equation, $I = I_{max}/[1 + (EC_{50}/[A])^{nH}]$ where I_{max} is the maximal response plateau, [*A*] is the log concentration of agonist, and *nH* is the Hill coefficient, using KaleidaGraph v3.6 software (Synergy Software, Reading, PA). A detailed error analysis of nonsense suppression experiments shows that data are reproducible to ±50% in EC_{50} (*29*). Relative efficacies (ε) of *m*CPBG,

are reported as $\varepsilon = I_{max\text{-}mCPBG}/I_{max\text{-}5\text{-}HT}$. Efficacy was calculated for individual cells and then averaged and reported as mean ± S.E.M.

4.4.4 Computation

All calculations were performed with the program SPARTAN (30).

4.5 REFERENCES

1. Lummis, S. C. (2012) 5-HT(3) receptors, *The Journal of biological chemistry 287*, 40239-40245.
2. Maricq, A. V., Peterson, A. S., Brake, A. J., Myers, R. M., and Julius, D. (1991) Primary structure and functional expression of the 5HT3 receptor, a serotonin-gated ion channel, *Science 254*, 432-437.
3. Davies, P. A., Pistis, M., Hanna, M. C., Peters, J. A., Lambert, J. J., Hales, T. G., and Kirkness, E. F. (1999) The 5-HT_{3B} subunit is a major determinant of serotonin-receptor function, *Nature 397*, 359-363.
4. Niesler, B., Walstab, J., Combrink, S., Moller, D., Kapeller, J., Rietdorf, J., Bonisch, H., Gothert, M., Rappold, G., and Bruss, M. (2007) Characterization of the novel human serotonin receptor subunits 5-HT3C,5-HT3D, and 5-HT3E, *Mol Pharmacol 72*, 8-17.
5. Walstab, J., Rappold, G., and Niesler, B. (2010) 5-HT(3) receptors: role in disease and target of drugs, *Pharmacol Ther 128*, 146-169.
6. Krzywkowski, K., Davies, P. A., Feinberg-Zadek, P. L., Brauner-Osborne, H., and Jensen, A. A. (2008) High-frequency HTR3B variant associated with major depression dramatically augments the signaling of the human 5-HT3AB receptor, *Proc Natl Acad Sci U S A 105*, 722-727.
7. Jensen, A. A., Davies, P. A., Brauner-Osborne, H., and Krzywkowski, K. (2008) 3B but which 3B and that's just one of the questions: the heterogeneity of human 5-HT3 receptors, *Trends Pharmacol Sci 29*, 437-444.
8. Miles, T. F., Dougherty, D. A., and Lester, H. A. (2013) The 5-HT3AB receptor shows an A3B2 stoichiometry at the plasma membrane, *Biophys J 105*, 887-898.
9. Lochner, M., and Lummis, S. C. (2010) Agonists and antagonists bind to an A-A interface in the heteromeric 5-HT3AB receptor, *Biophys J 98*, 1494-1502.
10. Thompson, A. J., Price, K. L., and Lummis, S. C. (2011) Cysteine modification reveals which subunits form the ligand binding site in human heteromeric 5-HT3AB receptors, *J Physiol 589*, 4243-4257.
11. Michaelson, S. D., Paulsen, I. M., Kozuska, J. L., Martin, I. L., and Dunn, S. M. (2013) Importance of recognition loops B and D in the activation of human 5-HT(3) receptors by 5-HT and meta-chlorophenylbiguanide, *Neuropharmacology 73*, 398-403.
12. Hapfelmeier, G., Tredt, C., Haseneder, R., Zieglgansberger, W., Eisensamer, B., Rupprecht, R., and Rammes, G. (2003) Co-expression of the 5-HT3B serotonin

receptor subunit alters the biophysics of the 5-HT3 receptor, *Biophys J 84*, 1720-1733.

13. Kilpatrick, G. J., Butler, A., Burridge, J., and Oxford, A. W. (1990) 1-(m-chlorophenyl)-biguanide, a potent high affinity 5-HT3 receptor agonist, *Eur J Pharmacol 182*, 193-197.
14. Beene, D. L., Brandt, G. S., Zhong, W., Zacharias, N. M., Lester, H. A., and Dougherty, D. A. (2002) Cation-p interactions in ligand recognition by serotonergic (5-$HT3_A$) and nicotinic acetylcholine receptors: the anomalous binding properties of nicotine, *Biochemistry 41*, 10262-10269.
15. Price, K. L., Bower, K. S., Thompson, A. J., Lester, H. A., Dougherty, D. A., and Lummis, S. C. (2008) A hydrogen bond in loop A is critical for the binding and function of the 5-HT3 receptor, *Biochemistry 47*, 6370-6377.
16. Miles, T. F., Bower, K. S., Lester, H. A., and Dougherty, D. A. (2012) A coupled array of noncovalent interactions impacts the function of the 5-HT3A serotonin receptor in an agonist-specific way, *ACS Chem Neurosci 3*, 753-760.
17. Thompson, A. J., Verheij, M. H., de Esch, I. J., and Lummis, S. C. (2012) VUF10166, a novel compound with differing activities at 5-HT(3)A and 5-HT(3)AB receptors, *J Pharmacol Exp Ther 341*, 350-359.
18. Thompson, A. J., and Lummis, S. C. (2013) Discriminating between 5-HT A and 5-HT AB receptors, *Br J Pharmacol*.
19. Mazzaferro, S., Benallegue, N., Carbone, A., Gasparri, F., Vijayan, R., Biggin, P. C., Moroni, M., and Bermudez, I. (2011) Additional acetylcholine (ACh) binding site at alpha4/alpha4 interface of (alpha4beta2)2alpha4 nicotinic receptor influences agonist sensitivity, *The Journal of biological chemistry 286*, 31043-31054.
20. Tavares Xda, S., Blum, A. P., Nakamura, D. T., Puskar, N. L., Shanata, J. A., Lester, H. A., and Dougherty, D. A. (2012) Variations in binding among several agonists at two stoichiometries of the neuronal, alpha4beta2 nicotinic receptor, *J Am Chem Soc 134*, 11474-11480.
21. Van Arnam, E. B., and Dougherty, D. A. (2014) Functional Probes of Drug-Receptor Interactions Implicated by Structural Studies: Cys-Loop Receptors Provide a Fertile Testing Ground, *J Med Chem*.
22. Beene, D. L., Price, K. L., Lester, H. A., Dougherty, D. A., and Lummis, S. C. (2004) Tyrosine residues that control binding and gating in the 5-hydroxytryptamine3 receptor revealed by unnatural amino acid mutagenesis, *The Journal of neuroscience : the official journal of the Society for Neuroscience 24*, 9097-9104.
23. Duffy, N. H., Lester, H. A., and Dougherty, D. A. (2012) Ondansetron and granisetron binding orientation in the 5-HT(3) receptor determined by unnatural amino acid mutagenesis, *ACS Chem Biol 7*, 1738-1745.
24. Zhong, W., Gallivan, J. P., Zhang, Y., Li, L., Lester, H. A., and Dougherty, D. A. (1998) From ab initio quantum mechanics to molecular neurobiology: a cation-pi binding site in the nicotinic receptor, *Proc Natl Acad Sci U S A 95*, 12088-12093.
25. Gao, F., Mer, G., Tonelli, M., Hansen, S. B., Burghardt, T. P., Taylor, P., and Sine, S. M. (2006) Solution NMR of acetylcholine binding protein reveals

agonist-mediated conformational change of the C-loop, *Mol Pharmacol 70*, 1230-1235.

26. Hansen, S. B., Sulzenbacher, G., Huxford, T., Marchot, P., Taylor, P., and Bourne, Y. (2005) Structures of Aplysia AChBP complexes with nicotinic agonists and antagonists reveal distinctive binding interfaces and conformations, *Embo J 24*, 3635-3646.
27. Lummis, S. C., D, L. B., Harrison, N. J., Lester, H. A., and Dougherty, D. A. (2005) A cation-pi binding interaction with a tyrosine in the binding site of the GABAC receptor, *Chem Biol 12*, 993-997.
28. Nowak, M. W., Gallivan, J. P., Silverman, S. K., Labarca, C. G., Dougherty, D. A., Lester, H. A., and Conn, P. M. (1998) In vivo incorporation of unnatural amino acids into ion channels in Xenopus oocyte expression system, In *Methods in Enzymology*, pp 504-529, Academic Press.
29. Torrice, M. M. (2009) Chemical-scale studies of nicotinic and muscarinic acetylcholine receptors, In *Chemistry and Chemical Engineering*, California Institute of Technology, Pasadena.

Chapter 5

Efforts Toward the Application of Unnatural Amino Acid Mutagenesis in Ligand-Gated Transcription Factors

5.1 ABSTRACT

Nuclear receptors are a broad class of ligand-gated transcription factors. This family of receptors is responsible for sensing steroids, sterols, fatty acids, and retinoids, and their function has been implicated in diverse physiological processes such as metabolism, inflammation, and immunity. RARα/RXRα heterodimeric nuclear receptor activation requires more than simply ligand binding and is surprisingly complex. The process of activation terminates in phosphorylation at S77 of RARα. Interestingly, S77 is immediately succeeded by a proline residue. This constitutes the minimal known recognition motif for the prolyl-isomerase Pin1. Unnatural amino acid mutagenesis with proline analogues of varying *cis* preference would be an elegant proof of this activation mechanism. Here, I describe progress toward the reconstitution of a RARα/RXRα pathway in *Xenopus laevis* oocytes and the detection of reporter mRNA by quantitative reverse transcription PCR as a functional assay for the detection of unnatural amino acid bearing transcription factors.

5.2 INTRODUCTION

Given that a multicellular organism contains the same DNA in its genome across all of its cells, the specialization required by multicellularity is generated through the

differential selection of subsets of that genome to be transcribed into RNA. This selection is enacted by a broad class of proteins termed transcription factors. Upon becoming activated via either the sensation of ligand or post-translational modification, these proteins access the nucleus and bind to specific sequences in the genome termed promoters. In eukaryotes, combinatorial and cooperative action by collections of transcription factors bound at promoters recruit the RNA polymerase and its associated cofactors, enabling them to generate functional RNA.

While crystallography has elucidated the structures of a multitude of transcription factors, the structural logic of what constitutes an activated transcription factor, and in turn an activated promoter capable of recruiting RNA polymerase, is largely unknown. Transcription factors display a high degree of intrinsic disorder and complex dependent structure (*1*). Thus, even for proteins in which structures of certain domains exist, much of their function may lie in more fluid regions that orient those structured domains. Unfortunately, it is precisely these variable regions on which crystallography is void.

Nuclear receptors are a broad class of ligand-gated transcription factors, with 48 unique receptors identified in humans thus far (*2*). This family of receptors is responsible for sensing steroids, sterols, fatty acids, and retinoids, and their function has been implicated in diverse physiological processes such as metabolism, inflammation, and immunity. Nuclear receptors have two conserved domains, a ligand-binding domain and a DNA-binding domain. The two domains are linked by variable hinge domains. These receptors also possess a highly variable N-terminal domain.

Nuclear receptors are generally grouped into three classes: I, those that act as monomers, such as Nur77, and steroidogenic factor 1 (SF1), II, those that homodimerize,

such as the androgen receptor, the estrogen receptor (ER), and the glucocorticoid receptor (GR), and III, those that form heterodimers with the retinoid receptor (RXR), such as peroxisome proliferator-activated receptors (PPAR) and retinoic acid receptors (RAR) (*2*).

Each nuclear receptor subunit binds to a unique six base consensus DNA sequence and dimers have a receptor-specific distance between each of their six base sequences. This combined stretch of bases is referred to as the receptor's response element (*2*). While DNA-binding domains are capable of binding their consensus sequences in isolation, there is ample evidence of allosteric communication between the domains (*3, 4*). Recently, full-length crystal structures of dimeric nuclear receptors have been reported (*5-7*). These suggest a critical role for the hinge region in conveying allostery by controlling the relative orientation of the ligand-binding and DNA-binding domains. This communication is further modulated by the binding of one of the over 150 co-activators of nuclear receptors (*2*). These co-activators bind at one of two sites: activating factor 1 (AF1) in the ligand-binding domain or AF2 in the N-terminal domain.

The RARα/RXRα heterodimeric nuclear receptor has been thoroughly biochemically characterized, and many structures exist for each of its domains in isolation (*8, 9*). Upon binding of retinoic acid, RARα dimerizes with RXRα, migrates to the nucleus where it binds its response element, and recruits the transcriptional machinery. The process of receptor activation requires more than simply ligand binding however and is surprisingly complex (Figure 5.1). Retinoic acid, in addition to being bound by RAR, activates the p38MAPK pathway (*10*). This, coupled with RAR/RXR ligand binding, allows MSK1 to phosphorylate RAR at S369 of the ligand-binding

domain adjacent to AF1 (*10*). S369 phosphorylation, in turn, allows Cyclin H and cdk7 of the TFIIH complex to phosphorylate S77 of the N-terminal domain near AF2 (*11*). This latter phosphorylation is necessary and sufficient for transcription factor activation and results in higher DNA binding efficiency at the response element (*11, 12*).

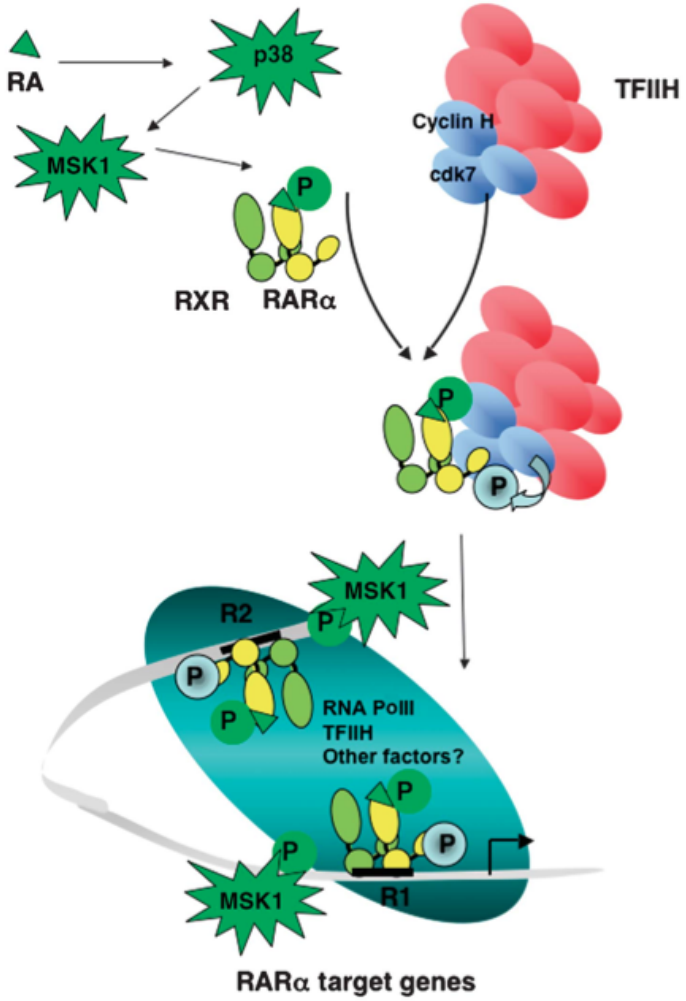

Figure 5.1 The RAR/RXR activation pathway. Adapted from reference 10.

The exact structural mechanism of how phosphorylation in the N-terminal domain affects the adjacent DNA-binding domain remains to be explored. Interestingly, S77 is immediately succeeded by a proline residue. This constitutes the minimal known

recognition motif for the enzyme Pin1 (*13, 14*). Pin1 is a phospho-directed proline isomerase. Proline is the only natural amino acid that is capable of existing to any appreciable extent (about five percent) in a *cis* conformation (*15*). Isomerization is still disfavored, however, and is exceedingly slow. Augering the hypothesis that S77 marks a recognition site is the finding that Pin1 interacts with other nuclear receptors (*16-18*).

Pin1 is capable of catalyzing both the *trans* to *cis* and *cis* to *trans* reactions (*13, 14, 19*). Most kinases, however, are only capable of phosphorylation adjacent to *trans* substrates. Phosphorylation has been found to raise the energetic barrier between the *trans* and *cis* conformations, essentially locking the backbone in its set conformation unless acted upon by Pin1. Therefore, *in vivo*, Pin1 is likely to predominantly catalyze the proline backbone from *trans* to *cis*.

Assays for detecting Pin1 activity are crude however. The best and most used method is to reconstitute the system in question and dope in peptides containing Pin1 recognition sequences (*20, 21*). These peptides are expected to outcompete the endogenous substrate for catalysis, resulting in the diminishment of the ultimate functional output. Such an assay is both indirect and difficult to accomplish for complex systems such as RAR/RXR activation.

Here we hope to establish a system in which we can perform a more direct and elegant test of Pin1 function. A number of unnatural proline analogues have been created that show a diverse range of *cis* preferences (Figure 5.2) (*22, 23*). If mutation to a heavily *cis* biased unnatural amino acid at P78 can rescue an otherwise inactive S77A RAR/RXR, it is likely that proline isomerization at P78 is crucial for activation.

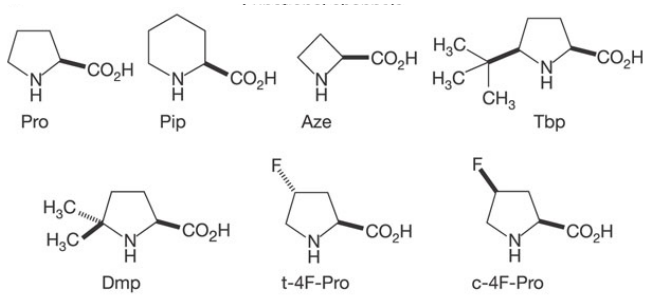

Figure 5.2 Unnatural proline analogues of varying *cis* preference.

Unnatural amino acid mutagenesis brings complications of its own. First, to date there are a limited variety of amenable systems for heterologous expression in which unnatural amino acid incorporation is well tolerated (*24, 25*). The best characterized and most precedented is the *Xenopus laevis* oocyte . There is precedence for the heterologous expression of the RAR/RXR nuclear receptor in *Xenopus* oocytes by introducing mRNA for the receptor subunits and a simple luciferase reporter plasmid containing the appropriate response element (*26, 27*). RAR/RXR function in this system was confirmed by detecting luciferase bioluminescence.

A second limitation of unnatural amino acid mutagenesis is that, even in *Xenopus* oocytes, expression of unnatural amino acid containing proteins is extremely limited (*28*). Thus a supremely sensitive functional assay is required. There are reasons to be hopeful however, as transcription is an amplifying process, e.g., each activated transcription factor is capable of generating many RNA molecules.

Each of those RNA molecules can, in turn, be amplified and detected using quantitative Reverse-Transcribed PCR (qRT-PCR). In fact, qRT-PCR protocols have

been shown to reliably detect roughly 20 copies of target RNA (*29*). In this technique isolated RNA is reverse transcribed into DNA that is then subject to amplification by PCR. Oligonucleotide primers specific to the target of interest are combined with those for various reference genes whose expression levels are known to be unaffected by the target (*30*). After each PCR cycle a fluorescence reading is taken to detect a fluorescent DNA intercalator included in the reaction. The higher the copy number of the target, the fewer PCR cycles it will take before the target fragment is amplified above the fluorescence background. The cycle at which the target reaches a fluorescence threshold can then be normalized to that of the reference genes in the same sample, allowing for calculation of relative abundances across experimental conditions.

Thus, we hope to develop an experimental system for unnatural amino acid mutagenesis and qRT-PCR analysis in *Xenopus laevis* oocytes to investigate potential enzyme directed proline isomerization of nuclear receptors as a structural mechanism of activation. We expect to see robust activation in the wild type RAR/RXR that is abolished by S77A mutation and rescued by the introduction of *cis* biased unnatural amino acids.

5.3 RESULTS AND DISCUSSION

5.3.1 Luciferase reporter plasmid qPCR calibration

A luciferase reporter plasmid containing a minimal promoter with three sites for RAR/RXR heterodimer binding, akin to that reported in prior studies in *Xenopus laevis* oocytes, was obtained. Primers were designed to specifically amplify a section of the luciferase coding region. To determine the sensitivity of the qPCR protocol and the

effectiveness of the luciferase primers, a calibration experiment was devised. Dilutions of the reporter plasmid were created at every order of magnitude from three million copies per μL down to three copies of the plasmid per μL. These dilutions seeded qPCR reactions with each condition run in triplicate. An additional condition with no reporter plasmid was also included.

The results of this experiment showed the expected pattern, with the fluorescence of higher copy number conditions rising above threshold at a lower number of amplification cycles (Cq) (Figure 5.3A). Tight grouping of replicates within each condition was also observed, demonstrating the precision of the qPCR technique. A thermal denaturation experiment was performed on the amplified product, or amplicon, showing a sharp characteristic melting temperature for the amplicon that is consistent across experimental conditions, with one exception (Figure 5.3B). The tightness of the melting curve peak suggests that only one DNA species is amplified during the qPCR procedure. The one exception shows a second peak of higher thermal stability, suggesting contamination or nonspecific amplification in this condition. As only one of twenty-one samples using the luciferase primers shows this second peak, it is likely that the primers are generally sound and that the thermal denaturation experiment may be used to identify and remove rare events of contamination from inclusion in future analysis.

The cycle at which fluorescence surpasses threshold for each condition shows a strong correlation with the plasmid copy number of the condition, as expected (Figure 5.3C). The difference in number of cycles between conditions that increase an order of magnitude, 3.29 ± 0.35 cycles, agrees well with that expected given amplicon doubling during every cycle (3.32 cycles). Thus it appears that the qPCR is a reliable

measure of relative sample copy number within an experiment. Also, given this calibration experiment, the Cq value of future experiments may be related back to absolute copy number.

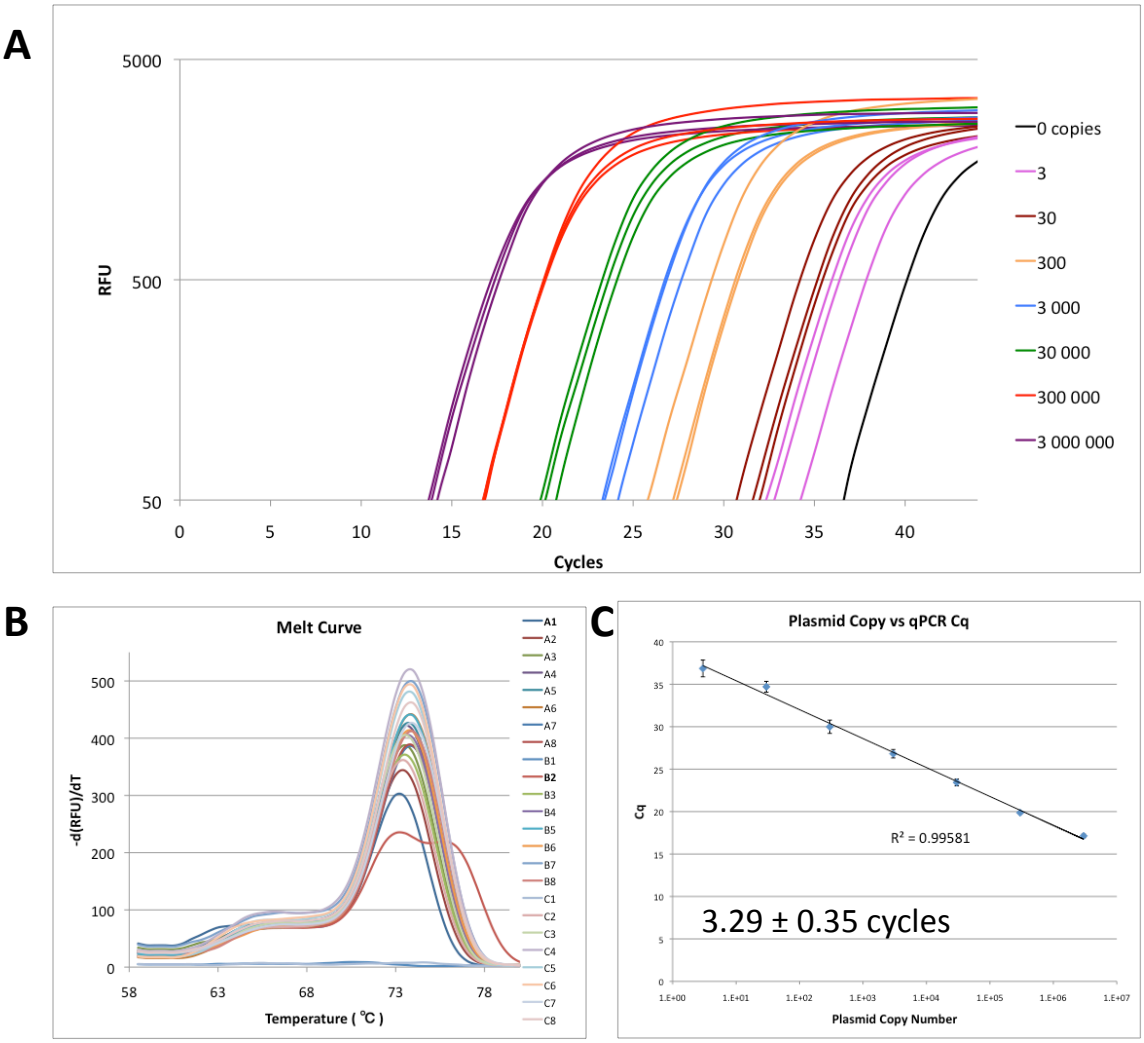

Figure 5.3 Luciferase reporter plasmid qPCR calibration. (A) Fluorescence response of samples of varying plasmid copy number as the PCR cycle count increases. (B) Melting curve of luciferase primer amplicon, plotted as the rate of fluorescence change versus temperature. (C) The relationship between the cycle at which fluorescence surpasses threshold, Cq, and the plasmid copy number. The average spacing of 3.29 agrees well with the order of magnitude difference in sample plasmid abundance. RFU, relative fluorescence units.

The variability between replicates of the same condition does increase as copy number decreases below 300, suggesting a lower threshold. There eventually is amplification of the condition with zero plasmid, however with significant fluorescence from the cycle numbers in the high 30s, suggesting that Cq values in this range are not indicative of real signal.

5.3.2 qRT-PCR on mRNA from uninjected oocytes

To ensure that the luciferase primers used above are specific to only the reporter plasmid, they were tested against the pool of mRNA produced by naive oocytes that have not been injected with any foreign constructs. To do this, the mRNA must first be extracted from the oocytes. Then the isolated mRNA must be reverse transcribed into DNA so that PCR amplification may proceed.

To limit the effects of cell to cell variability in expression and to ensure sufficient RNA isolate, four oocytes were combined for each RNA extraction sample. Extraction was supplemented with a half hour on column DNAse I digestion at room temperature to ensure RNA purity. RNA isolate was analyzed by UV-Vis spectroscopy, showing a concentration of 113 ng per μL and the ratio of absorbances at 260 nm / 280nm was 2.05. Ratios over 2.0 are indicative of an enriched RNA sample. Lower ratios indicate mixture with DNA or RNA degredation.

Reverse transcription was performed using 1 μg of the extracted RNA in a 20 μL reaction. A poly-thymine primer, $[dT]_{18}$, was used to selectively catalyze the reverse transcription of the mRNA minority within the RNA isolate. The process finishes with RNAse digestion. After reverse transcription the sample was again analyzed by UV-Vis spectroscopy. The reverse transcribed sample showed a concentration of 2222 ng per μL

and an A260/280 ratio of 1.84. The increase in concentration shows that the reaction amplified the mRNA within the sample. This is a potential source of concern as it could bias results if not all target mRNAs amplify with equal efficiency. The marked decrease to 1.8 is consistent with a relatively pure and non-degraded DNA sample.

As positive controls, glyceraldehyde 3-phosphate dehydrogenase (GAPDH) and ornithine decarboxylase (ODC) were selected, as they had previously been shown to exist at invariant abundance in *Xenopus laevis* oocytes. Such general housekeeping genes are also of great utility as reference marks against which to interpret the luciferase reporter abundance so that differences in the quality and quantity of RNA extracted can be accounted for. qPCR primers were designed for both of these genes so that conditions probing their abundance could be run in parallel with the luciferase primers.

The reverse transcription reaction mixture was split into three replicates of each of the three primer sets for a total of nine qPCR reactions. GAPDH and ODC show high abundances in the reverse transcribed sample with Cq values of 23.2 and 24.2 cycles, respectively (Figure 5.4). This is roughly equivalent to ten thousand copies each in the fraction of the sample probed in each reaction based on the luciferase calibration experiment, though slight corrections may need to account for differences in amplicon length. The luciferase samples on the other hand have a Cq value of 36.6 cycles. This is equivalent to that seen for samples with three or fewer copies in the calibration experiment.

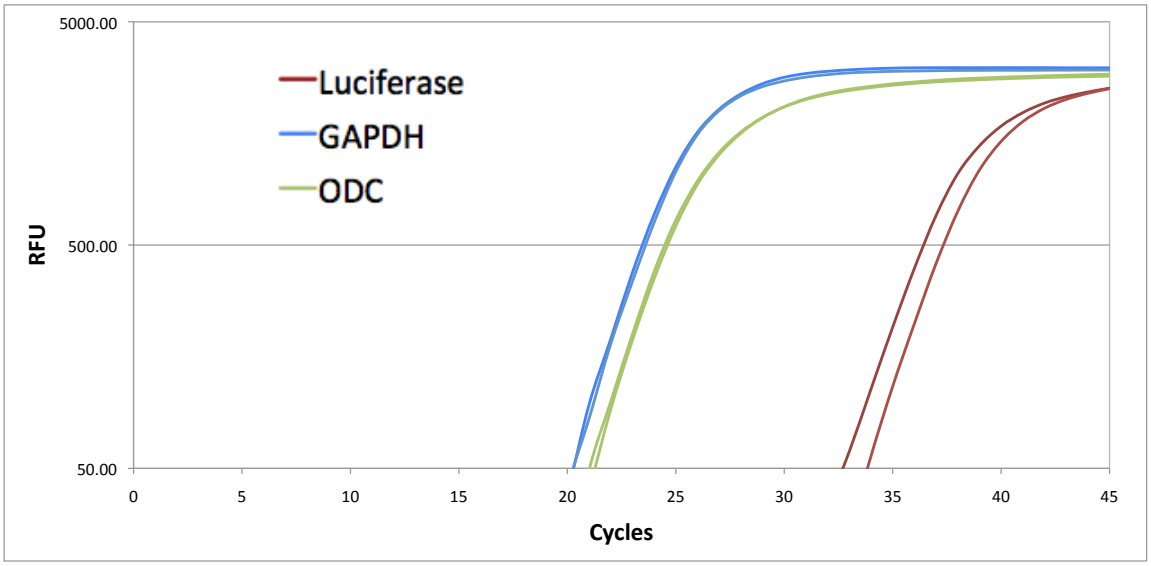

Figure 5.4 qPCR controls tested on uninjected oocytes. RFU, relative fluorescence units.

Unfortunately the thermal denaturation experiment shows a sharp peak in the luciferase amplicon melt curve equivalent to that seen at high copy numbers in the calibration experiment (Figure 5.5A). This suggests that the nonspecific amplification has a similar thermal stability and that, unfortunately, the denaturation experiment may not root out all false positives. The thermal denaturation of GAPDH and ODC amplicons show similarly sharp peaks at 75 and 78 °C, respectively (Figure 5.5B and C).

These results suggest that GAPDH and ODC fall within a robust region of qPCR detection, making them well suited as reference genes against which to evaluate luciferase expression levels. The lack of amplification of the luciferase amplicon in naïve uninjected oocytes shows that the luciferase primers are specific to that construct and background off-target amplification will not significantly contribute to the apparent abundance of luciferase in future experiments.

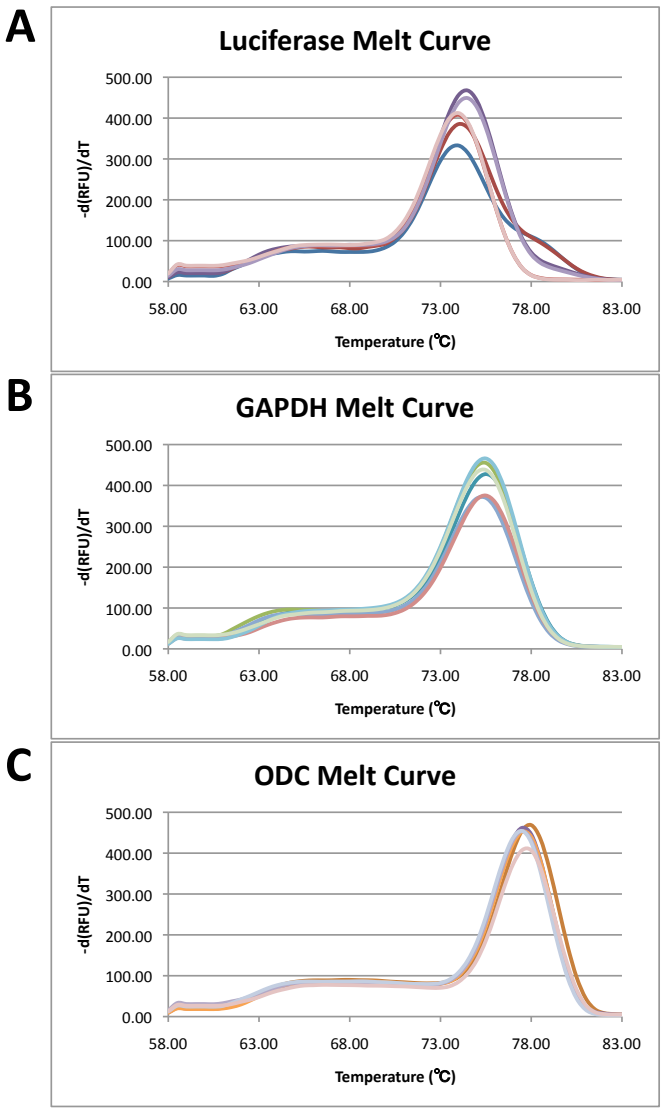

Figure 5.5 Thermal denaturation of qPCR amplicons. Plots are the rate of fluorescence change versus temperature for luciferase (A), GAPDH (B), and ODC (C) primers.

5.3.3 Reconstitution of the RAR/RXR dependent luciferase reporter system

With the above controls in place, reconstitution of the RAR/RXR dependent luciferase reporter system in *Xenopus laevis* oocytes as reported previously was attempted. The experimental work-flow was as follows (Figure 5.6):

1. injection of the oocyte nuclei with luciferase reporter plasmid

2. injection of *in vitro* transcribed mRNA for RARα and RXRα

3. incubation with or without retinoic acid

4. RNA isolation for reverse transcription and qPCR as previously described.

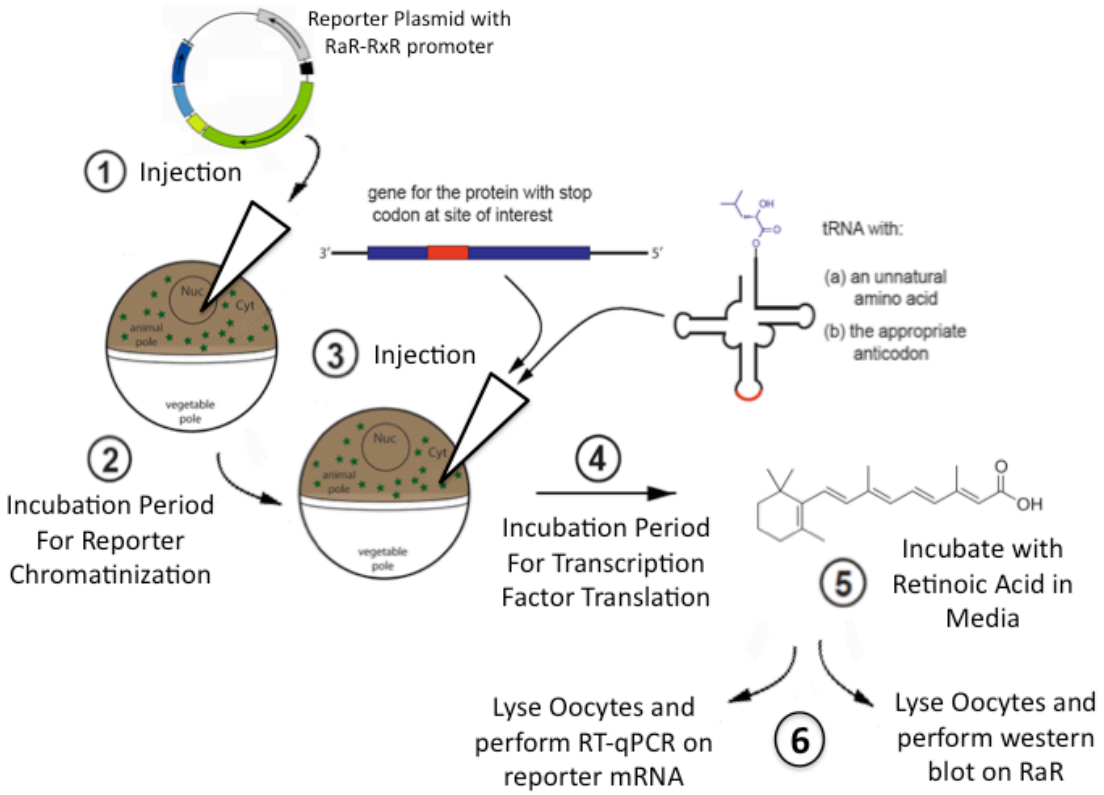

Figure 5.6 Schematic of experimental work-flow.

The first step proved to be non-trivial, with multiple methods for nuclear injection attempted. These methods are premised on the finding that the nucleus is fluid within the oocyte. Low-speed centrifiguation of oocytes individually situated animal pole down in conical tubes was performed to force the nucleus up against the plasma membrane of the animal pole. This should result in an area of reduced pigment that marks the presence of the nucleus into which one should inject. Centrifugation is harsh on the oocytes and removal of the oocytes from the tubes without disrupting the nucleus' placement is delicate.

A second, and preferred, method is to rely on the observed relative low density of the nucleus relative to the cytoplasm. If left animal pole up, the nucleus will float to the top of the oocyte, resulting in a similar displacement of pigment in the animal pole by which it may be identified. The injection needle was placed perpendicular to the nucleus and inserted slightly deeper into the oocyte than typical cytoplasmic injections. 10 nL containing 2 ng of luciferase reporter plasmid was injected into each oocyte.

After an overnight incubation during which the oocytes were allowed to recover and to chromatinize the reporter construct, they received a second cytoplasmic injection. This contained *in vitro* transcribed mRNA for RARα and RXRα. 10 ng of each mRNA was delivered in a 50 nL shallow injection at the boundary between the animal and vegetal poles of the oocytes. Following an hour incubation in which the oocytes were allowed to recover, the cells were randomly split into two equal groups, with one receiving 10 μM retinoic acid. Retinoic acid solubility was increased by supplementation with 0.1 percent DMSO and sonication at 37 °C for a half hour prior to addition.

After an additional overnight incubation in a blacked out container to limit retinoic acid photo-degradation, total RNA was extracted from oocytes from conditions with and without retinoic acid exposure and mRNA was reverse transcribed into DNA as detailed previously. UV-Vis spectroscopy showed the sample to be of good quality (Table 5.1) Each reverse transcription reaction seeded qPCR reactions for luciferase, GAPDH and ODC. Each condition was run in triplicate.

GAPDH and ODC reference genes show amplification at around 30 cycles regardless of incubation with retinoic acid (Table 5.1). The lack of meaningful change in Cq between the conditions confirms the validity of the targets as reference genes. The

lack of a significant change in Cq between GAPDH and ODC also suggests that their expression levels are relatively invariant. The fact that GAPDH and ODC amplify at roughly 6 cycles higher than observed in the experiment on uninjected oocytes may imply that the RNA extraction was less efficient in this experiment or that the oocyte repair process following puncture results in fewer housekeeping gene mRNA.

As hoped, the luciferase sample that has been exposed to retinoic acid shows strong signal with a Cq of roughly 24 cycles (Table 5.1). Unfortunately, this high expression is also observed in the absence of retinoic acid.

	RNA extracted		DNA reverse transcribed		qPCR Cq		
	Conc	A260/ 280	Conc	A260 / 280	Luciferase	GAPDH	ODC
No ligand	263	2.05	1824	1.84	22.2 ± 1.1	30.0 ± 0.8	30.0 ± 0.8
RA	296	2.05	2070	1.83	23.9 ± 0.8	29.4 ± 0.8	28.5 ± 0.8

Table 5.1 UV-Vis and qPCR data for DNA and RNA injected oocytes. Concentrations are in ng per μL. Cq are in cycles. RA is retinoic acid. Values are reported as mean and standard error.

5.3.4 Determining the origin of luciferase reporter signal

There are several possible explanations for this high apparent expression of luciferase that is unresponsive to retinoic acid exposure. The first is that the RARα and RXRα may be constitutively active, resulting in the production of luciferase mRNA even in the absence of activating ligand. It is also possible that endogenous activated nuclear receptors within the oocytes are stimulating the production of luciferase mRNA.

To distinguish between these two cases, the experiment was repeated identically, except that the second injection containing the RARα and RXRα mRNA was skipped. If

the luciferase signal is due to their constitutive activation, this sample should have negligible luciferase response. Samples with and without retinoic acid exposure were again created and run in duplicate. UV-Vis spectroscopy again confirmed high sample quality and conversion to DNA (Table 5.2).

	RNA extracted		DNA reverse transcribed		qPCR Cq		
	Conc	A260/ 280	Conc	A260 / 280	Luciferase	GAPDH	ODC
No ligand	259	2.07	2015	1.80	22.0	25.6	24.3
RA	240	2.07	2245	1.82	22.1	26.7	25.7

Table 5.2 UV-Vis and qPCR data for DNA injected oocytes. Concentrations are in ng per μL. Cq are in cycles. RA is retinoic acid. Cq values are the average of 2 replicates.

GAPDH and ODC samples amplified at around 25 cycles and luciferase again showed high copy numbers with a Cq value of 22 cycles regardless of retinoic acid presence (Table 5.2). The difference between the Cq of luciferase and the Cq of the reference genes in this experiment was roughly three cycles, whereas the difference when the transcription factor mRNA is injected is roughly seven cycles. If real, this suggests that the luciferase transcript is 2^4 or 16 times more abundant when RARα and RXRα mRNA are supplied. The response is still invariant with regard to retinoic acid, suggesting constitutive activation.

The high basal level of luciferase response, even when the transcription factors are not supplied, suggests that there may be either endogenous transcription factors that are acting on the reporter plasmid, or that there is contamination from undigested DNA plasmid that remains in the extracted RNA despite the on-column DNAse I digestion. It is possible that if the basal level of luciferase response could be lowered, the fold increase

upon expression of the transcription factors might appear much larger. This would provide a larger window in which to reliably observe partial recovery of function when it comes time to attempt unnatural amino acid mutagenesis.

To determine whether DNA contamination persists after the DNAse I digestion, two different initial approaches were attempted. First, a primer was designed to amplify from a non-coding region of the luciferase reporter plasmid. In a calibration curve experiment, this primer, called pGL3, showed similar fidelity as the luciferase primer, with the spacing between order of magnitude dilutions of plasmid of 3.34 cycles or 10.1 fold (Figure 5.7).

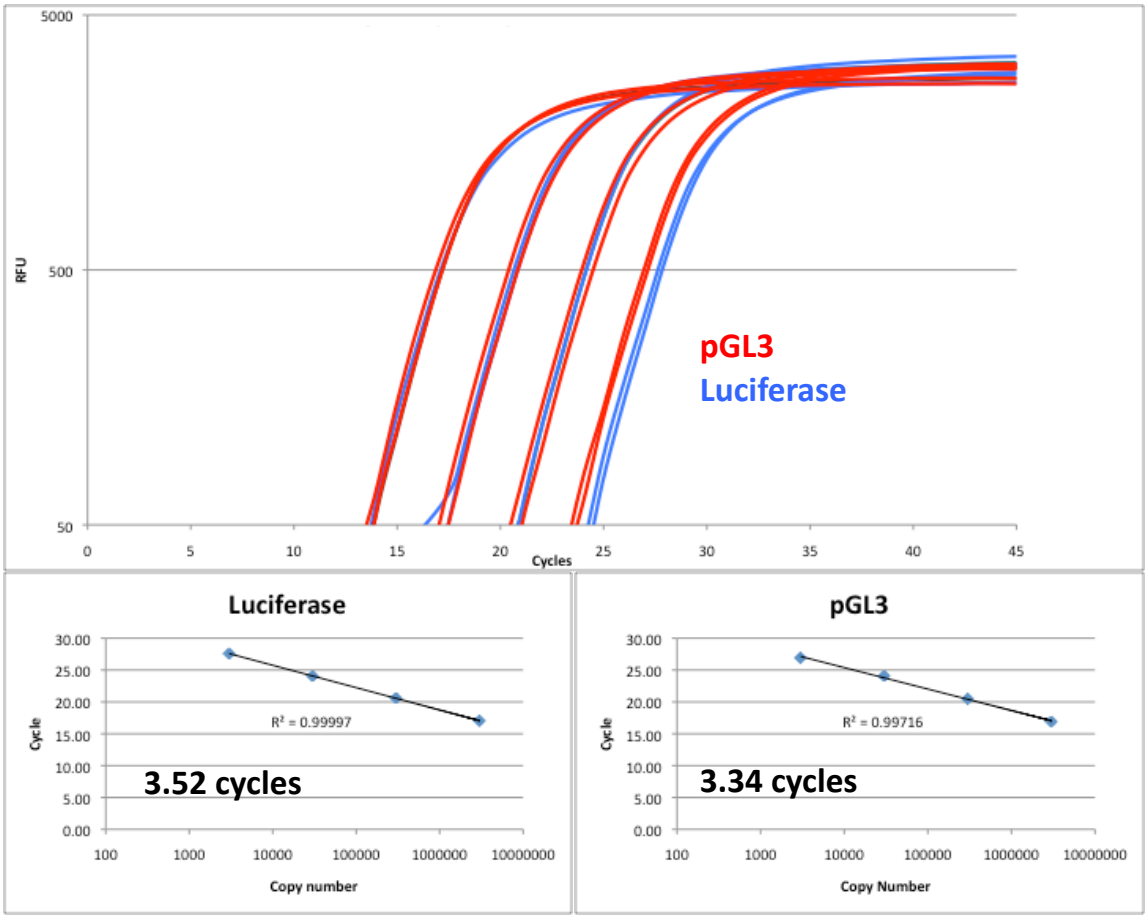

Figure 5.7 pGL3 primer qPCR calibration. Fluorescence as a function of PCR cycle shows pGL3 primer to function similarly to previous luciferase primers.

When tested against reverse transcribed RNA isolate from naïve ununinjected oocytes however, the pGL3 reaction amplified at 26 cycles. This suggests that the primers are not specific for the luciferase reporter plasmid and amplify endogenous constructs. The second method attempted was to perform an additional DNAse I digestion for 10 min at 37 °C on the extracted total RNA prior to reverse transcription. Oocytes injected with only the luciferase reporter plasmid were lysed after overnight incubation in the absence of retinoic acid. Total RNA was extracted from two sets of four oocytes with equivalent yields and quality (Table 5.3) Each sample received the standard on-column DNAse I digestion, while one sample received the addition re-digestion. This re-digested sample showed marked degradation, however, with the concentration dropping from 230 ng per μL after the first digestion to 53 ng per μL. Additionally the A260/280 ratio dropped from 2.05 to 1.97, supporting the conclusion that the sample had degraded (Table 5.3).

	RNA extracted		DNA reverse transcribed		qPCR Cq		
	Conc	A260/ 280	Conc	A260 / 280	Luciferase	GAPDH	ODC
Single	267	2.04	1994	1.82	23.8 ± 0.7	24.8 ± 0.2	27.4 ± 0.8
First	230	2.05	-	-	-	-	-
Second	53	1.97	2333	1.81	24.3 ± 1.1	27.4 ± 0.4	30.4 ± 0.9

Table 5.3 UV-Vis data for DNAse I re-digestion experiment. Single refers to the standard condition of a single DNAse I digestion. First refers to a sample after the first of two DNAse I digestions. Second refers to a sample after the second of two DNAse I digestions. Concentrations are in ng per μL. Cq are in cycles. Values are reported as mean and standard error.

When this re-digested sample was reverse transcribed and compared to a parallel sample that had only the standard single on-column digestion, the difference in

absorbance profiles disappeared with each showing high abundance and A260/280 ratios typtical of DNA samples. qPCR revealed that the Cq of luciferase remained unchanged between the two samples and that the difference in Cq between luciferase and the reference genes actually increased upon re-digestion (Table 5.3). This suggests that while the reference genes degraded during the second DNAse I digestion, the luciferase construct remained stable. It is possible that the heat of the re-digestion had a greater effect on the comparatively labile RNA than the DNAse did on the plasmid.

The difference between luciferase and the reference genes in the single digestion condition is different than that observed in the prior experiment. If this sample were compared with the transcription factor injected condition, it would appear that there was no increase in luciferase abundance with the addition of transcription factor mRNA. This variable response may be due to imprecision of the amount of reporter plasmid delivered, as 10 nL is at the lower limit of detection for the standard micro-injection needles used.

The final and most elegant method to determine the source of the luciferase signal was to perform qPCR reactions on the total isolated RNA without reverse transcription. Leftover RNA isolate from the above singly digested sample was added directly to qPCR reactions for luciferase and GAPDH. Amplification should be impossible for single stranded RNA so neither construct should show signal unless there is DNA contamination in the RNA isolate with the required template sequences. Amplification does occur for luciferase with a Cq of 25.8 ± 0.1 cycles while the GAPDH Cq is 38.4 ± 0.1 cycles (Figure 5.8). Thus, it appears that the luciferase signal arises nearly entirely from DNA contamination in the total RNA extract despite DNAse I digestion. The Cq of luciferase is roughly 3 cycles lower than the Cq after reverse transcription,

which tracks well with the roughly 10 fold increase in nucleic acid concentration recorded by UV-Vis after reverse transcription. The Cq of GAPDH corresponds to less than three copies according to the luciferase calibration curve, showing that the reference gene signal in prior experiments did indeed arise from reverse transcribed mRNA.

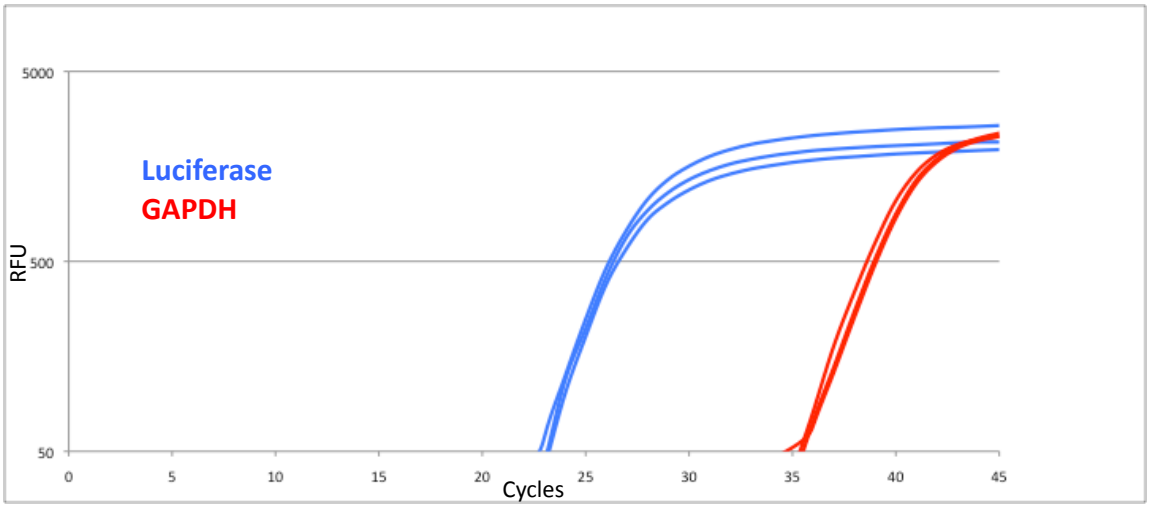

Figure 5.8 qPCR of the total RNA isolate of luciferase reporter plasmid injected oocytes

5.3.5 Introducing selectivity for the luciferase transcript

Given the high background level (equivalent to tens of thousands of copies) of luciferase response in qPCR experiments due to the amplification of contaminating plasmid DNA, it is possible that the signal from smaller retinoic acid dependent increases in luciferase mRNA production is swamped out. In order to see these potential effects, specificity of amplification for the mRNA over the DNA plasmid must be introduced. The conventional way in which this specificity is generated is to create amplification primers that span the intron-exon junction of a gene. If the primer contains only coding sequence from adjacent exons, it will only be able to anneal and allow amplification after intron excision during mRNA maturation.

Unfortunately, the introns of the luciferase gene were removed from the reporter construct. Therefore a short intron original to the firefly luciferase gene was reintroduced by PCR. The intron is short enough that it could be chemically synthesized in its entirety with overlaps into the adjacent exons, allowing the oligo to be used as one large amplification primer. qPCR primers were then designed that anneal across the intron-exon boundary, referred to as plasmid primer, and those that anneal only to the edges of the exons split by the intron, referred to as intron-spanning primer (Figure 5.9).

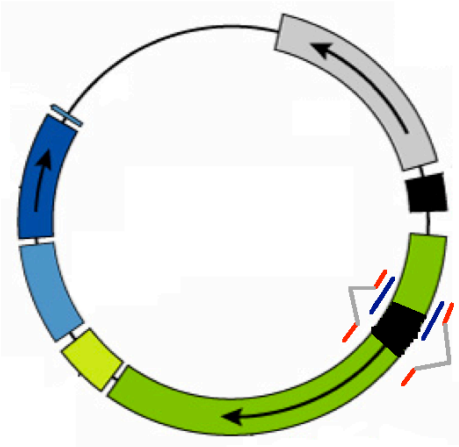

Figure 5.9 Diagram of qPCR primers for an intron-containing luciferase reporter plasmid. The black section of the green coding region is an intron. The blue primers bridge these sections and anneal along the whole length. The red primer spans the intron and anneals only on the two exons that will be brought together after splicing.

These primers were then used in qPCR reactions to find conditions that promote maximal selectivity between the two. Ideally conditions would require annealing along the full sequence of the primer to allow amplification. The best way to regulate stringency of primer binding is to adjust the annealing temperature of the PCR method. Thus, side by side reactions of the intron-spanning and plasmid primers were performed at a range of annealing temperatures from 50.8 °C to 69.7 °C (Table 5.4). The largest difference between the efficiency of amplification of the two sets of primers while still allowing any amplification occurred at an annealing temperature of 63.5 °C.

Annealing Temperature	plasmid Cq	intron-spanning Cq
69.7	-	-
66.9	-	-
63.5	16	29.3
59.6	17.4	25.5
56.5	17.4	23.9
53.5	17.9	21.3
50.8	18.4	20.3

Table 5.4 qPCR data for intron-containing luciferase primer annealing temperature experiment. Temperatures are in ºC. Cq are in cycles. Values are the mean of three replicates. -, no amplification.

This qPCR protocol was then applied to the total RNA extracted from 4 oocytes injected with the standard 2 ng per cell of the luciferase reporter plasmid. It was found that while the plasmid primers amplified as expected with a Cq of 26 cycles, the intron-spanning primers displayed a Cq of 37.9 cycles (Figure 5.10). As this Cq reflects an absolute abundance of the luciferase DNA in single digit or even zero copies, this result suggests that the intron-spanning primers are sufficient to discriminate between mRNA and the DNA plasmid in the *Xenopus laevis* oocyte.

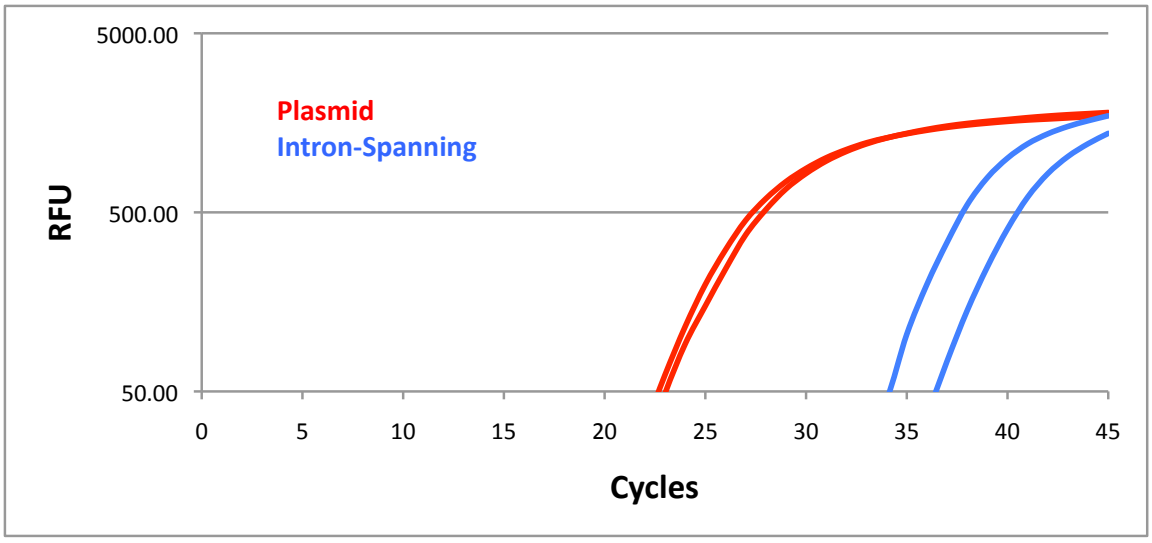

Figure 5.10 qPCR using intron-spanning primers of the total RNA lysate from modified luciferase resporter plasmid injected oocytes.

Having validated the intron-spanning primers and established a true negative control, the full expression system was again reconstituted in hopes of establishing a positive response. Oocyte nuclei were injected with 2 ng per cell of the luciferase reporter construct, and allowed to repair and chromatinize the plasmid for 18 hours. Then the oocyte was cytoplasmically injected with 5 ng or 0.5 ng each of RARα and RXRα mRNA. After one hour for the oocytes to recover from injection, they were incubated in 10 μM retinoic acid for an additional 18 hours. At this time, total RNA was extracted and reverse transcribed according to the established protocol, creating two parallel conditions culled from four oocytes each that are identical except in the amount of transcription factor mRNA injected.

These two samples were split into qPCR reactions using the intron-primers with an annealing temperature of 63.5 °C, in addition to those for the reference genes with the standard annealing temperature of 48 °C. The results of these reactions show the expected abundances of the reference genes with GAPDH Cq values around 25 cycles and ODC Cq values around 28 cycles (Table 5.5). Unfortunately, the luciferase Cq values were around 35 cycles, firmly in a range that suggests there is no detectable expression. The amount of transcription factor mRNA injected seems to have no effect on these results.

	0.5 ng mRNA	5 ng mRNA
Intron-Spanning	35.7	35.1
GAPDH	28.2	29.4
ODC	24.5	26.0

Table 5.5 qPCR data for intron-containing DNA and RNA injected oocytes. 0.5 and 5 ng mRNA refers to the amount of RARα/RXRα mRNA injected per oocyte. Values are the average Cq for two replicates of each condition.

5.3.6 Future Directions

The lack of signal observed with the intron-spanning primers may arise from a number of possibilities. It is possible that the *Xenopus laevis* spliceosome is incapable of recognizing the firefly intron for excision. It is also possible that in the oocyte developmental state the spliceosome is not active or the mRNA is sequestered from it. In this case the experiment should be repeated with the intron-less luciferase reporter assay. The protein fraction of the cell lysate should then be subjected to the luciferase enzymatic luminescence assay. If luciferase mRNA is made, and that mRNA is translated to protein, this assay should give an observable signal.

It is also possible that the transcription factors themselves are not being created. It is possible that there is an undetected defect in the coding region of the DNA for RARα or RXRα that precludes functional expression, or that there was a mistake in their subcloning into *Xenopus laevis* expression vectors. Western blotting of the protein fraction of the oocyte lysate for the transcription factors should reveal whether they are being produced to any appreciable extent within the oocyte.

Alternative methods for micro-injecting the oocyte nuclei with the luciferase reporter plasmid must also be attempted. There appears to be some sample to sample heterogeneity in the amount of plasmid delivered due to the small volume injected. A more reliable system for such small volumes may be to use the *Nano-ject II* by Drummond, which is on hand.

It is also worth considering that, even given a working expression system with retinoic acid inducible luciferase mRNA production, it may be that our unnatural proline analogues are ill-suited to the question at hand. It may be that the activation of the

receptor depends on a certain lifetime of the *cis* proline. The proline analogues increase the population percent *cis* bias but there is still rapid interconversion between the *cis* and *trans* states. Aside from the reasonableness of this particular biological question, the expansion of the unnatural amino acid mutagenesis methodology to an important new class of protein by the application of alternative highly sensitive functional assays would be an important step forward for this technology.

5.4 MATERIALS AND METHODS

5.4.1 Materials

pSV Sport RXRα (ID: 8882), pcDNA FLAG-RARα (ID: 35555), and pGL3 RARE Luciferase (ID: 13458) constructs were obtained from Addgene. Retinoic acid was purchased as a powder from Sigma, suspended as a 10 mM stock in DMSO and stored at -80 ºC.

5.4.2 Preparation of cRNA and Oocytes

Harvested stage V–VI *Xenopus* oocytes were washed in four changes of Ca^{2+}-free OR2 buffer (82.5 mM NaCl, 2 mM KCl, 1 mM $MgCl_2$, 5 mM HEPES, pH = 7.5), defolliculated in 1 mg/mL collagenase for approximately 1 h, washed again in four changes of Ca^{2+}-free OR2, and transferred to ND96 (96 mM NaCl, 2 mM KCl, 1.8 mM $CaCl_2$, 1 mM $MgCl_2$, 5 mM HEPES, pH = 7.5) supplemented with 0.28 mg/mL pyruvate, 0.05 mg/mL Gentamicin, and 0.12 mg/mL theophylline. Oocytes were injected with either cDNA plasmids or mRNA produced by *in vitro* transcription using the mMESSAGE mMACHINE kit (Ambion, Austin, Texas, USA) from cDNA subcloned into pGEMHE as previously described (28).

Oocyte nuclei were injected by allowing the nucleus to rise against the animal pole by incubation, vegetal pole down in the ridge of the disk that sits within petri dishes used for micro-injection for 90 minutes at room temperature. Oocytes were injected deeply and directly into the center of discolored regions the animal pole that appeared after such incubation with 0.2 or 2 ng of reporter plasmid per oocytes. Oocyte cytoplasms were injected shallowly at the edge of the animal pole with 0.5, 5, or 10 ng of mRNA for each transcription factor.

5.4.3 RNA isolation and Reverse Transcription

RNA isolation was performed using RNeasy kit (Qiagen). Deviations from standard protocol are detailed below. Four oocytes were lysed in buffer RLT and vortexed to homogenize until no macroscopic oocyte structure remains intact. Ethanol precipitation proceeds directly on this sample without centrifugation. 3 -5 μL DNAse I in a 70 μL buffered solution was applied to the column and incubated at room temperature for 30 min. RNA was eluted in 20 μL of RNAse-free water. This eluent was then passed through the column a second time for complete recovery. Samples were stored at -80 ºC until ready for reverse transcription.

Reverse transcription was performed using the Transcriptor First-Strand cDNA Synthesis kit (Roche). Deviations from standard protocol are detailed below. 1 μL (~300 ng) of total RNA extract was added to a 20 μL reaction containing polythymine $[dT]_{18}$ primer. RNA, primer, and water were denatured at 65 ºC for 10 minutes and cooled on ice before the addition of buffer, dNTP, RNase Inhibitor, and reverse transcriptase. This reaction was incubated for 30 min at 50 ºC before transcriptase denaturation by incubation at 85 ºC for 5 min.

5.4.4 quantitative Real-Time PCR

20 μL qPCR reactions employed the 2X SYBR Green Master Mix (Roche). 1.25 μL each from 10 μM forward and reverse primer stocks was added along with 2 μL from the reverse transcription reaction. cDNA for reactions with luciferase for each of the reference gene primers was split from the same reverse transcription product. Each condition was run in triplicate.

19.5 μL of each sample was transferred to a 96-well plate, taking care to avoid bubbles, covered, and run on a Bio-Rad CFX96 Real-Time system qPCR with a 2-step cycle. An initial denaturation of 95 ºC for 10 min preceded 40 cycles of 10 s at 95 ºC and 30 s at the annealing temperature (48 ºC for all conditions except those specified otherwise in the main text). Following the final cycle, a temperature gradient ramping from 58 – 88 ºC, raising two degrees per minute, was run.

5.5 REFERENCES

1. Liu, J., Perumal, N. B., Oldfield, C. J., Su, E. W., Uversky, V. N., and Dunker, A. K. (2006) Intrinsic disorder in transcription factors, *Biochemistry 45*, 6873-6888.
2. Helsen, C., and Claessens, F. (2014) Looking at nuclear receptors from a new angle, *Mol Cell Endocrinol 382*, 97-106.
3. Putcha, B. D., Wright, E., Brunzelle, J. S., and Fernandez, E. J. (2012) Structural basis for negative cooperativity within agonist-bound TR:RXR heterodimers, *Proc Natl Acad Sci U S A 109*, 6084-6087.
4. Osz, J., Brelivet, Y., Peluso-Iltis, C., Cura, V., Eiler, S., Ruff, M., Bourguet, W., Rochel, N., and Moras, D. (2012) Structural basis for a molecular allosteric control mechanism of cofactor binding to nuclear receptors, *Proc Natl Acad Sci U S A 109*, E588-594.
5. Chandra, V., Huang, P., Hamuro, Y., Raghuram, S., Wang, Y., Burris, T. P., and Rastinejad, F. (2008) Structure of the intact PPAR-gamma-RXR- nuclear receptor complex on DNA, *Nature 456*, 350-356.
6. Chandra, V., Huang, P., Potluri, N., Wu, D., Kim, Y., and Rastinejad, F. (2013) Multidomain integration in the structure of the HNF-4alpha nuclear receptor complex, *Nature 495*, 394-398.

7. Orlov, I., Rochel, N., Moras, D., and Klaholz, B. P. (2012) Structure of the full human RXR/VDR nuclear receptor heterodimer complex with its DR3 target DNA, *Embo J 31*, 291-300.
8. Bourguet, W., Vivat, V., Wurtz, J. M., Chambon, P., Gronemeyer, H., and Moras, D. (2000) Crystal structure of a heterodimeric complex of RAR and RXR ligand-binding domains, *Mol Cell 5*, 289-298.
9. Renaud, J. P., Rochel, N., Ruff, M., Vivat, V., Chambon, P., Gronemeyer, H., and Moras, D. (1995) Crystal structure of the RAR-gamma ligand-binding domain bound to all-trans retinoic acid, *Nature 378*, 681-689.
10. Bruck, N., Vitoux, D., Ferry, C., Duong, V., Bauer, A., de The, H., and Rochette-Egly, C. (2009) A coordinated phosphorylation cascade initiated by p38MAPK/MSK1 directs RARalpha to target promoters, *Embo J 28*, 34-47.
11. Gaillard, E., Bruck, N., Brelivet, Y., Bour, G., Lalevee, S., Bauer, A., Poch, O., Moras, D., and Rochette-Egly, C. (2006) Phosphorylation by PKA potentiates retinoic acid receptor alpha activity by means of increasing interaction with and phosphorylation by cyclin H/cdk7, *Proc Natl Acad Sci U S A 103*, 9548-9553.
12. Sun, K., Montana, V., Chellappa, K., Brelivet, Y., Moras, D., Maeda, Y., Parpura, V., Paschal, B. M., and Sladek, F. M. (2007) Phosphorylation of a conserved serine in the deoxyribonucleic acid binding domain of nuclear receptors alters intracellular localization, *Mol Endocrinol 21*, 1297-1311.
13. Lu, K. P., Finn, G., Lee, T. H., and Nicholson, L. K. (2007) Prolyl cis-trans isomerization as a molecular timer, *Nat Chem Biol 3*, 619-629.
14. Lu, K. P., and Zhou, X. Z. (2007) The prolyl isomerase PIN1: a pivotal new twist in phosphorylation signalling and disease, *Nat Rev Mol Cell Biol 8*, 904-916.
15. Jabs, A., Weiss, M. S., and Hilgenfeld, R. (1999) Non-proline cis peptide bonds in proteins, *J Mol Biol 286*, 291-304.
16. Chen, H. Z., Li, L., Wang, W. J., Du, X. D., Wen, Q., He, J. P., Zhao, B. X., Li, G. D., Zhou, W., Xia, Y., Yang, Q. Y., Hew, C. L., Liou, Y. C., and Wu, Q. (2012) Prolyl isomerase Pin1 stabilizes and activates orphan nuclear receptor TR3 to promote mitogenesis, *Oncogene 31*, 2876-2887.
17. Gianni, M., Boldetti, A., Guarnaccia, V., Rambaldi, A., Parrella, E., Raska, I., Jr., Rochette-Egly, C., Del Sal, G., Rustighi, A., Terao, M., and Garattini, E. (2009) Inhibition of the peptidyl-prolyl-isomerase Pin1 enhances the responses of acute myeloid leukemia cells to retinoic acid via stabilization of RARalpha and PML-RARalpha, *Cancer Res 69*, 1016-1026.
18. Lucchetti, C., Caligiuri, I., Toffoli, G., Giordano, A., and Rizzolio, F. (2013) The prolyl isomerase Pin1 acts synergistically with CDK2 to regulate the basal activity of estrogen receptor alpha in breast cancer, *PLoS One 8*, e55355.
19. Shaw, P. E. (2007) Peptidyl-prolyl cis/trans isomerases and transcription: is there a twist in the tail?, *EMBO Rep 8*, 40-45.
20. Brondani, V., Schefer, Q., Hamy, F., and Klimkait, T. (2005) The peptidyl-prolyl isomerase Pin1 regulates phospho-Ser77 retinoic acid receptor alpha stability, *Biochem Biophys Res Commun 328*, 6-13.
21. Lu, K. P., Liou, Y. C., and Zhou, X. Z. (2002) Pinning down proline-directed phosphorylation signaling, *Trends Cell Biol 12*, 164-172.

22. Limapichat, W., Lester, H. A., and Dougherty, D. A. (2010) Chemical scale studies of the Phe-Pro conserved motif in the cys loop of Cys loop receptors, *J Biol Chem 285*, 8976-8984.
23. Lummis, S. C., Beene, D. L., Lee, L. W., Lester, H. A., Broadhurst, R. W., and Dougherty, D. A. (2005) Cis-trans isomerization at a proline opens the pore of a neurotransmitter-gated ion channel, *Nature 438*, 248-252.
24. Beene, D. L., Dougherty, D. A., and Lester, H. A. (2003) Unnatural amino acid mutagenesis in mapping ion channel function, *Curr Opin Neurobiol 13*, 264-270.
25. Monahan, S. L., Lester, H. A., and Dougherty, D. A. (2003) Site-specific incorporation of unnatural amino acids into receptors expressed in Mammalian cells, *Chem Biol 10*, 573-580.
26. Minucci, S., Wong, J., Blanco, J. C., Shi, Y. B., Wolffe, A. P., and Ozato, K. (1998) Retinoid receptor-induced alteration of the chromatin assembled on a ligand-responsive promoter in Xenopus oocytes, *Mol Endocrinol 12*, 315-324.
27. Tomita, A., Buchholz, D. R., Obata, K., and Shi, Y. B. (2003) Fusion protein of retinoic acid receptor alpha with promyelocytic leukemia protein or promyelocytic leukemia zinc finger protein recruits N-CoR-TBLR1 corepressor complex to repress transcription in vivo, *J Biol Chem 278*, 30788-30795.
28. Nowak, M. W., Gallivan, J. P., Silverman, S. K., Labarca, C. G., Dougherty, D. A., and Lester, H. A. (1998) In vivo incorporation of unnatural amino acids into ion channels in Xenopus oocyte expression system, *Methods Enzymol 293*, 504-529.
29. Tokmakov, A. A., Hashimoto, T., Hasegawa, Y., Iguchi, S., Iwasaki, T., and Fukami, Y. (2014) Monitoring gene expression in a single Xenopus oocyte using multiple cytoplasmic collections and quantitative RT-PCR, *Febs J 281*, 104-114.
30. Sindelka, R., Ferjentsik, Z., and Jonak, J. (2006) Developmental expression profiles of Xenopus laevis reference genes, *Dev Dyn 235*, 754-758.

Appendix 1

Investigation of Potential 5-HT_3 Receptor Molecular Chaperoning

A1.1 ABSTRACT

Cys-loop receptors undergo a slow and highly inefficient maturation process before arriving at the plasma membrane. Several proteins, termed molecular chaperones, facilitate this process. Two such chaperones of Cys-loop receptors are RIC-3 and Lynx1. Here we test the abilities of these proteins to facilitate 5-HT_3 receptor expression on the plasma membrane of *Xenopus laevis* oocytes. We find that, across a wide range of relative abundances, RIC-3 decreases 5-HT_3A expression on the plasma membrane. Maximal serotonin currents suggest that Lynx1 has a bimodal interaction with 5-HT_3 subunits. At high relative abundances, Lynx1 inhibits 5-HT_3 assembly, while at lower abundances Lynx1 appears to selectively chaperone 5-HT_3A and not 5-HT_3AB receptors. Lynx1 is unable to bias assembly toward 5-HT_3A receptors in oocytes expressing a mixed population of receptors however, suggesting either that the maximal serotonin current data were misleading or that the B subunit has a higher affinity for the A subunit than does Lynx1.

A1.2 INTRODUCTION

Cys-loop receptors, as multimeric integral membrane proteins, undergo a complex process of maturation. Individual receptor subunits complex to form pentamers in the endoplasmic reticulum (ER) before passage through the Golgi and insertion in the plasma

membrane (*1*). The assembly process is slow and highly inefficient however (*2*). Receptor subunits must overcome a varied mixture of ER retention and exit motifs, be decorated at various glycosylation sites, oxidize proper disulfide bonds, cleave N-terminal signaling sequences, and find complementary subunits with which to assemble in acceptable functional stoichiometries (*1, 3, 4*). Perhaps unsurprisingly then, a large majority of translated subunits remain unassembled in the ER, where they lead to the activation of ER stress signaling responses (*5-7*).

Given this landscape, one could imagine that increased subunit translation levels might lead to increased ER stress rather than to increased mature functional receptor. Thus, in some cases, in order to efficiently modulate the amount of mature receptor on the plasma membrane, accessory proteins facilitate the assembly process (*8, 9*). These facilitators, known as molecular chaperones, bind to and stabilize subunits in partially assembled receptors within the ER (*8, 9*). There are two major molecular chaperones for nicotinic acetylcholine receptors (nAChR): RIC-3 and Lynx (*10, 11*).

RIC-3 was identified by a mutagenic screen in *C. elegans*, where it is required for expression of nAChRs (*12*). The human homologue of RIC-3 was found to greatly increase the expression of α7 nAChRs in heterologous systems (*13-15*). Further, the endogenous expression level of RIC-3, which is primarily located in the ER, correlates with the functional expression of α7 nAChRs on the plasma membrane. While it is known that RIC-3 directly binds to nAChRs, and its function is contingent on nAChR transmembrane region or intracellular loop identity, the exact mechanism of its interaction is unclear (*13, 16-18*). Converse to its actions on α7, RIC-3 inhibits functional expression of many other nAChR subtypes (*11*).

For non-nicotinic Cys-loop receptors the data are less clear. In *Xenopus laevis* oocytes, it appears that RIC-3 blocks the expression of 5-HT_3A receptors (*13*). However, other studies in human cell lines show up-regulation of plasma membrane 5-HT_3A receptor (*19*). This up-regulation also appears to be subunit-specific, as RIC-3 does not bind the 5-HT_3B subunit (*20, 21*). Thus, it appears either that there may be additional cell type specific factors that enable RIC-3 function or that one set of studies is mistaken.

Lynx1 was identified through sequence homology with a family of toxins, including α-bungarotoxin, known to target and bind nAChRs (*22*). Lynx1 is widely expressed in the brain and experiments in heterologous expression systems demonstrate that co-expression of Lynx1 and α4β2 nAChRs results in many changes to the acetylcholine response, including current intensity, receptor desensitization rate, and ligand potency (*23*). *In vivo,* these changes have been found to underlie the closure of the early developmental period of synaptic plasticity in the visual cortex (*24*).

Lynx1's functional effects result from its direct binding to the receptor (*23*). Co-immunoprecipitation experiments show that Lynx is capable of binding many different nAChR subunits. NMR studies have confirmed that Lynx1 forms a three finger toxin-like β-fold (*25*). Like those toxins, Lynx1 is believed to bind to the receptor at the interface of adjacent subunits just below the orthosteric binding site (*25, 26*). Lynx1 is decorated with a GPI-linker in the ER and recent evidence suggests that Lynx1 binding to nAChRs in the ER may facilitate receptor assembly (*10*).

In attempting to determine the relationships between structure and function in the 5-HT_3 receptor, many mutations that decrease receptor assembly and efficacy are encountered. This effect is compounded by the inefficiency of the nonsense suppression

methodology. Therefore we attempted to characterize the effects of RIC-3 and of Lynx1 on 5-HT_3 receptors.

A1.3 RESULTS AND DISCUSSION

A1.3.1 RIC-3 Inhibits 5-HT_3A Functional Expression at the Plasma Membrane

In order to determine if RIC-3 is capable of chaperoning 5-HT_3A receptors in *Xenopus laevis* oocytes, the mRNA of both proteins were co-injected at varying relative abundances. The total maximal serotonin current elicited from these oocytes was then compared to paired ooctyes bearing the same amount of receptor subunit mRNA but lacking RIC-3 mRNA. The paired oocytes were taken from the same batch, had been injected and assayed at the same time as the RIC-3 bearing oocytes, and handled identically in between. Despite the normal variability of maximal currents across oocytes, given a large sample size culled from multiple oocyte preparations, it was hoped that meaningful interpretations could be made.

RIC-3 : 5-HT_3A mass ratios of 1:1, 1:10, and 1:100 were compared to oocytes injected with 5-HT_3A alone (Figure A1.1). In all cases of RIC-3 coinjection, maximal serotonin response was significantly decreased ($p < 0.05$, student's T-test). The strongest inhibition occurs at the highest relative abundance of RIC-3, with the effect trailing off as RIC-3 scarcity increases. This is

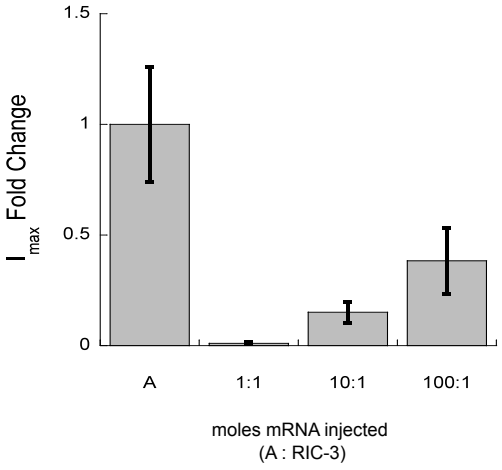

Figure A1.1 Effects of RIC-3 on 5-HT_3A receptor maximal current. Normalized to the 5-HT I_{max} for 5-HT_3A receptor in the absence of RIC-3.

in agreement with the effects reported previously in *Xenopus laevis* oocytes and contrary to findings in human cell lines, confirming the validity of the early oocyte work and suggesting that addition factors present in human cells influence RIC-3 function.

A1.3.2 Lynx1 Appears to Selectively Regulate 5-HT$_3$A but not 5-HT$_3$AB Receptors

When Lynx1 and 5-HT$_3$A subunits were co-injected at various relative abundances according to the protocol delineated above for RIC-3, two different effects became apparent (Figure A1.2, *A*; Table A1.1). Similarly to RIC-3, at high Lynx1 relative abundances the serotonin maximal current was inhibited. Unlike RIC-3 however, there exists a ratio at which the serotonin maximal current meaningfully increases ($p < 0.01$, student's T-test) before trailing off again toward levels seen in the absense of Lynx1. This suggests that Lynx1 is capable of chaperoning 5-HT$_3$A receptors to the plasma membrane. Assuming equally efficient translation of the constructs, the ratio at which increases in maximal current are observed equates to one Lynx1 molecule per ten assembled receptors. This sub-stoichiometric effect is somewhat puzzling until one remembers the strong inhibitory effect at ten lynx molecules per one assembled receptor. It is possible that current increases are not seen at one Lynx1 molecule per receptor, because this overall ratio likely is a combination of mono-liganded receptors that potentiate and multi-liganded receptors that inhibit observed currents.

When the same experiment is repeated with oocytes injected with both 5-HT$_3$A and 5-HT$_3$B subunits, the reduction of maximal serotonin current is again observed at high ratios of Lynx1 to receptor subunit (Figure A1.2, *B*; Table A1.1). There is no further effect, however, as currents resemble those for oocytes lacking Lynx1 at all other

injection ratios. This suggests that the potentiating effect seen above for the 5-HT_3A receptor is subunit specific.

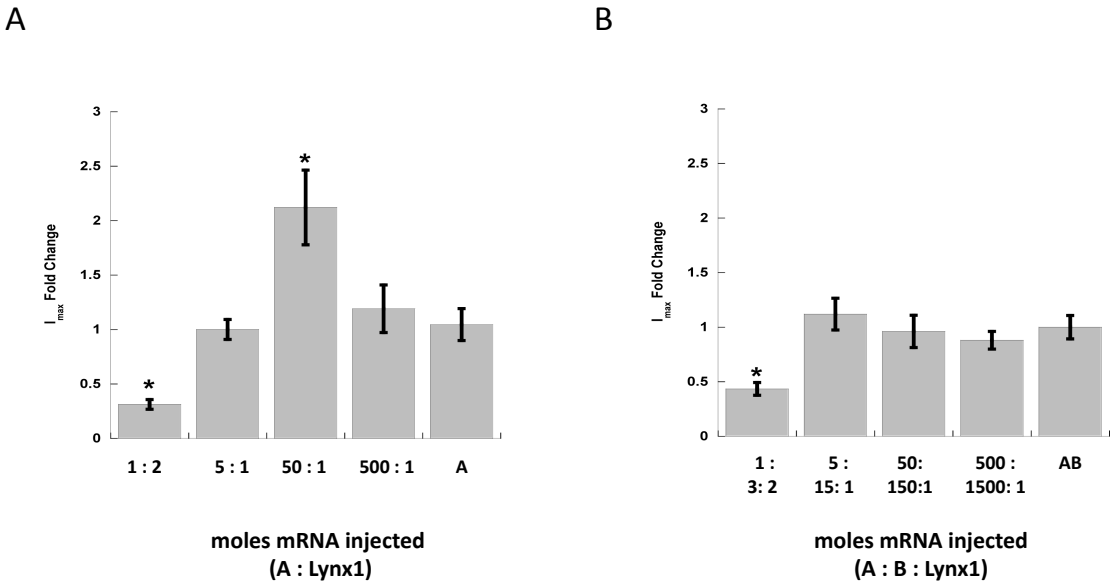

Figure A1.2 Effect of Lynx1 co-expression on 5-HT maximal currents. (A) 5-HT_3A receptor responses normalized to maximal current in the absence of Lynx1. (B) 5-HT_3AB receptor responses normalized to maximal current in the absence of Lynx1. Asterisks mark conditions that are significantly ($p < 0.01$) deviated from the reference condition.

Receptor	5-HT_3A : Lynx1	Normalized I_{max}	$p < 0.01$	# Cells
A	-	1.00 ± 0.15		30
A	1:2	0.31 ± 0.04	*	30
A	5:1	0.96 ± 0.09		43
A	50:1	2.12 ± 0.34	*	36
A	500:1	1.19 ± 0.22		21
AB	-	1.00 ± 0.11		29
AB	1:2	0.43 ± 0.06	*	27
AB	5:1	1.12 ± 0.15		31
AB	50:1	0.96 ± 0.15		30
AB	500:1	0.88 ± 0.08		33

Table A1.1 Effect of Lynx1 co-expression on 5-HT maximal currents. In all cases, the injection ratio of A to B subunits in 5-HT_3AB receptors is 1:3. P-values are determined by student's t-test. Values are reported as mean ± standard error.

A1.3.3 Lynx1 Appears Unable to Bias Assembly in Mixed Populations of 5-HT$_3$A and 5-HT$_3$AB Receptors

The subunit selectivity of 5-HT$_3$ receptor upregulation by Lynx1 observed above raises the possibility that Lynx1 acts to shape the serotonin receptor expression profile *in vivo*, biasing toward assembly of the homomeric receptor. To test this hypothesis, oocytes were injected with a ratio of 5-HT$_3$A and 5-HT$_3$B subunits shown to generate a mixed population of homomeric and heteromeric receptors (Figure A1.3). The dose-response curve resulting from this mixed population shows a biphasic response with components relating to each of receptor subtypes. The fit of this biphasic response provides the proportion of total serotonin response arising from each receptor subtype.

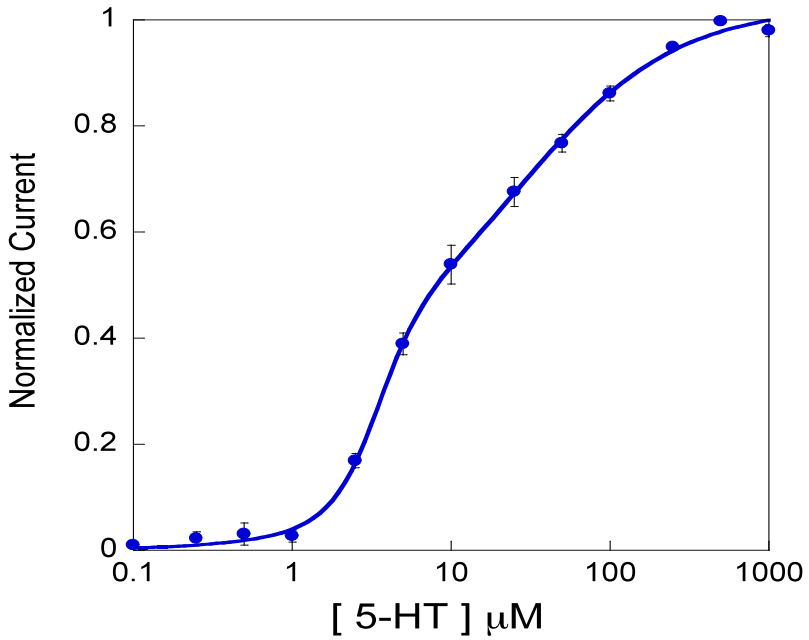

Figure A1.3 Biphasic dose-response relationship resulting from co-expression of 5-HT$_3$A and 5-HT$_3$AB receptors. Injected subunit mRNA ratio is 100:1 5-HT$_3$A:5-HT$_3$B. The fit of the biphasic curve shows 40 % of total response to arise from homomeric channels at this subunit injection ratio.

Varying amounts of Lynx1 were then co-injected along with this mix of receptor subunits. If Lynx1 increases the likelihood of 5-HT_3A receptor assembly at the expense of 5-HT_3AB receptor assembly, it would be expected that the components of the biphasic dose response curve arising from the homomeric channel would increase as a proportion of the normalized total response. Unfortunately, this is not what is observed (Table A1.2). The proportion of homomeric and heteromeric receptors is unaffected by any relative abundance of Lynx1. This can mean either of two things: one, that the Lynx effect on 5-HT_3A maximal currents was a statistical aberration arising from an inherently noisy metric, or two, that the effect on maximal currents was real but that it is mitigated by the presence of competing 5-HT_3B subunits. The latter scenario could be possible if B subunit association with A subunits is stronger than that of Lynx1.

5-HT_3A : Lynx1	% Response Homomer	# Cells
-	28 ± 3	10
1:2	24 ± 2	5
5:1	30 ± 3	8
50:1	29 ± 2	10
500:1	26 ± 2	10

Table A1.2 Effect of Lynx1 on a mixed population of 5-HT_3A and 5-HT_3AB receptors. In all conditions the ratio of A and B subunits is 100:1. The percent of normalized 5-HT response corresponding to each receptor type was calculated from the fit of the biphasic dose-response curve and the percentage corresponding to homomeric 5-HT_3A receptors is reported here.

A1.4 METHODS

A1.4.1 Mutagenesis and Preparation of cRNA and Oocytes

Wild type 5-HT_3A and 5-HT_3B receptor subunits, within the complete coding sequence for the human 5-HT_3A and 5-HT_3B receptor subunit (accession numbers P46098-1; NP_006019), were cloned into pGEMhe. Mouse Lynx1 was cloned into pDH105 vector. Harvested stage V-VI *Xenopus* oocytes were washed in four changes of Ca^{2+}-free OR2 buffer (82.5 mM NaCl, 2 mM KCl, 1 mM $MgCl_2$, 5 mM HEPES, pH 7.5), de-folliculated in 1 mg/ml collagenase for approximately 1 h, washed again in four changes of Ca^{2+}-free OR2, and transferred to ND96 (96 mM NaCl, 2 mM KCl, 1.8 mM $CaCl_2$, 1 mM $MgCl_2$, 5 mM HEPES, pH 7.5) supplemented with 0.28 mg/ml pyruvate, 0.05 mg/ml Gentamicin, and 0.12 mg/ml theophylline. Oocytes were injected with 5-25 ng mRNA produced by *in vitro* transcription using the mMESSAGE MACHINE kit (Ambion, Austin, Texas, USA) from cDNA subcloned into pGEMhe as previously described (*27*). All 5-HT_3AB receptor experiment injections contained a 1:3 A:B subunit mole ratio. Electrophysiological measurements were performed after incubation for 24 - 72 h post-injection at 18^o C.

A1.4.2 Characterization of receptors

Agonist-induced currents were recorded at 22-25^o C from individual oocytes using the OpusXpress system (Molecular Devices Axon Instruments, Union City, CA). 5-HT, and *m*-chlorophenylbiguanide (*m*CPBG) (Sigma) were stored as 25 mM aliquots at -20^o C, diluted in Ca^{2+}-free ND96 buffer (96 mM NaCl, 2 mM KCl, 1 mM $MgCl_{2,,}$ 5 mM HEPES, pH 7.5), and delivered to cells via the automated perfusion system of the OpusXpress. Glass microelectrodes were backfilled with 3 M KCl and had a resistance of

~1 MΩ. The holding potential was -60 mV. Agonist doses in Ca^{2+}-free ND96 were applied for 15 s followed by a 116 s wash with the running buffer. Dose-response data were obtained for ≥ 8 agonist concentrations on ≥ 8 cells. To determine EC_{50} values, concentration-response data were fitted to the four-parameter logistic equation $I = I_{max}/[1 + (EC_{50}/[A])^{nH}]$, where I_{max} is the maximal response plateau, [*A*] is the log concentration of agonist, and *nH* is the Hill coefficient, using KaleidaGraph v3.6 software (Synergy Software, Reading, PA). A detailed error analysis of nonsense suppression experiments shows that data are reproducible to ±50% in EC_{50} (*28*). Efficacy was calculated for individual cells and then averaged and reported as mean ± S.E.M.

A1.5 REFERENCES

1. Tsetlin, V., Kuzmin, D., and Kasheverov, I. (2011) Assembly of nicotinic and other Cys-loop receptors, *J Neurochem 116*, 734-741.
2. Ilegems, E., Pick, H. M., Deluz, C., Kellenberger, S., and Vogel, H. (2004) Noninvasive imaging of 5-HT3 receptor trafficking in live cells: from biosynthesis to endocytosis, *The Journal of biological chemistry 279*, 53346-53352.
3. Boyd, G. W., Doward, A. I., Kirkness, E. F., Millar, N. S., and Connolly, C. N. (2003) Cell surface expression of 5-hydroxytryptamine type 3 receptors is controlled by an endoplasmic reticulum retention signal, *The Journal of biological chemistry 278*, 27681-27687.
4. Boyd, G. W., Low, P., Dunlop, J. I., Robertson, L. A., Vardy, A., Lambert, J. J., Peters, J. A., and Connolly, C. N. (2002) Assembly and cell surface expression of homomeric and heteromeric 5-HT3 receptors: the role of oligomerization and chaperone proteins, *Mol Cell Neurosci 21*, 38-50.
5. Srinivasan, R., Richards, C. I., Xiao, C., Rhee, D., Pantoja, R., Dougherty, D. A., Miwa, J. M., and Lester, H. A. (2012) Pharmacological chaperoning of nicotinic acetylcholine receptors reduces the endoplasmic reticulum stress response, *Mol Pharmacol 81*, 759-769.
6. Christianson, J. C., and Green, W. N. (2004) Regulation of nicotinic receptor expression by the ubiquitin-proteasome system, *Embo J 23*, 4156-4165.
7. Merlie, J. P., and Lindstrom, J. (1983) Assembly in vivo of mouse muscle acetylcholine receptor: identification of an alpha subunit species that may be an assembly intermediate, *Cell 34*, 747-757.

8. Wanamaker, C. P., and Green, W. N. (2007) Endoplasmic reticulum chaperones stabilize nicotinic receptor subunits and regulate receptor assembly, *The Journal of biological chemistry 282*, 31113-31123.
9. Lester, H. A., Miwa, J. M., and Srinivasan, R. (2012) Psychiatric drugs bind to classical targets within early exocytotic pathways: therapeutic effects, *Biol Psychiatry 72*, 907-915.
10. Miwa, J. M., Lester, H. A., and Walz, A. (2012) Optimizing cholinergic tone through lynx modulators of nicotinic receptors: implications for plasticity and nicotine addiction, *Physiology (Bethesda) 27*, 187-199.
11. Millar, N. S. (2008) RIC-3: a nicotinic acetylcholine receptor chaperone, *Br J Pharmacol 153 Suppl 1*, S177-183.
12. Halevi, S., McKay, J., Palfreyman, M., Yassin, L., Eshel, M., Jorgensen, E., and Treinin, M. (2002) The C. elegans ric-3 gene is required for maturation of nicotinic acetylcholine receptors, *Embo J 21*, 1012-1020.
13. Castillo, M., Mulet, J., Gutierrez, L. M., Ortiz, J. A., Castelan, F., Gerber, S., Sala, S., Sala, F., and Criado, M. (2006) Role of the RIC-3 protein in trafficking of serotonin and nicotinic acetylcholine receptors, *J Mol Neurosci 30*, 153-156.
14. Wang, Y., Yao, Y., Tang, X. Q., and Wang, Z. Z. (2009) Mouse RIC-3, an endoplasmic reticulum chaperone, promotes assembly of the alpha7 acetylcholine receptor through a cytoplasmic coiled-coil domain, *The Journal of neuroscience : the official journal of the Society for Neuroscience 29*, 12625-12635.
15. Dau, A., Komal, P., Truong, M., Morris, G., Evans, G., and Nashmi, R. (2013) RIC-3 differentially modulates alpha4beta2 and alpha7 nicotinic receptor assembly, expression, and nicotine-induced receptor upregulation, *BMC Neurosci 14*, 47.
16. Haeger, S., Kuzmin, D., Detro-Dassen, S., Lang, N., Kilb, M., Tsetlin, V., Betz, H., Laube, B., and Schmalzing, G. (2010) An intramembrane aromatic network determines pentameric assembly of Cys-loop receptors, *Nat Struct Mol Biol 17*, 90-98.
17. Goyal, R., Salahudeen, A. A., and Jansen, M. (2011) Engineering a prokaryotic Cys-loop receptor with a third functional domain, *The Journal of biological chemistry 286*, 34635-34642.
18. Gee, V. J., Kracun, S., Cooper, S. T., Gibb, A. J., and Millar, N. S. (2007) Identification of domains influencing assembly and ion channel properties in alpha 7 nicotinic receptor and 5-HT3 receptor subunit chimaeras, *Br J Pharmacol 152*, 501-512.
19. Cheng, A., McDonald, N. A., and Connolly, C. N. (2005) Cell surface expression of 5-hydroxytryptamine type 3 receptors is promoted by RIC-3, *The Journal of biological chemistry 280*, 22502-22507.
20. Walstab, J., Hammer, C., Lasitschka, F., Moller, D., Connolly, C. N., Rappold, G., Bruss, M., Bonisch, H., and Niesler, B. (2010) RIC-3 exclusively enhances the surface expression of human homomeric 5-hydroxytryptamine type 3A (5-HT3A) receptors despite direct interactions with 5-HT3A, -C, -D, and -E subunits, *The Journal of biological chemistry 285*, 26956-26965.
21. Cheng, A., Bollan, K. A., Greenwood, S. M., Irving, A. J., and Connolly, C. N. (2007) Differential subcellular localization of RIC-3 isoforms and their role in

determining 5-HT3 receptor composition, *The Journal of biological chemistry 282*, 26158-26166.

22. Miwa, J. M., Ibanez-Tallon, I., Crabtree, G. W., Sanchez, R., Sali, A., Role, L. W., and Heintz, N. (1999) lynx1, an endogenous toxin-like modulator of nicotinic acetylcholine receptors in the mammalian CNS, *Neuron 23*, 105-114.
23. Ibanez-Tallon, I., Miwa, J. M., Wang, H. L., Adams, N. C., Crabtree, G. W., Sine, S. M., and Heintz, N. (2002) Novel modulation of neuronal nicotinic acetylcholine receptors by association with the endogenous prototoxin lynx1, *Neuron 33*, 893-903.
24. Morishita, H., Miwa, J. M., Heintz, N., and Hensch, T. K. (2010) Lynx1, a cholinergic brake, limits plasticity in adult visual cortex, *Science 330*, 1238-1240.
25. Lyukmanova, E. N., Shenkarev, Z. O., Shulepko, M. A., Mineev, K. S., D'Hoedt, D., Kasheverov, I. E., Filkin, S. Y., Krivolapova, A. P., Janickova, H., Dolezal, V., Dolgikh, D. A., Arseniev, A. S., Bertrand, D., Tsetlin, V. I., and Kirpichnikov, M. P. (2011) NMR structure and action on nicotinic acetylcholine receptors of water-soluble domain of human LYNX1, *The Journal of biological chemistry 286*, 10618-10627.
26. Lyukmanova, E. N., Shulepko, M. A., Buldakova, S. L., Kasheverov, I. E., Shenkarev, Z. O., Reshetnikov, R. V., Filkin, S. Y., Kudryavtsev, D. S., Ojomoko, L. O., Kryukova, E. V., Dolgikh, D. A., Kirpichnikov, M. P., Bregestovski, P. D., and Tsetlin, V. I. (2013) Water-soluble LYNX1 residues important for interaction with muscle-type and/or neuronal nicotinic receptors, *The Journal of biological chemistry 288*, 15888-15899.
27. Nowak, M. W., Gallivan, J. P., Silverman, S. K., Labarca, C. G., Dougherty, D. A., Lester, H. A., and Conn, P. M. (1998) In vivo incorporation of unnatural amino acids into ion channels in Xenopus oocyte expression system, In *Methods in Enzymology*, pp 504-529, Academic Press.
28. Torrice, M. M. (2009) Chemical-scale studies of nicotinic and muscarinic acetylcholine receptors, In *Chemistry and Chemical Engineering*, California Institute of Technology, Pasadena.